TR 81060

ROYAL AIRCRAFT ESTABLISHMENT

*

Technical Report 81060

May 1981

THE APPLICATION OF SUBSONIC THEORETICAL AERODYNAMICS TO ACTIVE CONTROLS

by

H.C. Garner

*

Procurement Executive, Ministry of Defence
Farnborough, Hants

UDC 629.13.014 : 533.6.048.1 : 533.6.013.13 : 517.956.224 :
533.6.011.32/34 : 533.6.011.1 : 533.6.013.2

ROYAL AIRCRAFT ESTABLISHMENT

Technical Report 81060

Received for printing 11 May 1981

THE APPLICATION OF SUBSONIC THEORETICAL AERODYNAMICS TO ACTIVE CONTROLS.

by

H. C. Garner

SUMMARY

Analytical and numerical studies are made of aerodynamic forces for wing and control-surface motion with general time-dependence in linearized subsonic flow. Alternative formulations are discussed, with particular attention to one in the time domain where quasi-steady displacement and rate terms are combined with a residual history term. An accurate calculation procedure is devised, and results are illustrated for a high-aspect-ratio wing at Mach number 0.8 with trailing-edge, leading-edge and all-moving-tip controls. Emphasis is placed on asymptotic behaviour at small and large times.

Individual control characteristics are compared over a wide range of control rate. The usefulness of the quasi-steady approximation is established for hinge moments and is analysed for lift, where the rate and history terms become important together. The rapid lift response to the leading-edge control and the sluggish lift response to the trailing-edge control are explained. These forces in the time domain are confirmed by Fourier transform calculations in the frequency domain, which show the extent to which the range of frequency can be truncated.

The control-surface motion to produce a known time-dependent force is determined. It is remarkable how rapidly the controls can neutralize the growth of lift as the wing enters a step gust.

Departmental Reference: Structures BF/B/0860

LIST OF CONTENTS

1 INTRODUCTION

The concept of active control technology has become associated with many aspects of unsteadiness in flight, which together cover a wide range of frequency. The use of an autopilot to control height and speed defines the low-frequency end of the spectrum. Next comes the control of short-period pitching oscillations and the application to the relaxed static stability of aircraft, for which it is sufficient to adopt low-frequency aerodynamics. Moderate frequencies arise in the damping of structural modes and are prominent in aircraft response to gusts, where active controls can enhance ride control or alleviate structural loads. Higher frequencies may arise in the efficiency and safety aspects of manoeuvre control, and still higher frequencies are invoked in problems of flutter suppression. At the top of the range comes the fatigue problem of buffet loads. These applications make demands in the field of unsteady aerodynamic theory.

Active controls are potentially of many types. The present investigation concerns wing aerodynamics in attached subsonic flow, and the treatment covers the conventional aileron or trailing-edge control and also leading-edge and all-moving-tip controls. Other possible types involve greater theoretical difficulty. Discontinuities in planform arise with extended flaps: controls such as spoilers incur problems of flow separation: canards or elevators involve interfering surfaces. Whatever control devices are considered, the technology calls for their rapid deployment. It is necessary to be able to calculate the time-dependent aerodynamic forces for arbitrary control motion and, moreover, to solve the inverse problem of how to deploy a control to produce a given unsteady force.

When linearized subsonic lifting-surface theory is adequate, it is convenient to apply the well-established principles of superposing oscillatory motions to give step changes, as has been described in the review of indicial aerodynamics by Lomax[1]. The practical application to the response of a flexible aircraft to gusts is illustrated by Mitchell[2] using a Fourier transform technique. Subsequent to Refs 1 and 2 the accuracy and scope of numerical methods for aerodynamic load calculation have improved. Indeed Körner's[3] recent survey of theoretical aerodynamic methods for active control devices contains over a hundred references later than 1965 and discusses not only subsonic flow but transonic, supersonic and separated flows as well. The role of unsteady aerodynamics in problems of aircraft dynamics is discussed by Hancock[4]. When the mathematical modelling of the aerodynamics can satisfactorily be expressed in terms of the instantaneous motion, the solution of the equations of aircraft dynamics is numerically straightforward. The synthesis of active control systems is the current problem calling for most accuracy and generality in time-dependent aerodynamics.

The present investigation gives detailed consideration to wing and control motion with general time dependence in linearized subsonic flow. We shall look at alternative formulations of the aerodynamic forces and the practical merits of the various functions introduced to account for the history of the motion. We shall seek to develop numerical procedures and to test them for the gross wing planform and aileron in Fig 1 typical of a modern medium-sized high-subsonic airliner, and also with leading-edge and all-moving-tip controls. The characteristics of the various controls will be compared over a range of

control rate for the Mach number 0.8, and the usefulness of the low-frequency approximation will be analysed. For a particular form of transient control motion, we shall also express the aerodynamic forces as integrals with respect to frequency, so that with the aid of a Fourier transform technique the consistency of the numerical results and the permissible truncation of the infinite range of frequency can be examined. As an illustrative solution of the inverse problem, we shall demonstrate how rapidly the three types of control can be deployed to neutralize the growth of lift due to entry into a step gust.

2 BASIC TIME-DEPENDENT WING FORCES

For many years the primary requirement for high-frequency unsteady aerodynamics has arisen from the need for flutter calculations, which continue to rely heavily on small-perturbation theories for wings in simple harmonic motion. Frequency parameter is therefore a basic independent variable. In the linearized treatment of active controls one approach is to use the frequency spectrum to build a step change, and hence to derive a time integral to represent any specified motion. The corresponding aerodynamic forces are then obtainable by linear superposition. This is analogous to the representation of an arbitrary gust profile and its aerodynamics in terms of those for sinusoidal gusts via an intermediate step gust.

A somewhat different approach is to define an arbitrary smooth motion of a wing or control surface with finite acceleration starting at time $t = 0$. This expresses the reality that any such motion can be created by the application of a finite force, which may be of finite duration t_1. Double integral expressions for resulting aerodynamic forces are obtained in Appendix A, and the relative merits of working in the time domain or the frequency domain are discussed in section 2.3. This leads to the concept of hereditary functions, for which various alternatives are considered in section 2.4.

2.1 Oscillatory forces

The present calculations are made with the subsonic lifting-surface method of Davies[5]. The oscillatory load distribution is taken to be continuous and finite over the planform apart from the inverse-square-root singularity at the leading edge and to be independent of the wing thickness and the mean flow. For an oscillatory upward wing displacement given by

$$z = \mathcal{R}\left[z_j(x,y)e^{i\omega t}\right] \tag{2-1}$$

the surface boundary condition imposes a complex upwash angle

$$\frac{w_j}{U} = \frac{\partial z_j}{\partial x} + \frac{i\omega z_j}{U} \quad , \tag{2-2}$$

and the theory yields the integral equation

$$\frac{w_j(x,y)}{U} = \frac{1}{4\pi\bar{c}^2}\iint \ell_j(x_0,y_0)K\left(\frac{x-x_0}{\bar{c}}, \frac{y-y_0}{\bar{c}}\right)\exp\left\{\frac{-i\bar{\nu}(x-x_0)}{\bar{c}}\right\}dx_0dy_0 \quad . \tag{2-3}$$

Here the integral is taken over the planform where the typical length is chosen to be the geometric mean chord $\bar{c}$, the unknown oscillatory loading over the planform is defined by

$$\text{Lift per unit area} = \Re\left[\rho U^2 \ell_j(x,y) e^{i\omega t}\right] , \tag{2-4}$$

and corresponding to the circular frequency ω the frequency parameter is

$$\bar{\nu} = \frac{\omega \bar{c}}{U} . \tag{2-5}$$

The main stream has density ρ, velocity U parallel to the x-axis and Mach number M. The kernel* function K in equation (2-3) is given by equation (17) of Ref 5 as a function of $\bar{\nu}$, M and the two space variables. For a set of displacement modes, designated by equation (2-1) with subscript i, there is a complex matrix of generalized aerodynamic forces given by the integrals

$$Q_{ij} = \frac{1}{\bar{c}^3} \iint z_i(x_0,y_0) \ell_j(x_0,y_0) dx_0 dy_0 \tag{2-6}$$

over the planform from tip to tip.

The displacement or force modes to be used in the present calculations are defined in Table 1. Modes 1 to 5 correspond to heaving motion and the four rotational motions of the wing and control surfaces indicated in Fig 1, and equation (2-2) is seen to apply to w_j/U in Table 1. The theory of Ref 5 obtains rigorous approximations to Q_{ij} with the replacement of z_i and w_j by equivalent smooth complex functions, which avoid discontinuities in the equivalent ℓ_j at the hinge line in modes 3 and 4. A modal data program to evaluate these equivalent functions at the required locations on the planform is described in section 5 of Ref 6. Very simple changes to that program make possible its extension from an arbitrary trailing-edge control to one selected from the three types in Fig 1. There is one slight complication, however, in the case of the all-moving-tip control; the hinge axis must not intersect the leading or trailing edge, and to acquire results for the forward axis, chosen to give aerodynamic balance, it becomes necessary to take two axes further aft and to extrapolate linearly in x_{h5}. The remaining mode 6 in Table 1 is different from the other five in that w_j represents a sinusoidal gust and the corresponding quantity z_j that would be obtained from the differential equation (2-2) is complex and useless as a force mode. The modal data program is therefore replaced by a direct evaluation of the already smooth function w_j at the required locations, and the force mode is replaced by the unrelated function $|y|/s$ which yields a generalized force proportional to the root bending moment.

The Fortran program for the numerical solution of equation (2-3) and the evaluation of the generalized force coefficients Q_{ij} in equation (2-6) is described in section 3 of

---

* At a recent colloquium in Göttingen to celebrate the eightieth birthday of Professor H.G. Küssner, it was proposed internationally that this function should henceforth be known as the Küssner kernel in recognition of his fundamental work on the subject published in 1940.

Ref 6. One minor change is made to both this and the modal data program, so that the subroutine CHORD can handle any polygonal planform with provision for arbitrary extents and alternative shapes of rounding at the corners; numerical input data are read on the first occasion that the subroutine is entered. The actual planform is defined in Fig 1, but after smoothing around the central and trailing-edge crank sections with the aid of the function

$$g(\lambda) = \frac{1}{16}(1-\lambda)^4(5+4\lambda+\lambda^2) \quad , \qquad 0 \leqslant \lambda \leqslant 1, \qquad (2\text{-}7)$$

the modified shape is as follows. For the leading edge

$$\left.\begin{aligned} \frac{x_\ell}{\bar{c}} &= 1.6934\,\frac{y}{s} + 0.1660\,g(\lambda) \quad , && 0 \leqslant \frac{y}{s} \leqslant 0.0980 \\ \frac{x_\ell}{\bar{c}} &= 1.6934\,\frac{y}{s} \quad , && 0.0980 \leqslant \frac{y}{s} \leqslant 1 \end{aligned}\right\} \qquad (2\text{-}8)$$

with $\lambda = (y/s)/0.0980$. For the trailing edge

$$\left.\begin{aligned} \frac{x_t}{\bar{c}} &= 1.6896 \quad , && 0 \leqslant \frac{y}{s} \leqslant 0.2496 \\ \frac{x_t}{\bar{c}} &= 1.6896 + 0.0362\,g(\lambda) \quad , && 0.2496 \leqslant \frac{y}{s} \leqslant 0.3476 \\ \frac{x_t}{\bar{c}} &= 1.4331 + 0.7380\,\frac{y}{s} + 0.0362\,g(\lambda) \quad , && 0.3476 \leqslant \frac{y}{s} \leqslant 0.4456 \\ \frac{x_t}{\bar{c}} &= 1.4331 + 0.7380\,\frac{y}{s} \quad , && 0.4456 \leqslant \frac{y}{s} \leqslant 1 \end{aligned}\right\} \qquad (2\text{-}9)$$

with $\lambda = \left|(y/s) - 0.3476\right|/0.0980$.

In addition to the planform data, including the typical length $\bar{c}$ and the semi-span $s = 3.9960\bar{c}$, it is necessary to specify certain parameters to define the calculation. These control the output and ensure that the number of modes is consistent with the modal data and are treated as symmetric in y in the present calculations or as antisymmetric, if required. There are parameters to fix the numbers of spanwise loading points and upwash points, both of which are set to $m = 23$ in this instance; similarly the numbers of chordwise loading and upwash points are set to $N = 8$. To enhance the accuracy of spanwise integration of equation (2-3), integers q_i ($i = 1$ to N) and their lowest common multiple are increased from unity, and their values in the present calculations are

$$q_i = (16, 8, 6, 4, 4, 6, 8, 16) \quad \text{with an LCM of } 48 \; . \qquad (2\text{-}10)$$

The Mach number is set to 0.8 and the frequency parameter takes in turn the 24 values

$$\bar{\nu} = 0,\ 0.05,\ 0.15,\ 0.4,\ 0.6,\ 0.75,\ 1.0 \ \text{ and } \ 1.2\ (0.3)\ 6.0 \; . \qquad (2\text{-}11)$$

Selected force coefficients have been tabulated against $\bar{\nu}$. Tables 2 to 4 give the coefficients $-Q_{1j}$, $-Q_{2j}$ and $-Q_{jj}$ for the trailing-edge, leading-edge and all-moving-tip controls respectively. Each of these complex coefficients is split into its in-phase and in-quadrature components written as

$$Q_{ij}(\bar{\nu}) = Q'_{ij}(\bar{\nu}) + i\bar{\nu}Q''_{ij}(\bar{\nu}) \quad . \tag{2-12}$$

The signs in Tables 1 to 4 may call for clarification. The rotational modes 2 to 5 are nose-down, as are the pitching and hinge moment coefficients with $i = 2$ and $i = j$ in equation (2-6). The positive values of $-Q'_{1j}$ represent negative in-phase lift corresponding to each nose-down control. The corresponding in-quadrature coefficients $-Q''_{1j}$ involve rapid changes when $\bar{\nu}$ is small, and for each control it changes sign in the frequency range of equation (2-11). The positive values of $-Q'_{2j}$ represent in-phase nose-up pitching moments about the axis $x = x_a$ in Fig 1 corresponding to nose-down control angles. The hinge moment coefficients include equal contributions from the pair of control surfaces. They appear as small quantities because the non-dimensionalizing volume in equation (2-6) is $\bar{c}^3$ instead of the more typical product of the area and mean chord of the control surfaces, which is $0.04\bar{c}^3$ in modes 3 and 4. Both parts of $-Q_{jj}$ change fairly slowly with $\bar{\nu}$. Positive $-Q'_{33}$ indicates a restoring moment on the trailing-edge control, unlike $-Q'_{44}$ for the leading-edge control. The all-moving-tip is almost neutral with static balance and small values of $-Q'_{55}$ of varying sign. Positive values of $-Q''_{jj}$ show that free motion in any one of the three control-surface modes will decay.

An Argand diagram of the complex quantity $Q_{13}(\bar{\nu})/Q'_{13}(0)$ is drawn in .g 2(a) over the frequency range $0 \leq \bar{\nu} \leq 6$, and it shows an undulatory behaviour the range $1 \leq \bar{\nu} \leq 3$ and an asymptote at $Q'_{13}(\infty)/Q'_{13}(0) = 0.32_5$, both of which will be discussed later. It is sufficient here to contrast this behaviour with that of the smooth Argand diagram of $Q_{16}(\bar{\nu})/Q'_{16}(0)$ corresponding to sinusoidal gusts of varying wavelength, which spirals to the origin as wavelength decreases or $\bar{\nu} \to \infty$.

2.2 Indicial aerodynamics

The term 'indicial aerodynamics' has been in the technical vocabulary for decades, but its origin is obscure to many who use it. It seems unlikely that the term is derived from 'index' in the mathematical sense, although the exponent in equation (2-1) provides a stepping stone from simple harmonic motion to one of growing or decaying amplitude with complex frequency ω. It is probably derived from 'indicium' (= mark, sign) and refers to the signature of a discrete event in time such as a step change. The fact remains that the term is applied to the classical work of Wagner (1925) and Küssner (1936) who solved analytically the growth of lift in two-dimensional incompressible flow arising respectively from a sudden change of angle of attack and from entry into a uniform vertical gust.

The developments in this field up to the late 1950s have been reviewed by Lomax[1]. An additional paper of this period by Drischler[7] also gives useful analytical and numerical data. Without restriction to two-dimensional or incompressible flow there are basic linear relationships between indicial and oscillatory aerodynamics. These provide

alternative expressions for the lift due to a step motion of a wing or control surface, and, following equations (41) of Ref 1, we can take for $\sigma > 0$

$$L(\sigma) = \rho U^2 \bar{c}^2 \left[Q_{1j}(0) + \frac{2}{\pi} \int_0^\infty \{Q''_{1j}(\bar{\nu}) - Q''_{1j}(\infty)\} \cos \bar{\nu}\sigma \, d\bar{\nu} \right] \tag{2-13}$$

or

$$L(\sigma) = \frac{2}{\pi} \rho U^2 \bar{c}^2 \int_0^\infty \frac{Q'_{1j}(\bar{\nu}) \sin \bar{\nu}\sigma}{\bar{\nu}} \, d\bar{\nu} \quad . \tag{2-14}$$

Here the oscillatory coefficients $Q_{ij}(\bar{\nu})$ with $i = 1$ and j arbitrary are split into their real and imaginary parts from equation (2-12), and

$$\sigma = \frac{Ut}{\bar{c}} \tag{2-15}$$

is the travel in mean chords following the step motion. The mathematical derivation of aerodynamic forces for general time-dependent motion and full details of their evaluation are covered in sections 2.3 to 3.3. In the limit as $\sigma \to \infty$ equations (2-13) and (2-14) give

$$L(\infty) = \rho U^2 \bar{c}^2 Q'_{1j}(0) \quad . \tag{2-16}$$

Hence the ratio $L(\sigma)/L(\infty)$ for the trailing-edge control ($j = 3$) can be evaluated from the lift data in Table 2 or Fig 2a, and the results are plotted as the broken curve in Fig 2b. The full curve for entry into a step gust is obtained similarly from equations (2-13) to (2-16) from the lift data for sinusoidal gusts ($j = 6$) in Fig 2a.

Some contrasts and comparisons between the pairs of curves for the oscillatory and step motions in Fig 2 for $M = 0.8$ will set the scene. As will be explained in the following sections, there is an impulsive lift at $\sigma = 0$ proportional to $Q''_{1j}(\infty)$; this is finite and non-zero for the control surface, but is zero for the gust case where the Argand diagram indicates a curve spiralling to the origin at $\bar{\nu} \to \infty$. The limiting value $L(0)$ as σ tends to zero through positive values is proportional to $Q'_{1j}(\infty)$ which, also, is finite and non-zero for the control and zero for the gust. The larger variations in curvature of $L(\sigma)$ for the trailing-edge control in Fig 2b are thought to follow from the distinctive undulations of $\bar{\nu}Q''_{13}(\bar{\nu})$ in Fig 2a, about which more will be said later. Similarly it is worth noting at this stage that as $\sigma \to \infty$ the two curves in Fig 2b have the same asymptotic behaviour

$$\frac{L(\sigma)}{L(\infty)} \simeq 1 - \frac{1.009}{\sigma^2} \tag{2-17}$$

which, as will be seen, relates to a common feature of the Argand diagrams near $\bar{\nu} = 0$.

2.3 Non-sinusoidal motion

In indicial aerodynamics the step change is one of the usual basic elements. It is unrealistic, but serves as a practical mathematical device for the linear construction of arbitrary time-dependent wing motion or a gust of arbitrary profile. In the present treatment of non-sinusoidal motion the wing and control surfaces are regarded as being activated by finite forces and involve finite acceleration. In the context of active controls it is therefore postulated that the upward wing displacement in the mode $z_j(x,y)$ has a smooth time dependence so that

$$z = q_j(\tau) z_j(x,y) \tag{2-18}$$

where $\tau = Ut/\bar{c}$ and $q_j(\tau)$ and its first derivative are continuous and its second derivative is bounded.

In Appendix A, alternative expressions are derived for the generalized force in mode i due to the wing motion in equation (2-18) with $q_j(\tau) = 0$ for $\tau < 0$. With the addition of subscripts to equations (A-12) and (A-13), we have

$$Q_i(\tau) = Q''_{ij}(\infty) \frac{dq_j(\tau)}{d\tau} + Q'_{ij}(0) q_j(\tau) + \frac{2}{\pi} \int_0^\tau \int_0^\infty \frac{dq_j(\tau_0)}{d\tau_0} \left\{ Q''_{ij}(\bar{\nu}) - Q''_{ij}(\infty) \right\} \cos\left[\bar{\nu}(\tau - \tau_0)\right] d\bar{\nu} d\tau_0 \tag{2-19}$$

and

$$Q_i(\tau) = Q''_{ij}(\infty) \frac{dq_j(\tau)}{d\tau} + \frac{2}{\pi} \int_0^\tau \int_0^\infty \frac{dq_j(\tau_0)}{d\tau_0} \frac{Q'_{ij}(\bar{\nu})}{\bar{\nu}} \sin\left[\bar{\nu}(\tau - \tau_0)\right] d\bar{\nu} d\tau_0 \tag{2-20}$$

where $Q'_{ij}(\bar{\nu})$ and $Q''_{ij}(\bar{\nu})$ are defined in equations (2-6) and (2-12). These quantities can be calculated, as in Tables 2 to 4, for particular values of $\bar{\nu}$, but they each require approximate smooth representation over the complete frequency spectrum. On the other hand $q_j(\tau_0)$ may be specified by a simple formula, whereby the integrations with respect to τ_0 in equations (2-19) and (2-20) can be carried out analytically, so as to leave a single integral for $Q_i(\tau)$ with respect to $\bar{\nu}$ in the frequency domain. The two double integrals for $Q_i(\tau)$ are equivalent to those derived from reciprocal Fourier transform relationships between the indicial aerodynamic force and the corresponding complex coefficient $Q_{ij}(\bar{\nu})$ for oscillatory motion (see equations (5) and (6) of Ref 7).

The classical approach is to integrate first with respect to $\bar{\nu}$ to give in the time domain

$$Q_i(\tau) = Q''_{ij}(\infty) \frac{dq_j(\tau)}{d\tau} + Q'_{ij}(0) \int_0^\tau \frac{dq_j(\tau_0)}{d\tau_0} F_1(\tau - \tau_0) d\tau_0 \quad , \tag{2-21}$$

where we have alternative expressions

$$F_1(\sigma) = 1 + \frac{2}{\pi}\int_0^\infty \frac{Q''_{ij}(\bar{\nu}) - Q''_{ij}(\infty)}{Q'_{ij}(0)} \cos \bar{\nu}\sigma \, d\bar{\nu} \tag{2-22}$$

and

$$F_1(\sigma) = \frac{2}{\pi}\int_0^\infty \frac{Q'_{ij}(\bar{\nu})}{\bar{\nu}Q'_{ij}(0)} \sin \bar{\nu}\sigma \, d\bar{\nu} \tag{2-23}$$

from equations (2-19) and (2-20) respectively. These are readily identified with equations (2-13) and (2-14). The advantage of this formulation is that $F_1(\sigma)$, which has often been called a Wagner function, can be calculated without reference to the wing motion $q_j(\tau)$. Thus equation (2-21) can be used whether $q_j(\tau)$ is regarded as known or unknown.

2.4 Hereditary functions

We now introduce and appraise some hereditary functions, which embody the history of the wing motion in a general expression for the resulting instantaneous aerodynamic force. The function $F_1(\sigma)$ in equation (2-22) or (2-23) is one of them, and others arise when equation (2-21) is integrated by parts. Thus,

$$\begin{aligned} Q_i(\tau) &= Q''_{ij}(\infty)\frac{dq_j(\tau)}{d\tau} + Q'_{ij}(0)\left[q_j(\tau_0)F_1(\tau-\tau_0)\right]_0^\tau - Q'_{ij}(0)\int_0^\tau q_j(\tau_0)\frac{dF_1(\tau-\tau_0)}{d\tau_0}d\tau_0 \\ &= Q''_{ij}(\infty)\frac{dq_j(\tau)}{d\tau} + Q'_{ij}(0)F_1(0)q_j(\tau) + Q'_{ij}(0)\int_0^\tau q_j(\tau_0)F_0(\tau-\tau_0)d\tau_0 \end{aligned} \tag{2-24}$$

where

$$\begin{aligned} F_0(\sigma) &= \frac{dF_1(\sigma)}{d\sigma} \\ &= -\frac{2}{\pi}\int_0^\infty \frac{Q''_{ij}(\bar{\nu}) - Q''_{ij}(\infty)}{Q'_{ij}(0)}\bar{\nu}\sin\bar{\nu}\sigma\,d\bar{\nu} = \frac{2}{\pi}\int_0^\infty \frac{Q'_{ij}(\bar{\nu}) - Q'_{ij}(\infty)}{Q'_{ij}(0)}\cos\bar{\nu}\sigma\,d\bar{\nu} \end{aligned} \tag{2-25}$$

and

$$\begin{aligned} F_1(0) &= \lim_{\sigma\to 0}\left[\frac{2}{\pi}\int_0^\infty \frac{Q'_{ij}(\bar{\nu})}{\bar{\nu}Q'_{ij}(0)}\sin\bar{\nu}\sigma\,d\bar{\nu}\right] \\ &= \lim_{\sigma\to 0}\left[\frac{2}{\pi}\int_0^\infty \frac{Q'_{ij}(\bar{\nu}) - Q'_{ij}(\infty)}{\bar{\nu}Q'_{ij}(0)}\sin\bar{\nu}\sigma\,d\bar{\nu} + \frac{2Q'_{ij}(\infty)}{\pi Q'_{ij}(0)}\int_0^\infty \frac{\sin\bar{\nu}\sigma}{\bar{\nu}}d\bar{\nu}\right] = \frac{Q'_{ij}(\infty)}{Q'_{ij}(0)}\,. \end{aligned} \tag{2-26}$$

By equations (2-24) and (2-26)

$$Q_i(\tau) = Q''_{ij}(\infty)\frac{dq_j(\tau)}{d\tau} + Q'_{ij}(\infty)q_j(\tau) + Q'_{ij}(0)\int_0^\tau q_j(\tau_0)F_0(\tau-\tau_0)d\tau_0 \qquad (2\text{-}27)$$

where $F_0(\sigma)$ is given by either of the integrals in equations (2-25).

Another hereditary function is found when equation (2-21) is rewritten in the form

$$Q_i(\tau) = Q''_{ij}(\infty)\frac{dq_j(\tau)}{d\tau} - Q'_{ij}(0)\left[\frac{dq_j(\tau_0)}{d\tau_0}F_2(\tau-\tau_0)\right]_0^\tau + Q'_{ij}(0)\int_0^\tau \frac{d^2q_j(\tau_0)}{d\tau_0^2}F_2(\tau-\tau_0)d\tau_0 \qquad \ldots\ldots (2\text{-}28)$$

where
$$F_2(\sigma) = \int_0^\sigma F_1(\tau_0)d\tau_0 + \frac{Q''_{ij}(\infty)}{Q'_{ij}(0)} \quad . \qquad (2\text{-}29)$$

The constant in equation (2-29) is chosen to cancel the first term on the right hand side of equation (2-28). Remembering that $dq_j(\tau_0)/d\tau_0 = 0$ at $\tau_0 = 0$, we obtain

$$Q_i(\tau) = Q'_{ij}(0)\int_0^\tau \frac{d^2q_j(\tau_0)}{d\tau_0^2}F_2(\tau-\tau_0)d\tau_0 \qquad (2\text{-}30)$$

where, from equations (2-22) and (2-29)

$$F_2(\sigma) = \sigma + \frac{2}{\pi}\int_0^\infty \frac{Q''_{ij}(\bar{\nu}) - Q''_{ij}(\infty)}{Q'_{ij}(0)}\frac{\sin\bar{\nu}\sigma}{\bar{\nu}}d\bar{\nu} + \frac{Q''_{ij}(\infty)}{Q'_{ij}(0)}$$

$$= \sigma + \frac{2}{\pi}\int_0^\infty \frac{Q''_{ij}(\bar{\nu})}{Q'_{ij}(0)}\frac{\sin\bar{\nu}\sigma}{\bar{\nu}}d\bar{\nu} \quad . \qquad (2\text{-}31)$$

Thus we have three hereditary functions $F_n(\sigma)$ with $n = 0, 1, 2,$ such that

$$F_0(\sigma) = \frac{dF_1(\sigma)}{d\sigma} = \frac{d^2F_2(\sigma)}{d\sigma^2} \quad . \qquad (2\text{-}32)$$

The first of these from equations (2-25) is used in equation (2-27) as a factor of $q_j(\tau_0)$ in the integrand. As $q_j(\tau_0)$ is proportional to the displacement or position of the wing surface, we call $F_0(\sigma)$ the 'hereditary position factor'. Similarly, from equation (2-22) or (2-23), the 'hereditary velocity factor' $F_1(\sigma)$ multiplies $dq_j(\tau_0)/d\tau_0$ in equation (2-21), and the 'hereditary acceleration factor' $F_2(\sigma)$ in equation (2-31)

multiplies $d^2q_j(\tau_0)/d\tau_0^2$ in equation (2-30). Although the three formulations are analytically equivalent, each $F_n(\sigma)$ has its merits and defects in numerical, graphical and practical terms.

The outstanding merit of the position factor $F_0(\sigma)$ is that it applies even when $q_j(\tau)$ is discontinuous. Equation (2-27) shows clearly the characteristics described in the last paragraph of section 2.2, the impulsive force proportional to $Q''_{ij}(\infty)$ due to the step change and the subsequent value proportional to $Q'_{ij}(\infty)$ before the hereditary function begins to contribute. Because $F_0(\sigma)$ tends to zero for large σ, the integral in equation (2-27) is particularly suitable for residual effects. However, it has the defect that $F_0(\sigma)$ is very difficult to compute for small σ. Moreover, in the present application to active controls with smoothly varying $q_j(\tau)$ it may seem unnatural that the limiting values $Q'_{ij}(\infty)$ and $Q''_{ij}(\infty)$ for infinite frequency should play such major roles. However, the extraneous terms in equation (2-27) can be transferred into the integrand by adding a linear combination of the delta function and its first derivative to $F_0(\sigma)$ and so creating a unified hereditary function (see equation (2-9) of Ref 8).

The velocity function $F_1(\sigma)$ in equation (2-22) or (2-23) seems to contain a satisfactory balance between what is required at small and large times. Apart from some uncertainty in the calculation of its limiting value in equation (2-26), it can be fairly well represented graphically. But it still requires the addition of a delta function at $\sigma = 0$ to account for the first term on the right hand side of equation (2-21). It will be seen to have some of the characteristics of the original Wagner function, with the slight disadvantage that it remains finite as $\sigma \to \infty$.

One obvious merit of the acceleration factor $F_2(\sigma)$ is that it defines $Q_i(\tau)$ in equation (2-30) without extraneous terms. Moreover, of these hereditary functions it is the easiest to compute for small σ. Unfortunately, it diverges for large σ because of the first term on the right hand side of equation (2-31). This difficulty can be overcome by further manipulation.

If equation (2-31) is rewritten as

$$F_2(\sigma) = \sigma + \frac{Q''_{ij}(0)}{Q'_{ij}(0)} + \frac{2}{\pi}\int_0^\infty \frac{Q''_{ij}(\bar{\nu}) - Q''_{ij}(0)}{Q'_{ij}(0)} \frac{\sin \bar{\nu}\sigma}{\bar{\nu}}\, d\bar{\nu} , \qquad (2\text{-}33)$$

then equation (2-30) becomes

$$Q_i(\tau) = Q'_{ij}(0)\int_0^\tau \frac{d^2q_j(\tau_0)}{d\tau_0^2}(\tau-\tau_0)d\tau_0 + Q''_{ij}(0)\int_0^\tau \frac{d^2q_j(\tau_0)}{d\tau_0^2}d\tau_0 + Q'_{ij}(0)\int_0^\tau \frac{d^2q_j(\tau_0)}{d\tau_0^2}H(\tau-\tau_0)d\tau_0$$

$$= Q'_{ij}(0)q_j(\tau) + Q''_{ij}(0)\frac{dq_j(\tau)}{d\tau} + Q'_{ij}(0)\int_0^\tau \frac{d^2q_j(\tau_0)}{d\tau_0^2}H(\tau-\tau_0)d\tau_0 \qquad (2\text{-}34)$$

where* $$H(\sigma) = \frac{2}{\pi}\int_0^\infty \frac{Q''_{ij}(\bar{\nu}) - Q''_{ij}(0)}{Q'_{ij}(0)} \frac{\sin \bar{\nu}\sigma}{\bar{\nu}}\, d\bar{\nu} \quad . \qquad (2\text{-}35)$$

This result presupposes that $q(\tau)$ and $dq(\tau)/d\tau$ vanish at $\tau = 0$ and that $d^2q(\tau)/d\tau^2$ exists throughout $0 < \tau_0 < \tau$ apart from the admissibility of discrete discontinuities in the range. This last assumption is compatible with a pilot applying a stick force that is continuous apart from isolated sudden changes. The first two terms of equation (2-34) are equivalent to the force on a wing to first order in frequency parameter and are particularly appropriate while a control surface is being deployed quite slowly. The residual integral involves the hereditary function $H(\sigma)$ in equation (2-35), which we shall call the 'history function'. This is a slight misnomer in that, although $Q'_{ij}(0)q_j(\tau)$ represents the steady force due to the instantaneous displacement of the control, $Q''_{ij}(0)dq_j(\tau)/d\tau$ includes not only the quasi-steady force due to the instantaneous velocity of the control but the additional effect of an implied low-frequency oscillation. Nevertheless, the third term of equation (2-34) will be seen to make a negligible contribution when the control rate is fairly small and slowly varying. In other situations $H(\sigma)$ will be required to higher accuracy than the position factor $F_0(\sigma)$.

3 CALCULATION OF HEREDITARY FUNCTIONS

The mathematical principles underlying the whole of section 2 are well-established, but there is a tendency to take their numerical implementation for granted. Our objective is therefore to tackle the calculations as thoroughly as circumstances permit and to discover the difficulties that are likely to matter in practical applications of active control technology. It is necessary to discover when approximations may be expected to succeed and when they are likely to fail. At the other extreme it is desirable to establish the relevance of the refinements that can be made.

Practical numerical approximations to indicial aerodynamics have been developed for two-dimensional subsonic compressible flows[1,7], but not enough is known about high-frequency effects in linearized three-dimensional flows. It is not merely that the range of frequency in experimental work is too restricted, but the purely theoretical work is seldom taken above flutter frequencies with consequent lack of physical insight into what to expect. An object lesson was taught during the present investigation concerning the unexpected undulations shown in the Argand diagram of lift for the oscillating trailing-edge control in Fig 2a. The phenomenon is discussed and explained in Ref 9 in terms of even larger undulations in chordwise and spanwise loadings remote from the control and associated with the acoustic propagation and convection of disturbances created as the control oscillates. For the present calculations the undulatory behaviour reinforces the need for closely spaced values of $\bar{\nu}$ to define the quantities $Q'_{ij}(\bar{\nu})$ and $Q''_{ij}(\bar{\nu})$. It is considered that the 24 values of $\bar{\nu}$ in equation (2-11) will provide an adequate cubic spline representation.

* $H(\sigma)$ should not be confused with the Heaviside step function.

In regions of both very low and very high frequency a cubic spline fit contradicts the forms of the asymptotic expansions, and the special treatment of these regions is covered in sections 3.1 and 3.2 respectively. The procedures for calculating the hereditary functions and the numerical results are then discussed in sections 3.3 and 3.4 respectively. Ideas for empirical correction factors are put forward in section 3.5.

3.1 Logarithmic terms at low frequency

Woodcock[8] has made an independent study of the modelling of linearized three-dimensional subsonic time-dependent aerodynamics. While he is concerned more especially with approximations to $Q_{ij}(\bar{\nu})$ suitable for analysis by Fourier transform methods, he also considers the complex quantity as a double power series in $i\bar{\nu}$ and $\log(i\bar{\nu})$. His analysis confirms the leading terms of the series to be used in the present investigation

$$Q'_{ij}(\bar{\nu}) = B'_0 + B'_1\bar{\nu}^2 \log \bar{\nu} + B'_2\bar{\nu}^2 + B'_3\bar{\nu}^3 \tag{3-1}$$

and

$$Q''_{ij}(\bar{\nu}) = B''_0 + B''_1\bar{\nu} + B''_2\bar{\nu}^2 \log \bar{\nu} + B''_3\bar{\nu}^2 \quad , \tag{3-2}$$

where log denotes the natural logarithm. Of course B'_0 and B''_0 are identified with the known quantities $Q'_{ij}(0)$ and $Q''_{ij}(0)$. Milne and the present author[10] have shown that both B'_1 and B''_1 are obtainable from steady aerodynamic forces. Equations (10), (11) and (16) of Ref 10 give

$$B''_1 = \frac{\pi}{2} B'_1 = -\frac{1}{16} Q'_{1j}(0)Q'_{i2}(0) \quad ; \tag{3-3}$$

the aspect ratio factor has disappeared because the reference area in equation (2-6) is $\bar{c}^2$ in place of planform area as used in Ref 10, and the change of sign occurs because the upwash mode w_2/U in Table 1 is of opposite sign to equation (15) of Ref 10. The values of $-B'_1$ are included in Tables 2 to 4.

The extension of low-frequency theory in Ref 10 supplies the leading transient term of the asymptotic expansion for large time of aerodynamic forces due to a step motion in mode j. From equation (26) of Ref 10 the generalized force in mode i becomes

$$Q_i(\sigma) \simeq Q'_{ij}(0) + \frac{Q'_{1j}(0)Q'_{i2}(0)}{8\pi\sigma^2} + O(\sigma^{-3}) \tag{3-4}$$

in the present notation. With reference to Fig 2b, we obtain for lift with $i = 1$ in equation (3-4)

$$\frac{L(\sigma)}{L(\infty)} = \frac{Q_1(\sigma)}{Q'_{1j}(0)} \simeq 1 + \frac{Q'_{12}(0)}{8\pi\sigma^2} + O(\sigma^{-3}) \quad . \tag{3-5}$$

The leading transient term is independent of the upwash mode j, and equation (2-17) follows after the substitution $Q'_{12}(0) = -25.368$ from Table 2 of Ref 9. Furthermore, from equations (3-1) to (3-3) and with reference to Fig 2a, the second terms in both $Q'_{1j}(\bar{\nu})/Q'_{1j}(0)$ and $\bar{\nu}Q''_{1j}(\bar{\nu})/Q'_{1j}(0)$ are seen to be independent of j.

The importance of the second terms in equations (3-1) and (3-2) grows with increasing aspect ratio, so that rapid variations in $Q''_{13}(\bar{\nu})$, $Q''_{14}(\bar{\nu})$ and $Q''_{15}(\bar{\nu})$ are found in Tables 2 to 4 for the present wing of aspect ratio 8.0. Without B'_1 and B''_1 the leading transient term in equation (3-5) would disappear. It is desirable to incorporate equations (3-1) and (3-2) in the calculation of hereditary functions. This is achieved by choosing a fairly small value $\bar{\nu} = \bar{\nu}_\ell$, by applying a cubic spline fit in a finite region $\bar{\nu}_\ell \leq \bar{\nu} \leq \bar{\nu}_u$, say, and by determining B'_2, B'_3, B''_2 and B''_3 to give continuity in $Q'_{ij}(\bar{\nu})$ and $Q''_{ij}(\bar{\nu})$ and their first derivatives at $\bar{\nu} = \bar{\nu}_\ell$. Thus in $0 \leq \bar{\nu} \leq \bar{\nu}_\ell$ we take equations (3-1) and (3-2) with

$$B'_2 = \frac{3Q'_{ij}(\bar{\nu}_\ell) - 3B'_0}{\bar{\nu}_\ell^2} - \frac{1}{\bar{\nu}_\ell}\left[\frac{dQ'_{ij}(\bar{\nu})}{d\bar{\nu}}\right]_{\bar{\nu}=\bar{\nu}_\ell} - B'_1(\log \bar{\nu}_\ell - 1) \tag{3-6}$$

$$B'_3 = \frac{-2Q'_{ij}(\bar{\nu}_\ell) + 2B'_0}{\bar{\nu}_\ell^3} + \frac{1}{\bar{\nu}_\ell^2}\left[\frac{dQ'_{ij}(\bar{\nu})}{d\bar{\nu}}\right]_{\bar{\nu}=\bar{\nu}_\ell} - \frac{B'_1}{\bar{\nu}_\ell} \tag{3-7}$$

$$B''_2 = \frac{-2Q''_{ij}(\bar{\nu}_\ell) + 2B''_0}{\bar{\nu}_\ell^2} + \frac{1}{\bar{\nu}_\ell}\left[\frac{dQ''_{ij}(\bar{\nu})}{d\bar{\nu}}\right]_{\bar{\nu}=\bar{\nu}_\ell} + \frac{B''_1}{\bar{\nu}_\ell} \tag{3-8}$$

and

$$B''_3 = \frac{Q''_{ij}(\bar{\nu}_\ell) - B''_0}{\bar{\nu}_\ell^2}(2\log \bar{\nu}_\ell + 1) - \frac{\log \bar{\nu}_\ell}{\bar{\nu}_\ell}\left[\frac{dQ''_{ij}(\bar{\nu})}{d\bar{\nu}}\right]_{\bar{\nu}=\bar{\nu}_\ell} - \frac{B''_1}{\bar{\nu}_\ell}(\log \bar{\nu}_\ell + 1) . \tag{3-9}$$

It is probably more important to curtail the low-frequency end of the cubic spline for $Q'_{ij}(\bar{\nu})$ than for $Q''_{ij}(\bar{\nu})$ as the logarithm only enters in the third term of equation (3-2). Although there is no reason to suppose that B''_2 is any smaller than B'_1, B'_2 is likely to have less influence on $F_0(\sigma)$ in equations (2-25) because of the factor $\bar{\nu}$ in the first integrand.

3.2 Piston theory at high frequency

There is some upper limit $\bar{\nu}_u$, say, where reliable calculations by subsonic lifting-surface theories become impracticable. For the present results at high $\bar{\nu}$ it was found to be necessary to increase the number of chordwise terms from N = 6 to 8 and sufficient to economize in computation time by decreasing the number of spanwise terms from m = 31 to 23. The choice $\bar{\nu}_u = 6$ is purely a matter of judgement.

For $\bar{\nu} > \bar{\nu}_u$ recourse is made to piston theory. Ashley and Zartarian[11] discuss piston theory primarily for its use in supersonic flow. As Mach number decreases, the theory becomes restricted to increasingly high values of the frequency parameter, but it has some application as $\bar{\nu}$ tends to infinity even in subsonic compressible flow. First-order piston theory relates the upwash angle and wing loading in equations (2-2) and (2-4) by the equation

$$\ell_j = -\frac{2}{M}\frac{w_j}{U} = -\frac{2}{M}\left(\frac{\partial z_j}{\partial x} + \frac{i\omega z_j}{U}\right) , \tag{3-10}$$

so that by equations (2-6) and (2-12)

$$Q'_{ij}(\infty) = -\frac{2}{M}\iint \frac{z_i}{\bar{c}} \frac{\partial z_j}{\partial x_0} \frac{dx_0 dy_0}{\bar{c}^2} \tag{3-11}$$

and

$$Q''_{ij}(\infty) = -\frac{2}{M}\iint \frac{z_i}{\bar{c}} \frac{z_j}{\bar{c}} \frac{dx_0 dy_0}{\bar{c}^2} \tag{3-12}$$

where the integrals are taken over the planform. But the argument is fallacious. It is likely that both the real and imaginary parts of ℓ_j have asymptotic expansions in inverse powers of $i\bar{\nu}$, so that we may write

$$\begin{aligned} \ell_j &= \left(a_0 + \frac{a_1}{i\bar{\nu}} + \frac{a_2}{(i\bar{\nu})^2} + \ldots\right) + i\bar{\nu}\left(b_0 + \frac{b_1}{i\bar{\nu}} + \frac{b_2}{(i\bar{\nu})^2} + \frac{b_3}{(i\bar{\nu})^3} + \ldots\right) \\ &= \left[(a_0 + b_1) - \frac{a_2 + b_3}{\bar{\nu}^2} + \ldots\right] + i\bar{\nu}\left[b_0 - \frac{a_1 + b_2}{\bar{\nu}^2} + \ldots\right] . \end{aligned} \tag{3-13}$$

Thus equation (3-11) only provides the a_0 part of $-Q'_{ij}(\infty)$ and excludes the unknown higher-order contribution denoted by b_1. On the other hand the single contribution from b_0 suffices for $-Q''_{ij}(\infty)$, and equation (3-12) is correct.

On substituting the values of $z_1/\bar{c}$ and $z_2/\bar{c}$ from Table 1 and the planform data from equations (2-8) and (2-9), we calculate $Q''_{ij}(\infty)$ analytically for $M = 0.8$. The smoothing terms with $g(\lambda)$ have the negligible effect of decreasing $-Q''_{11}(\infty)$ from 19.980 to 19.967 and have been ignored in obtaining

$$\left.\begin{aligned} -Q''_{11}(\infty) &= 19.980 \quad (19.450) \\ -Q''_{12}(\infty) &= 12.940 \quad (11.932) \\ -Q''_{21}(\infty) &= 12.940 \quad (13.040) \\ -Q''_{22}(\infty) &= 12.478 \quad (11.651) \end{aligned}\right\} \tag{3-14}$$

from equation (3-12). The values in brackets are those calculated for the highest frequency parameter $\bar{\nu} = 6$ by the lifting-surface theory of Ref 5 as detailed in section 2.1. The edge conditions of finite non-zero loading implied by equation (3-10) are incompatible with lifting-surface theory and inappropriate for finite frequency, and several considerations follow from this. It becomes clearer why larger numbers of chordwise and spanwise terms are needed as $\bar{\nu}$ increases, and why approximation in the upper frequency range is unavoidable. The choice of $N = 8$ and $m = 23$ must inhibit the accuracy of the results for $\bar{\nu} = 6$ to some extent, but there is no reason to expect rapid convergence to the piston theory limit. Nevertheless, the numerical comparisons beside equations (3-14) are close enough to encourage the use of a matching process at $\bar{\nu} = \bar{\nu}_u = 6$.

All these difficulties are intensified in both the chordwise and spanwise directions with the part-span leading-edge and trailing-edge control surfaces. Violations of edge conditions and continuity of loading become especially important, and the absence of a logarithmic behaviour in the loading at the hinge from piston theory brings further incompatibility. For the control-surface modes j = 3, 4 and 5 we have

$$\left.\begin{aligned} -Q''_{1j}(\infty) &= -Q''_{j1}(\infty) = \frac{2}{Mc^3}\iint (x_0 - x_{hj})\,dx_0 dy_0 \\ -Q''_{2j}(\infty) &= -Q''_{j2}(\infty) = \frac{2}{Mc^4}\iint (x_0 - x_a)(x_0 - x_{hj})\,dx_0 dy_0 \\ -Q''_{jj}(\infty) &= \frac{2}{Mc^4}\iint (x_0 - x_{hj})^2\,dx_0 dy_0 \end{aligned}\right\} \qquad (3\text{-}15)$$

where the integrals are taken over the combined planform area of the port and starboard control surfaces. For M = 0.8 and the geometry defined in Fig 1 we calculate analytically the values of $Q''_{ij}(\infty)$ included in Tables 2 to 4. The following comparisons of lift

$\bar{\nu}$	$-Q''_{13}(\bar{\nu})$	$-Q''_{14}(\bar{\nu})$	$-Q''_{15}(\bar{\nu})$
6	0.0177	0.0309	0.2442
∞	0.0514	-0.0514	0.2331

show large differences for the trailing-edge control (j = 3) and more especially the leading-edge control (j = 4). The case of the all-moving tip (j = 5) without any discontinuity at the hinge gives a percentage change from $\bar{\nu} = 6$ to ∞ comparable with those found for the wing modes in equations (3-14).

On the basis of equation (3-13) with real coefficients a_n and b_n, we postulate the asymptotic expansions with leading terms

$$Q'_{ij}(\bar{\nu}) = A'_0 + \frac{A'_1}{\bar{\nu}^2} + \frac{A'_2}{\bar{\nu}^4} \qquad (3\text{-}16)$$

and

$$Q''_{ij}(\bar{\nu}) = A''_0 + \frac{A''_1}{\bar{\nu}^2} + \frac{A''_2}{\bar{\nu}^4} \quad , \qquad (3\text{-}17)$$

where A'_0 is unknown and A''_0 equals $Q''_{ij}(\infty)$ from equation (3-12). Although A'_0 cannot be calculated directly, we can invoke the identity in equation (A-10) of Appendix A as $\sigma \to 0$. Since the second term becomes

$$-\frac{1}{\pi}\int_0^\infty \frac{Q'_{ij}(\bar{\nu}) - Q'_{ij}(\infty)}{\bar{\nu}} \sin \bar{\nu}\sigma \, d\bar{\nu} - \frac{Q'_{ij}(\infty)}{\pi}\int_0^\infty \frac{\sin \bar{\nu}\sigma}{\bar{\nu}}\, d\bar{\nu} \to -\tfrac{1}{2}Q'_{ij}(\infty) \quad ,$$

the identity yields

$$A_0' = Q_{ij}'(\infty) = Q_{ij}'(0) + \frac{2}{\pi}\int_0^{\infty}\left[Q_{ij}''(\bar{\nu}) - Q_{ij}''(\infty)\right]d\bar{\nu} \quad . \tag{3-18}$$

Unless this formula is used, equation (3-16) is ineffective. The values of $Q_{ij}'(\infty)$ in Tables 2 to 4 are only approximate and are the best that we can obtain from equation (3-18), but the results confirm the fallacy of equation (3-11). Then both equations (3-16) and (3-17) serve to match a cubic spline fit at the upper end of the region $\bar{\nu}_\ell \leq \bar{\nu} \leq \bar{\nu}_u$. Continuity in $Q_{ij}'(\bar{\nu})$ and $Q_{ij}''(\bar{\nu})$ and their first derivatives at $\bar{\nu} = \bar{\nu}_u$ is satisfied with

$$A_1' = 2\bar{\nu}_u^2\left\{Q_{ij}'(\bar{\nu}_u) - A_0'\right\} + \frac{\bar{\nu}_u^3}{2}\left[\frac{dQ_{ij}'(\bar{\nu})}{d\bar{\nu}}\right]_{\bar{\nu}=\bar{\nu}_u} \tag{3-19}$$

$$A_2' = -\bar{\nu}_u^4\left\{Q_{ij}'(\bar{\nu}_u) - A_0'\right\} - \frac{\bar{\nu}_u^5}{2}\left[\frac{dQ_{ij}'(\bar{\nu})}{d\bar{\nu}}\right]_{\bar{\nu}=\bar{\nu}_u} \tag{3-20}$$

$$A_1'' = 2\bar{\nu}_u^2\left\{Q_{ij}''(\bar{\nu}_u) - A_0''\right\} + \frac{\bar{\nu}_u^3}{2}\left[\frac{dQ_{ij}''(\bar{\nu})}{d\bar{\nu}}\right]_{\bar{\nu}=\bar{\nu}_u} \tag{3-21}$$

and

$$A_2'' = -\bar{\nu}_u^4\left\{Q_{ij}''(\bar{\nu}_u) - A_0''\right\} - \frac{\bar{\nu}_u^5}{2}\left[\frac{dQ_{ij}''(\bar{\nu})}{d\bar{\nu}}\right]_{\bar{\nu}=\bar{\nu}_u} \quad . \tag{3-22}$$

Because of the uncertainty in A_0' , implied by equation (3-18), it seems preferable to calculate the hereditary functions from expressions involving $Q_{ij}''(\bar{\nu})$ rather than $Q_{ij}'(\bar{\nu})$. This favours the first integral of equations (2-25) and equations (2-22) and (2-31) for $F_n(\sigma)$ with n = 0, 1 and 2 respectively. In particular for $F_0(\sigma)$ it should be noted that despite the factor $\bar{\nu}$ the first integrand of equations (2-25) tends to zero as $\bar{\nu}$ tends to infinity.

3.3 Numerical procedures

Our next consideration is the evaluation of the hereditary functions from equations (2-22), (2-25), (2-31) and (2-35) in the forms

$$\left.\begin{aligned} F_0(\sigma) &= -\frac{2}{\pi}\int_0^{\infty}\frac{Q_{ij}''(\bar{\nu}) - Q_{ij}''(\infty)}{Q_{ij}'(0)}\,\bar{\nu}\sin\bar{\nu}\sigma\,d\bar{\nu} \\ F_1(\sigma) &= 1 + \frac{2}{\pi}\int_0^{\infty}\frac{Q_{ij}''(\bar{\nu}) - Q_{ij}''(\infty)}{Q_{ij}'(0)}\cos\bar{\nu}\sigma\,d\bar{\nu} \end{aligned}\right\} \tag{3-23}$$

$$F_2(\sigma) = \sigma + \frac{Q''_{ij}(\infty)}{Q'_{ij}(0)} + \frac{2}{\pi}\int_0^\infty \frac{Q''_{ij}(\bar{\nu}) - Q''_{ij}(\infty)}{Q'_{ij}(0)} \frac{\sin \bar{\nu}\sigma}{\bar{\nu}}\, d\bar{\nu}$$

$$H(\sigma) = F_2(\sigma) - \sigma - \frac{Q''_{ij}(0)}{Q'_{ij}(0)} \qquad (3\text{-}23)$$

with the range of integration subdivided into $0 < \bar{\nu} < \bar{\nu}_\ell$, $\bar{\nu}_\ell < \bar{\nu} < \bar{\nu}_u$ and $\bar{\nu}_u < \bar{\nu} < \infty$. Different integration procedures are used in the three regions, Simpson's Rule in $0 < \bar{\nu} < \bar{\nu}_\ell$, Filon's Rule in $\bar{\nu}_\ell < \bar{\nu} < \bar{\nu}_u$ and analytical treatment in $\bar{\nu}_u < \bar{\nu} < \infty$. The necessary equations are set out in Appendix B.

The greatest computational effort lies in the evaluation of a sufficient number of values $Q''_{ij}(\bar{\nu})$ by the lifting-surface method of Refs 5 and 6. As found in Ref 9 and given in Table 2 for the oscillatory trailing-edge control (j = 3) at M = 0.8, it is necessary to take intervals in $\bar{\nu}$ as small as 0.3 to define the undulating curves against frequency parameter to reasonable accuracy, especially in the range $1 < \bar{\nu} < 3$. The quantity $\bar{\nu}_\ell$ must not be less than the lowest non-zero value of $\bar{\nu}$ for which $Q''_{ij}(\bar{\nu})$ is calculated, and likewise $\bar{\nu}_u$ must not exceed the highest value. The region $\bar{\nu}_\ell \leq \bar{\nu} \leq \bar{\nu}_u$ is treated by means of a standard program for the cubic spline through all the data points, excluding $\bar{\nu} = 0$, and this provides interpolated values of $Q''_{ij}(\bar{\nu})$ at each integration point and at $\bar{\nu} = \bar{\nu}_\ell$ and $\bar{\nu} = \bar{\nu}_u$ the values of its first derivative as well.

To carry out the integration procedure for $0 < \bar{\nu} < \bar{\nu}_\ell$, it is necessary to use the low-frequency solutions for $B''_0 = Q''_{ij}(0)$, the non-dimensional lift $Q'_{1j}(0)$ and the coefficient $Q'_{i2}(0)$ for pitching motion so as to evaluate B''_1 from equation (3-3). Then, using $Q''_{ij}(\bar{\nu})$ and its first derivative at $\bar{\nu} = \bar{\nu}_\ell$, we calculate B''_2 and B''_3 from equations (3-8) and (3-9) to complete the definition of $Q''_{ij}(\bar{\nu})$ in equation (3-2). Typically we take $\bar{\nu}_\ell = 0.08$ and subdivide the range into 16 equal parts, and the integration in equation (B-4) is a matter of routine.

For the region $\bar{\nu}_\ell < \bar{\nu} < \bar{\nu}_u$, typically 148 equal intervals between 0.08 and 6.00, the cubic spline and equations (B-5) to (B-8) are used to evaluate the integrals. The velocity and acceleration factors $F_1(\sigma)$ and $F_2(\sigma)$ are served by equations (B-6) and (B-7) respectively, but the contribution to the position factor $F_0(\sigma)$ requires an equation like (B-7) with the frequency parameters $\bar{\nu}_u$, $\bar{\nu}_\ell$, $(\bar{\nu}_\ell + 2kh)$ and $(\bar{\nu}_\ell + (2k-1)h)$ transferred from the denominator to the numerator. This procedure with Filon's Rule involves no restriction on the magnitude of σ.

The final contributions from $\bar{\nu}_u < \bar{\nu} < \infty$ involve $Q''_{ij}(\bar{\nu})$ and its first derivative at $\bar{\nu} = \bar{\nu}_u$ and piston theory for $A''_0 = Q''_{ij}(\infty)$ from equation (3-12). The quantities A''_1 and A''_2 are then calculated from equations (3-21) and (3-22) to complete the definition of $Q''_{ij}(\bar{\nu})$ in equation (3-17). Then for $F_0(\sigma)$ to $F_2(\sigma)$ the respective equations (B-11) to (B-13) can be evaluated with the aid of the integral $S_3(\bar{\nu}_u\sigma)$ defined in equation (B-10). Appendix B also includes highly accurate expressions for S_3 in equation (B-14) or (B-15) according to whether $\bar{\nu}_u\sigma$ is less than or greater than 7.

The matching of $Q''_{ij}(\bar{\nu})$ at $\bar{\nu} = \bar{\nu}_\ell$ and $\bar{\nu} = \bar{\nu}_u$ is illustrated in Fig 3. A program in ICL 1900 Extended Fortran is available with $Q''_{ij}(\bar{\nu})$ and related quantities as input and the four hereditary function in equations (3-23) as output.

3.4 Discussion of results

The calculations are confined to one planform (Fig 1), one Mach number $M = 0.8$, and the lift, pitching moment and hinge moments associated with pitching motion ($j = 2$) and the deployment of the three types of control surface ($j = 3, 4, 5$). These results are largely illustrative, but they will enable us to discuss the characteristic behaviour of the various hereditary functions and some general numerical aspects of their evaluation.

Figs 4a & 4b show the position factor $F_0(\sigma)$, velocity factor $F_1(\sigma)$ and acceleration factor $F_2(\sigma)$ for the trailing-edge and leading-edge controls respectively. Larger magnitudes of $F_0(\sigma)$ and $F_1(\sigma)$ occur for the leading-edge control in Fig 4b because $Q'_{14}(0)$ is so much smaller than $Q'_{13}(0)$. These hereditary functions are considered in relation to their asymptotic expansions for small and large σ. By equations (2-25) and (3-17)

$$F_0(\sigma) = -\frac{2}{\pi}\int_0^\infty \frac{Q''_{ij}(\bar{\nu}) - A''_0 - \left(A''_1/\bar{\nu}^2\right)}{Q'_{ij}(0)}\,\bar{\nu}\sin\bar{\nu}\sigma\,d\bar{\nu} - \frac{2}{\pi}\int_0^\infty \frac{A''_1 \sin\bar{\nu}\sigma}{Q'_{ij}(0)\bar{\nu}}\,d\bar{\nu}$$

where the first integral vanishes as $\sigma \to 0$ and in the limit

$$F_0(0) = -\frac{A''_1}{Q'_{ij}(0)} \quad . \tag{3-24}$$

Equation (2-26) already gives

$$F_1(0) = \frac{Q'_{ij}(\infty)}{Q'_{ij}(0)} \quad , \tag{3-25}$$

and it follows from equation (2-31) that

$$F_2(0) = \frac{Q''_{ij}(\infty)}{Q'_{ij}(0)} \quad . \tag{3-26}$$

Equations (2-32) and (3-24) to (3-26) combine to give the asymptotic expansion for small σ

$$Q'_{ij}(0)F_2(\sigma) \simeq Q''_{ij}(\infty) + Q'_{ij}(\infty)\sigma - \tfrac{1}{2}A''_1\sigma^2 \quad . \tag{3-27}$$

Thus the curves of acceleration factor can be drawn with confidence near $\sigma = 0$. The limiting values $F_1(0)$ are subject to a degree of inaccuracy in the evaluation of $Q'_{ij}(\infty)$ from equation (3-18), but the velocity factor is fairly well represented near $\sigma = 0$ in Figs 4a & 4b. Although a value of A''_1 is implied in the matching process in the lower diagram of Fig 3, for example, it would be rash to quantify it. Therefore the curves of $F_0(\sigma)$ are speculative near $\sigma = 0$, and so to a lesser extent are the undulations in the region $\sigma < 3$. Beyond this the influence of the region $\bar{\nu}_u < \bar{\nu} < \infty$ weakens and we can turn to the behaviour of the hereditary functions for large σ.

In conjunction with the series in equation (3-2) for small frequency, equation (2-31) may be rewritten as

$$F_2(\sigma) = \sigma + \frac{2}{\pi}\int_0^\infty \frac{B_0'' + B_1''\bar{\nu}}{Q_{ij}'(0)}\frac{\sin\bar{\nu}\sigma}{\bar{\nu}}\,d\bar{\nu} + \frac{2}{\pi}\int_0^\infty \frac{Q_{ij}''(\bar{\nu}) - B_0'' - B_1''\bar{\nu}}{Q_{ij}'(0)}\frac{\sin\bar{\nu}\sigma}{\bar{\nu}}\,d\bar{\nu}$$

$$= \sigma + \frac{B_0''}{Q_{ij}'(0)} + \frac{2B_1''}{\pi Q_{ij}'(0)\sigma} + O(\sigma^{-2}) \quad . \tag{3-28}$$

With $B_0'' = Q_{ij}''(0)$ and B_1'' from equation (3-3), we have the asymptotic expansion for large σ

$$F_2(\sigma) \simeq \sigma + \frac{Q_{ij}''(0)}{Q_{ij}'(0)} - \frac{Q_{1j}'(0)Q_{i2}'(0)}{8\pi Q_{ij}'(0)\sigma} + O(\sigma^{-2}) \quad , \tag{3-29}$$

and by equations (2-32)

$$F_1(\sigma) \simeq 1 + \frac{Q_{1j}'(0)Q_{i2}'(0)}{8\pi Q_{ij}'(0)\sigma^2} + O(\sigma^{-3}) \tag{3-30}$$

and

$$F_0(\sigma) \simeq -\frac{Q_{1j}'(0)Q_{i2}'(0)}{4\pi Q_{ij}'(0)\sigma^3} + O(\sigma^{-4}) \quad . \tag{3-31}$$

Thus $F_0(\sigma)$ tends to zero the most rapidly. Equation (3-30) is consistent with the rigorous analysis of Ref 10 leading to equation (3-4). Figs 4a & 4b show how the characteristics of the leading-edge and trailing-edge controls, that are so different for small σ, become remarkably similar for large σ. This is particularly the case for lift when $Q_{ij}'(0) = Q_{ij}'(0)$ and equations (3-30) and (3-31) become independent of the mode j, as we anticipated in equation (2-17).

The remarks in the paragraphs following equation (2-32) are brought into perspective by Figs 4a & 4b. While for the trailing-edge control $F_1(\sigma)$ in Fig 4a is reminiscent of the original Wagner function, the corresponding function in Fig 4b for the leading-edge control is less so. The lift characteristics of $F_1(\sigma)$ for the various types of motion are compared in Fig 5. It will be seen that for the pitching motion $F_1(\sigma)$ rises rapidly from 0.44 to 0.84 in the first half mean chord of travel and thereafter increases relatively slowly. Like the leading-edge control, the all-moving-tip control gives a minimum in $F_1(\sigma)$ in the range $\sigma < 1$. All four velocity factors for lift have the common asymptote for large σ.

The remaining hereditary function from equations (3-23) is the history function derived at the end of section 2.4. It is readily evaluated from $F_2(\sigma)$, and it follows that from equation (3-27) for small σ

$$Q_{ij}'(0)H(\sigma) \simeq [Q_{ij}''(\infty) - Q_{ij}''(0)] + [Q_{ij}'(\infty) - Q_{ij}'(0)]\sigma - \tfrac{1}{4}A_1''\sigma^2 \quad , \tag{3-32}$$

and that from equation (3-29) for large σ

$$H(\sigma) \simeq -\frac{Q'_{ij}(0)Q'_{i2}(0)}{8\pi Q'_{ij}(0)\sigma} + O(\sigma^{-2}) \quad . \tag{3-33}$$

Typical curves of $H(\sigma)$ are shown in Figs 6 and 7. The history functions for lift and their common asymptote in Fig 6 have similar falling trends in the range $\sigma > 0.5$. The leading-edge control produces the most distinctive behaviour, and it may be noted that in the important range $\sigma < 7$ the curve for the all-moving tip lies between those for the leading-edge and trailing-edge controls. Fig 7 gives $H(\sigma)$ for the lift, pitching moment and hinge moment due to the trailing-edge control. It is worth pointing out from Ref 10 that the wing loading associated with the leading term in equation (3-33) corresponds to $Q'_{i2}(0)$ and is that for an incremental change in angle of attack. This loading, which is large near the leading-edge and small near the trailing-edge, plays an interesting role in the behaviour of the history functions for moderately large σ, so that the residual quantities at $\sigma = 6$ in Fig 7 show relatively large lift, intermediate pitching moment and very small hinge moment.

Next we consider in Tables 5 and 6 the sensitivity of the position factor $F_0(\sigma)$ and the history function $H(\sigma)$ to the manner of calculation. The fullest calculations of lift due to the trailing-edge control appear in columns (d). As described in Ref 9, it became necessary to amplify the set of 14 frequency parameters

$$\bar{\nu} = 0,\ 0.05,\ 0.15,\ 0.4,\ 0.75,\ 1.2\ (0.6)\ 6.0 \tag{3-34}$$

used in the preliminary calculations by including 10 extra values to give the set of 24 values in equation (2-11). Results obtained in columns (c) from the 14 values of $Q''_{13}(\bar{\nu})$ corresponding to equation (3-34) and the quantity $Q''_{13}(\infty)$ from piston theory are reasonably close to those in columns (d) for the most part. Large discrepancies in $F_0(\sigma)$ arise in Table 5 for small σ, but in Table 6 $H(\sigma)$ shows nothing worse than differences of 0.004 in opposite senses at $\sigma = 2.6$ and 5.0 ; these amount to about 1%, where discrepancies of similar magnitude in $F_0(\sigma)$ represent more than 15%. Further degradation of the calculations is found when the values of $Q''_{13}(\bar{\nu})$ from lifting-surface theory are ignored where $\bar{\nu}$ exceeds 1.2. Columns (a) are obtained when the integrals in equations (3-23) are truncated at $\bar{\nu} = 1.2$, and the comparisons with columns (d) are poor, but within 0.01 for $\sigma > 6.0$; even for $H(\sigma)$ in Table 6 there are discrepancies of 0.035 at $\sigma = 0.6$ and 0.8, while for $F_0(\sigma)$ column (a) of Table 5 is quite hopeless. Substantial improvement on columns (a) is found in columns (b) when the value $Q''_{13}(\infty)$ from piston theory is used and the calculation is made with $\bar{\nu}_u = 1.2$, but the need for lifting-surface values with $\bar{\nu} > 1.2$ is still apparent. The final columns (e) are obtained when the low-frequency logarithmic behaviour in equation (3-2) is suppressed by falsely setting the quantities B'_1 and B''_1 of equation (3-3) to zero. The position factor is virtually unaffected in that the worst discrepancy between columns (d) and (e) of Table 5 is 0.0002. However, in Table 6 the inaccuracy in $H(\sigma)$ reaches the third decimal place for $\sigma \geq 10.0$; but, when it is borne in mind that the setting of $\bar{\nu}_\ell$ to zero would not

suppress the second term on the right hand side of equation (3-2), the conclusion is reached that the refinement in that equation is of little practical significance.

A similar conclusion may not apply to equation (3-1), if calculations of $F_1(\sigma)$ are made from equation (2-23). This alternative to equation (2-22) is less satisfactory on numerical grounds as being more sensitive both to the logarithmic behaviour at small $\bar{\nu}$ and to the uncertainty at high $\bar{\nu}$ implicit in equation (3-18). Nevertheless, a few comparisons from the alternative formulation in terms of $Q'_{ij}(\bar{\nu})$ have been obtained as accurately as possible. In particular calculations of lift due to the trailing-edge control, the worst discrepancies from equation (2-23) for $F_1(\sigma)$ are roughly 0.02 near $\sigma = 0.1$ and 0.01 near $\sigma = 1.0$, which are of little consequence in Fig 4a; very similar discrepancies are found in pitching moment and hinge moment.

Of the four hereditary functions, $F_0(\sigma)$ and $H(\sigma)$ in equations (3-31) and (3-33) tend asymptotically to zero for large σ. The slower convergence of the history function, proportional to σ^{-1} instead of σ^{-3} for $F_0(\sigma)$, reflects the more enduring transient effects of an acceleration. Thus the history term, given by the integral in equation (2-34), makes a substantial contribution from the more distant past when the variable τ_0 is fairly small. It is a mistake to suppose that equation (2-34) can be integrated by parts to give a series involving the higher derivatives of $q_j(\tau)$ and a residual integral of decreasing significance. The behaviour of $H(\sigma)$ proportional to σ^{-1} does not permit further integration without introducing a divergent hereditary function with a term in $\log \sigma$. This matter is discussed further in section 4.2.

3.5 Empirical correction factors

The preceding calculations of hereditary functions are linearized not only in the sense that the basic equations of Appendix A involve the principle of superposition, but since the oscillatory aerodynamics take no account of wing thickness or viscosity. If we suppose that the key equations (A-12) and (A-13) can be applied to compressible viscous flow past a thick wing, empirical correction becomes feasible. The history function $H(\sigma)$ is the most suitable hereditary function for this purpose, because of its smooth behaviour and the extent to which this is governed by the asymptotic forms for small and large σ in equations (3-32) and (3-33). Thus

$$\left.\begin{aligned} H(0) &= \frac{Q''_{ij}(\infty) - Q''_{ij}(0)}{Q'_{ij}(0)} \\ \left[\frac{dH(\sigma)}{d\sigma}\right]_{\sigma=0} &= \frac{Q'_{ij}(\infty) - Q'_{ij}(0)}{Q'_{ij}(0)} \\ \left[H(\sigma)\right]_{\sigma \text{ large}} &= -\frac{Q'_{ij}(0)Q'_{i2}(0)}{8\pi Q'_{ij}(0)\sigma} \end{aligned}\right\} . \qquad (3\text{-}35)$$

The last of these relationships implies a bold assumption that equation (3-3) for the first logarithmic term at small frequency remains valid in viscous flow.

It is reasonable to suppose that experimental or estimated values of the steady-flow quantities $Q'_{ij}(0)$, $Q'_{1j}(0)$ and $Q'_{i2}(0)$ are obtainable. The low-frequency in-quadrature component $Q''_{ij}(0)$ may be more difficult to estimate; one empirical approach is that used in section 7 of Ref 12 for control hinge moments, but which can be applied generally. In the perpetual absence of experimental data on $Q'_{ij}(\infty)$ and $Q''_{ij}(\infty)$, it is probably best to regard these as being independent of wing thickness and viscosity. Let us suppose then that equations (3-35) are used to obtain both theoretical and empirical values of $H(0)$, $[dH(\sigma)/d\sigma]$ at $\sigma = 0$, and $\sigma H(\sigma)$ for σ large. Then we seek an empirical correction factor $\kappa(\sigma)$ to apply to $H(\sigma)$.

Clearly the ratios of the empirical and theoretical quantities in the first and third of equations (3-35) determine $\kappa(0)$ and $\kappa(\infty)$, although they must both be regarded as somewhat tentative. Where $H(\sigma)$ is a monotonic function falling smoothly from $H(0)$ to zero, a simple practical scheme is to take

$$\kappa(\sigma) = \kappa(\infty) + [\kappa(0) - \kappa(\infty)] \frac{H(\sigma)}{H(0)} . \tag{3-36}$$

In some instances, such as the leading-edge control in Fig 6 and the hinge moment in Fig 7, $H(\sigma)$ rises to a maximum $H(\sigma_m)$ at $\sigma = \sigma_m$, say. Thus, perhaps, equation (3-36) can be replaced by

$$\left.\begin{aligned} \kappa(\sigma) &= \kappa(0) , && 0 < \sigma \leqslant \sigma_m \\ \kappa(\sigma) &= \kappa(\infty) + [\kappa(0) - \kappa(\infty)] \frac{H(\sigma)}{H(\sigma_m)} , && \sigma \geqslant \sigma_m \end{aligned}\right\} . \tag{3-37}$$

The second of equations (3-35) is available to check or refine equation (3-36) or (3-37), if desired. The application of the empirical history function $\kappa(\sigma)H(\sigma)$ would be to calculations associated with equation (2-34), where the experimental or estimated quantities $Q'_{ij}(0)$ and $Q''_{ij}(0)$ are needed in their own right.

There is a simpler alternative, which involves an empirical value of $[Q'_{ij}(0)]_e$ only. With reference to equations (2-25) for the position factor $F_0(\sigma)$, we consider the assumption that a constant correction factor

$$\bar{\kappa} = \frac{[Q'_{ij}(0)]_e - Q'_{ij}(\infty)}{Q'_{ij}(0) - Q'_{ij}(\infty)} \tag{3-38}$$

may be applied to both $Q''_{ij}(\bar{\nu}) - Q''_{ij}(\infty)$ and $Q'_{ij}(\bar{\nu}) - Q'_{ij}(\infty)$. Then the factor

$$\kappa = \frac{Q'_{ij}(0)\bar{\kappa}}{[Q'_{ij}(0)]_e} = 1 + \frac{Q'_{ij}(\infty)\{[Q'_{ij}(0)]_e - Q'_{ij}(0)\}}{[Q'_{ij}(0)]_e\{Q'_{ij}(0) - Q'_{ij}(\infty)\}} \tag{3-39}$$

may be applied to all values of $F_0(\sigma)$. With the empirical correction in this form, equation (2-27) has the advantage that its first two terms are unchanged. The same constant factor κ would apply similarly to the history function $H(\sigma)$ in equation (2-35). To use equation (2-34), it would be necessary to take a consistent empirical value

$$[Q''_{ij}(0)]_e = Q''_{ij}(\infty) + \bar{\kappa}\{Q''_{ij}(0) - Q''_{ij}(\infty)\}$$

$$= Q''_{ij}(0) + \frac{\{Q''_{ij}(0) - Q''_{ij}(\infty)\}\{[Q'_{ij}(0)]_e - Q'_{ij}(0)\}}{Q'_{ij}(0) - Q'_{ij}(\infty)} \quad . \qquad (3\text{-}40)$$

The merit of this simpler alternative would depend a good deal on how well equation (3-40) fits the low-frequency experimental data.

With either of these empirical rules it would become possible to modify the calculations in the following sections. This would permit some allowance for effects that are ignored in lifting-surface theory.

4 TRANSIENT DEPLOYMENT OF CONTROLS

A computer program has been written to use separately the position factor $F_0(\sigma)$, the velocity factor $F_1(\sigma)$ and the history function $H(\sigma)$ as obtained numerically by the procedure described in section 3.3, in order to calculate the force coefficient $Q_i(\tau)$ from the respective equations (2-27), (2-21) and (2-34). The deployment of a control surface $q_j(\tau)$ is given algebraically in $0 \leq \tau \leq \tau_1$ and is identically zero outside this range, but $q_j(\tau)$ and its first two derivatives are chosen to be continuous for all τ. The present calculations for control surfaces correspond to the transient deflection angle

$$\left.\begin{aligned} \frac{\delta}{\delta_0} = q_j(\tau) &= 64\left(\frac{\tau}{\tau_1}\right)^3\left(1 - \frac{\tau}{\tau_1}\right)^3 \quad , && 0 \leq \tau \leq \tau_1 \\ &= 0 \quad , && \tau < 0 \text{ and } \tau > \tau_1 \end{aligned}\right\} \qquad (4\text{-}1)$$

where δ_0 is the maximum control angle and $\tau_1 = Ut_1/\bar{c}$ is the duration of the excursion in mean chords of travel. To the accuracy of plotting the calculated quantities $Q_i(\tau)$ from the three equations are indistinguishable.

Some typical results for the trailing-edge control and the relative contributions of the individual terms in equations (2-27) and (2-34) are discussed in section 4.1. The influence of the rate of deployment or the duration τ_1 is analysed in section 4.2. Section 4.3 contrasts the characteristics of the leading-edge and trailing-edge controls. All these calculations are in the time domain, but section 4.4 considers the merits of working in the frequency domain and the additional conclusions that can be drawn from this.

4.1 Forces due to trailing-edge control

The concept of active controls envisages the facility to deploy them rapidly. The really significant range of τ_1 is probably $5 \leq \tau_1 \leq 40$. For example, in equation (4-1) $\tau_1 = 10$ would give a maximum control rate

$$\left(\frac{\partial\delta}{\partial t}\right)_{max} = 3.43\,\frac{\delta_0 U}{\tau_1 \bar{c}} = 0.343\,\frac{\delta_0 U}{\bar{c}} \quad , \qquad (4\text{-}2)$$

which is about 100 deg/s with $\delta_0 = 5$ deg, $U = 240$ m/s and $\bar{c} = 4$ m. With $\tau_1 = 10$ the results for the lift, pitching moment and hinge moment due to the trailing-edge

control at $N = 0.8$ are illustrated in Fig 8. The calculations are made with unit δ_0, and the coefficient of lift $Q_1(\tau)$ only just reaches 80% of its peak quasi-steady value $Q'_{13}(0)$. Moreover, this occurs at time $t/t_1 = \tau/\tau_1 = 0.535$ and lags behind the control angle which peaks at $\tau/\tau_1 = 0.5$. There is a correspondingly slow decay of the residual lift after the motion has ceased. In contrast to the lift, the hinge moment overshoots its peak quasi-steady value by 4% at $\tau/\tau_1 = 0.45$ and thus leads the control angle. There is a corresponding overshoot where $Q_3(\tau)/Q'_{33}(0)$ becomes negative before the motion is completed, and the residual effect after $\tau/\tau_1 = 1$ is negligible. As might be expected, the behaviour of the transient pitching moment has intermediate characteristics.

Fig 9 shows the individual contributions of the terms in equations (2-27) and (2-34) to the lift when $\tau_1 = 5$ and 20 respectively. The lift now reaches respectively 72% and 89% of its peak quasi-steady value, here denoted by L_0, at time $\tau/\tau_1 = 0.545$ and again lags behind the motion. When the history function is used in equation (2-34), the first term denotes the quasi-steady contribution proportional to δ. The second term is proportional to $d\delta/dt$ and turns out to be of opposite sign; this gives a qualitative explanation of the lag in the peak lift. However, there remains an important contribution from the history term, indicated by the vertical arrows in the upper diagram of Fig 9, which changes sign twice. For the more rapid motion the lower diagram similarly disects equation (2-27) with the infinite-frequency coefficients and the position factor. It can be seen that the major contributions are from the first term proportional to $d\delta/d\tau$ when $0 < \tau/\tau_1 < 0.05$ and from the second term proportional to δ when $0.05 < \tau/\tau_1 < 0.40$. But, thereafter, the position integral provides the major contribution which remains positive. Apart from the dominant role of the very high frequency parameters and the irrelevance of the low-frequency coefficients $Q'_{13}(0)$ and $Q''_{13}(0)$ in the very early stages, the analysis in terms of the history function has rather more to commend it.

We would hope to find circumstances where the first two terms of equation (2-34) suffice, so that the history term can be ignored. Suppose, for example, that such quantities as those in Figs 8 and 9 are required to an accuracy of about ±0.05, and consider the following cases at the extremes of the significant range of τ_1

(a) Lift, $\tau_1 = 5$,
(b) Lift, $\tau_1 = 40$,
(c) Hinge moment, $\tau_1 = 5$.

The quantities from the control-angle, control-rate and history terms of equation (2-34) are given in Table 7. In case (a) the control-angle term neglects contributions as high as 0.3; moreover, the history term is mostly of larger magnitude than the total lift and its main effect is to cancel large superfluous contributions from the control-rate term. For such a rapid motion at $\tau_1 = 5$ the analysis of equation (2-34) for lift ceases to be helpful. For the more gradual deployment with $\tau_1 = 40$ in case (b), Table 7 is more encouraging. The control-angle term neglects contributions between ±0.1 in lift, while the inclusion of the control-rate term reduces the gaps to within ±0.05 or thereabouts. Under such conditions the individual terms of equation (2-34) become useful and only a rough approximation to the history term is needed. The rapidly-produced hinge moment in

case (c) is an instance where the control-angle term neglects positive and negative contributions of magnitudes greater than 0.3, while those of the history term hardly exceed 0.05. This special result is closely linked to the small dependence of Q'_{33} and Q''_{33} on $\bar{v}$ in Table 2, whereby in Fig 7 the history function itself becomes small.

4.2 Duration of deployment

Before discussing in more detail the effect of τ_1 on the present calculations, we consider in general terms the influence of control rate. If a control angle is changed slowly from 0 to δ_1, it is reasonable to express a consequent time-dependent force in the form

$$Q_i(\tau) = Q'_{ij}(0)\delta(\tau) + Q_R \frac{d\delta(\tau)}{d\tau} + Q_H \qquad (4\text{-}3)$$

with some rate factor Q_R. The boundary condition representing an instantaneous control rate, equivalent to the second term on the right hand side of equation (2-2), can be treated separately from the first term as if it were a steady state. This would determine a value for Q_R different from the low-frequency quantity $Q''_{ij}(0)$ in equation (2-34). If this steady control-rate concept were used for Q_R, the residual term Q_H would represent the history of the motion as the influence of time dependence in the surface distribution of upwash angle. Because the very existence of a control rate implies a time-dependent upwash, such an approach is illogical and will be shown to be ineffective. If the deployment from 0 to δ_1 is carried out very rapidly, we have already established from equation (2-21) that the velocity factor $F_1(\sigma)$ defines the instantaneous force. Thus for $\tau > 0$

$$Q_i(\tau) = Q'_{ij}(0)\delta_1 F_1(\tau) \quad . \qquad (4\text{-}4)$$

If the deployment takes time $t_1 = \tau_1 \bar{c}/U$, then a good approximation to the force for $\tau \geq \tau_1$ is

$$Q_i(\tau) \simeq \frac{Q'_{ij}(0)\delta_1}{\tau_1} \int_0^{\tau_1} F_1(\tau - \tau_0)d\tau_0$$

$$\simeq \frac{Q'_{ij}(0)\delta_1}{\tau_1} \left[F_2(\tau) - F_2(\tau - \tau_1)\right] \quad . \qquad (4\text{-}5)$$

A more crude, but still useful, approximation is

$$Q_i(\tau) \simeq Q'_{ij}(0)\delta_1 F_1(\tau - \tfrac{1}{2}\tau_1) \qquad (4\text{-}6)$$

which tends to the limit in equation (4-4) as τ_1 decreases to zero.

Fig 10 shows the time-dependent lift as the trailing-edge control angle δ follows equation (4-1) for different values of τ_1. The quasi-steady limit $\tau_1 \to \infty$ identifies L/L_0 with δ/δ_0. The time scale is normalized with respect to the excursion time. The main characteristic of Fig 10 is the progressive fall in maximum L/L_0 from unity to 0.72 as τ_1 decreases to 5. Subsidiary features when $\tau_1 \leq 40$ are the lag in the

occurrence of maximum L/L_0 from $\tau/\tau_1 = 0.50$ to about 0.545 and the greater residual lift after the control angle has returned to zero. As supplementary information the following table gives the normalized times τ_2/τ_1 when the residual lift has fallen to $L/L_0 = 0.01$.

τ_1	80	40	20	10	5
τ_2/τ_1	1.00	1.12	1.36	1.83	2.68

The asymptotic limit for small τ_1 corresponds to $F_0(\tau_2) = 0.01$, which in this case is found to be $\tau_2 = 8.5$.

The contributions to Fig 10 from the history term in equation (2-34) are plotted as $\Delta L/L_0$ in Fig 11. The widely varying curves against $t/t_1 = \tau/\tau_1$ illustrate different aspects of the application of the history function. Provided that $\Delta L/L_0$ is everywhere small compared with unity, the isolated history term usefully provides a correction to the quasi-steady forces, and this is the case for $\tau_1 \geq 20$. It is interesting to observe how the curves change shape from $\tau_1 = 5$ to $\tau_1 = 80$.

When τ_1 is small, $H(\tau - \tau_0)$ is slowly varying compared with $d^2q_j(\tau_0)/d\tau_0^2$; thus, when $\tau \ll \tau_1$, the history term for lift may be written as

$$\frac{\Delta L}{L_0} = H(\tau - \bar{\tau}_0) \int_0^{\tau} \frac{d^2 q_j(\tau_0)}{d\tau_0^2} d\tau_0 = H(\tau - \bar{\tau}_0) \frac{dq_j(\tau)}{d\tau} \qquad (4\text{-}7)$$

where $\bar{\tau}_0$ is some average value. Similarity between $\Delta L/L_0$ for $\tau_1 = 5$ and $dq_j(\tau)/d\tau$ is apparent, and with further decrease in τ_1 the curve becomes increasingly anti-symmetric about $\tau/\tau_1 = 0.5$ and its maximum and minimum approach $\tau/\tau_1 = 0.276$ and 0.724 respectively, those of

$$\frac{\tau_1}{\delta_0} \frac{d\delta}{d\tau} = 192 \left(\frac{\tau}{\tau_1}\right)^2 \left(1 - \frac{\tau}{\tau_1}\right)^2 \left(1 - \frac{2\tau}{\tau_1}\right) \qquad (4\text{-}8)$$

from equation (4-1). Moreover, from equation (4-7) these stationary values will ultimately behave like

$$\pm H(0) \left[\frac{dq_j(\tau)}{d\tau}\right]_{max} = \pm \frac{Q''_{ij}(\infty) - Q''_{ij}(0)}{Q'_{ij}(0)} \left[\frac{3.43}{\tau_1}\right] = \pm \frac{5.2}{\tau_1} \qquad (4\text{-}9)$$

for $i = 1$ and $j = 3$, which gives values ± 1.04 when $\tau_1 = 5$ to compare with +0.83 and −1.03 in Fig 11.

The limiting shape for large τ_1 has academic interest. It is then $d^2q_j(\tau_0)/d\tau_0^2$ that is slowly varying compared with $H(\tau - \tau_0)$, so that

$$\frac{\Delta L}{L_0} \simeq \frac{d^2 q_j(\bar{\tau}_0)}{d\bar{\tau}_0^2} \int_0^{\tau} H(\tau - \tau_0) d\tau_0 \qquad (4\text{-}10)$$

where $\bar{\tau}_0$ is some average value and, as τ_1 increases, $\bar{\tau}_0/\tau_1$ approaches τ/τ_1. As $\Delta L/L_0$ decreases with increasing τ_1, its shape in Fig 11 tends to become symmetrical like $d^2 q_j(\tau)/d\tau^2$ and its zeros approach the positions $\tau/\tau_1 = 0.276$ and 0.724. The convergence is slow and is complicated by the fact that the integral in equation (4-10) is logarithmically divergent as $\tau \to \infty$. Nevertheless, for motions of finite duration, equation (2-34) can be expressed in the form

$$Q_i(\tau) \simeq Q'_{ij}(0) q_j(\tau) + Q''_{ij}(0) \frac{dq_j(\tau)}{d\tau} + Q'_{ij}(0) J(0) \frac{d^2 q_j(\tau)}{d\tau^2} + Q'_{ij}(0) \int_0^{\tau} \frac{d^3 q_j(\tau_0)}{d\tau_0^3} J(\tau - \tau_0) d\tau_0 \quad , \qquad (4\text{-}11)$$

where

$$J(\sigma) = J(0) + \int_0^{\sigma} H(\sigma_0) d\sigma_0 \quad . \qquad (4\text{-}12)$$

The practical significance of equation (4-11) is slight, because its only relevance is to situations where the history term is already becoming negligible. Nevertheless, equations (4-10) to (4-12) yield the academic result

$$Q_i(\tau) \simeq Q'_{ij}(0) q_j(\tau) + Q''_{ij}(0) \frac{dq_j(\tau)}{d\tau} + Q'_{ij}(0) \left[J(\tau) - J(0) \right] \frac{d^2 q_j(\tau)}{d\tau^2} \qquad (4\text{-}13)$$

for large τ_1.

Fig 12 shows how the curves of instantaneous centre of pressure due to the trailing-edge control vary with τ_1. There are three limiting values

$$\left.\begin{aligned} &\text{for small } \tau, && \frac{\bar{x}}{\bar{c}L} = \frac{Q''_{23}(\infty)}{Q''_{13}(\infty)} \\ &\text{for large } \tau, && \frac{\bar{x}}{\bar{c}L} = \frac{Q'_{22}(0)}{Q'_{12}(0)} \\ &\text{quasi-steady,} && \frac{\bar{x}}{\bar{c}L} = \frac{Q'_{23}(0)}{Q'_{13}(0)} \end{aligned}\right\} , \qquad (4\text{-}14)$$

the first of which follows from the first term on the right hand side of equation (2-24). The second limit follows from the history term of equation (2-34) in conjunction with the asymptotic expansion in equation (3-33) and is identified with the wing aerodynamic centre. Neither of these limits is of much practical significance, because in both cases

the associated lift force is very small. Nor is the quasi-steady value of much consequence, for it belies the fact that in the most important range $5 \leq \tau_1 \leq 40$ and even for $\tau_1 = 80$ the quantity $\mathscr{M}/\bar{c}L$ is rapidly varying. It is also of interest in Fig 12 that the limit for large τ is approached from below; thus for $\tau_1 = 5$ and 10 the residual lift is acting well forward of the aerodynamic centre.

Tables 8 and 9 have been prepared to develop the theme of Table 7, discussed at the end of section 4.1, and to consider the influence of τ_1 on the usefulness of equation (2-34) with the history term omitted

$$Q_i(\tau) \simeq Q'_{ij}(0)q_j(\tau) + Q''_{ij}(0)\frac{dq_j(\tau)}{d\tau} \quad . \tag{4-15}$$

Table 8 gives the maximum and root mean square (rms) errors from equation (4-15) with and without its second term for the 20 values $\tau/\tau_1 = 0.05\ (0.05)\ 1.00$. As far as lift is concerned, the addition of the second term often increases both errors, but clearly it will bring improvement if τ_1 is large enough. Table 9 lists the rms errors and the values of τ_1 when equation (4-15) changes from being more inaccurate to being more accurate as a result of including the second term; it also gives the lower bounds of τ_1 for which equation (4-15) with either one or two terms gives rms errors below 5% of the peak steady value. For the case of lift due to pitching motion there is no range of τ_1 for which equation (4-15) achieves an rms error below 5% and its first term alone fails to do so. For lift with trailing-edge control motion there is such a range $36 < \tau_1 < 65$; by contrast the corresponding range for hinge moment is $4 < \tau_1 < 24$.

A subsidiary study is made to optimize the rms error from equation (4-3) with $Q_H = 0$ and variable Q_R . The following results are obtained for the three examples in Table 7:

$$\left.\begin{array}{lll} \text{(a)} & \text{Lift, } \tau_1 = 5, & Q_R = 0.293 = Q''_{13}\ (1.0) \\ \text{(b)} & \text{Lift, } \tau_1 = 40, & Q_R = 1.913 = Q''_{13}\ (0.15) \\ \text{(c)} & \text{Hinge moment, } \tau_1 = 5, & Q_R = -0.00969 = Q''_{33}\ (1.4) \end{array}\right\} \quad . \tag{4-16}$$

Far from relating to the rejected steady control-rate concept, which would require values $Q_R = -0.187$ for (a) and (b) and -0.00420 for (c), equations (4-16) state that the minimum rms errors occur with $Q_R = Q''_{ij}(\bar{\nu})$ for frequency parameters $\bar{\nu}$ which are found to be fairly close to $2\pi/\tau_1$ corresponding to an oscillation of period $t_1 = \tau_1\bar{c}/U$. Nevertheless, the general approximation

$$Q_i(\tau) \simeq Q'_{ij}\left(\frac{2\pi}{\tau_1}\right)\delta(\tau) + Q''_{ij}\left(\frac{2\pi}{\tau_1}\right)\frac{d\delta(\tau)}{dt} \tag{4-17}$$

would be a poor substitute for the full calculation, unless the frequency parameter $2\pi/\tau_1$ is predominant.

4.3 Type of control

Although the load distribution due to each of the control surfaces is greatly influenced by the wing tip, it is instructive to recall the steady two-dimensional load

distributions associated with each type of control. In linearized incompressible flow the lift per unit area, $\frac{1}{2}\rho U^2 \Delta C_p$, for a control angle δ is given for the trailing-edge control by

$$\frac{\Delta C_p}{\delta} = \frac{4}{\pi}\left[(\pi - \phi_h)\cot\tfrac{1}{2}\phi - \log\left\{\frac{\sin\tfrac{1}{2}|\phi - \phi_h|}{\sin\tfrac{1}{2}(\phi + \phi_h)}\right\}\right] , \tag{4-18}$$

for the leading-edge control by

$$\frac{\Delta C_p}{\delta} = \frac{4}{\pi}\left[\phi_h \cot\tfrac{1}{2}\phi + \log\left\{\frac{\sin\tfrac{1}{2}|\phi - \phi_h|}{\sin\tfrac{1}{2}(\phi + \phi_h)}\right\}\right] , \tag{4-19}$$

and for the all-moving-tip control, as for a flat plate, by

$$\frac{\Delta C_p}{\delta} = 4\cot\tfrac{1}{2}\phi \ . \tag{4-20}$$

In equations (4-18) to (4-20) with x and x_h measured from the leading-edge the angles ϕ and ϕ_h are defined as usual by

$$\left.\begin{aligned} \frac{x}{c} &= \tfrac{1}{2}(1 - \cos\phi) \\ \frac{x_h}{c} &= \tfrac{1}{2}(1 - \cos\phi_h) \end{aligned}\right\} . \tag{4-21}$$

If required, the simple compressibility factor $(1 - M^2)^{-\frac{1}{2}}$ enters on the right hand sides of equations (4-18) to (4-20). The load distributions at $M = 0$ for the trailing-edge control with $x_h = 0.75c$, the leading-edge control with $x_h = 0.25c$ and the all-moving tip are drawn in Fig 13. Positive δ is defined as nose-up, so that the discontinuities in surface slope at the hinge are in opposite senses for the leading-edge and trailing-edge controls. It follows from equations (4-18) and (4-19) that for a given control chord, not only are the logarithmic singularities at the hinge equal and opposite, but the inverse-square-root singularities at the leading-edge are identical in the two cases. Fig 13 also shows that the loading aft of the hinge of the leading-edge control remains negative. The cancellation effect is such that the two-dimensional lift due to the leading-edge control is only 9.5% of that produced by the trailing-edge control; the ratio 9.3% in three dimensions for the particular planform at $M = 0.8$ is remarkably close. The familiar flat-plate distribution for the all-moving-tip control in Fig 13 is less relevant, because the centre of pressure near the tip moves well forward of quarter chord to the extent that the hinge line in Fig 1 is taken to balance the control.

The calculations of lift due to the transient deflection angle in equation (4-1) are recorded in Table 10 when $\tau_1 = 5$ and 40 for pitching motion θ/θ_0 and for deployment of the three control surfaces at $M = 0.8$. For the slower motion with $\tau_1 = 40$, the trailing-edge control stands out as the slowest in producing and relinquishing lift. Pitching and leading-edge control rotation give remarkably similar time histories of L/L_0, while that of the all-moving tip is intermediate to the other two controls.

This pattern is largely repeated for the rapid motion $\tau_1 = 5$. The leading-edge control shows rapidity of aerodynamic response in that the lift overshoots the quasi-steady range $0 < L/L_0 < 1$. This behaviour is nearly matched by the case of pitching motion where $L/L_0 = -0.012$ at $\tau = 4.5$. As we have already seen, the trailing-edge control produces a sluggish behaviour in lift, which only reaches 72% of the quasi-steady maximum and retains 13% of this at the conclusion of the control motion. Figs 10, 14 and 15 show the influence of excursion time on lift for the trailing-edge, leading-edge and all-moving-tip controls respectively.

The results for $\tau_1 = 5$ can be analysed further in relation to equation (4-17), which gives for unit δ_0

$$\frac{L}{L_0} = \frac{Q_1(\tau)}{Q'_{1j}(0)} \simeq \frac{Q'_{1j}(2\pi/\tau_1)}{Q'_{1j}(0)} \left[\delta(\tau) + \frac{Q''_{1j}(2\pi/\tau_1)}{Q'_{1j}(2\pi/\tau_1)} \frac{d\delta(\tau)}{d\tau} \right] \quad . \tag{4-22}$$

For convenience we shall take the approximate value $2\pi/\tau_1 = 1.2$ and use the data in Tables 2 to 4. It can be seen from the following table that equation (4-22) provides a qualitative description of the differing characteristics of the three controls.

	$\tau_1 = 5$	j = 3 TE control	j = 4 LE control	j = 5 All-moving-tip
	Peak L/L_0	0.72	1.05	0.81
	at $\tau/\tau_1 =$	0.54	0.40	0.45
$Q'_{1j}(1.2)/Q'_{1j}(0)$		0.611	0.940	0.728
$Q''_{1j}(1.2)/Q'_{1j}(1.2)$		-0.225	0.688	0.274
From equation (4-22)	Peak L/L_0	0.87	2.75	1.14
	at $\tau/\tau_1 =$	0.64	0.30	0.34

The peak values of L/L_0 from Figs 10, 14 and 15 are ordered according to the values of the factor $Q'_{1j}(1.2)/Q'_{1j}(0)$. The location of the peak along the time scale is ordered by the ratio $Q''_{1j}(1.2)/Q'_{1j}(1.2)$ which governs the influence of the rate term. When this ratio is negative for $j = 3$ the peak is seen to be delayed, and when the ratio is larger and positive for $j = 4$ the peak is advanced from 0.50 to a larger extent. But the quantitative predictions of equations (4-22) are shown to caricature the behaviour and are included to emphasize the particular danger of using oscillatory aerodynamics for a discrete frequency in response studies of active control systems.

Fig 16 contrasts the normalized time-dependent lift from leading-edge and trailing-edge controls when deployed very briefly with $\tau_1 = 2$. This could correspond to a rapid on-off situation over a small range of control angle. The trailing-edge control only reaches 58% of the quasi-steady peak lift, while the leading-edge control gives a peak-to-peak variation that is nearly three times the quasi-steady one. Clearly the growth of

lift remote from the control surface is subject to the major time delay. Fig. 9 indicates that with a positive control rate this delay gives lift reduction for the trailing-edge control and lift enhancement for the leading-edge control, and the effect is reversed as the controls return to their initial positions. Similar reasoning leads us to expect the fairly close correlation between time-dependent hinge moments and their quasi-steady values implied in Tables 8 and 9. For the leading-edge control this correlation is particularly close, because the ratio $Q''_{44}(\bar{\nu})/Q'_{44}(\bar{\nu})$ from Table 3 is as small as -0.06 for $\bar{\nu} = 0$ and virtually remains between half and twice this value over the whole frequency range. There seems to be little point in isolating the history terms for the lift due to the leading-edge and all-moving-tip controls because, as Tables 8 and 9 show, the two-term approximation from equation (2-34) has virtually no advantage over the one-term approximation if 5% rms accuracy is sought. Full calculations are needed if $\tau_1 < 30$, and a similar conclusion can be reached for pitching moment as well as lift.

4.4 Use of Fourier transform

We now return to equations (2-19) and (2-20), derived in Appendix A. Instead of integrating with respect to frequency parameter and using hereditary functions, we consider the evaluation of $Q_i(\tau)$ in the frequency domain, when $q_j(\tau)$ is defined by equation (4-1). It is more convenient, however, to work in complex numbers and to take

$$Q_i(\tau) = \mathcal{R}\left[\tfrac{1}{2}q_j(\infty)Q_{ij}(0) - \frac{i}{\pi}\int_0^\infty\int_0^\infty \frac{dq_j(\tau_0)}{d\tau_0}\,\frac{Q_{ij}(\bar{\nu})e^{i\bar{\nu}(\tau-\tau_0)}}{\bar{\nu}}\,d\tau_0 d\bar{\nu}\right] \qquad (4\text{-}23)$$

from equations (A-5) to (A-7) of Appendix A. From equation (4-1) the analytical integration with respect to τ_0 yields

$$I(\bar{\nu}\tau_1) = \int_0^\infty \frac{dq_j(\tau_0)}{d\tau_0}\,e^{-i\bar{\nu}\tau_0}\,d\tau_0$$

$$= 64\left[\left\{\frac{6}{(-i\bar{\nu}\tau_1)^3} + \frac{360}{(-i\bar{\nu}\tau_1)^5}\right\}\left(-e^{-i\bar{\nu}\tau_1} - 1\right) + \left\{\frac{72}{(-i\bar{\nu}\tau_1)^4} + \frac{720}{(-i\bar{\nu}\tau_1)^6}\right\}\left(e^{-i\bar{\nu}\tau_1} - 1\right)\right] . \qquad \ldots\ldots (4\text{-}24)$$

If $\bar{\nu}\tau_1 < 1.25$, $I(\bar{\nu}\tau_1)$ is better evaluated from the expansion

$$I(\bar{\nu}\tau_1) = \left[\frac{8}{35}(\bar{\nu}\tau_1)^2 - \frac{4}{315}(\bar{\nu}\tau_1)^4 + \frac{2}{7425}(\bar{\nu}\tau_1)^6 - \frac{1}{315315}(\bar{\nu}\tau_1)^8 + \frac{1}{41277600}(\bar{\nu}\tau_1)^{10}\right]$$

$$+ i\left[\frac{16}{35}(\bar{\nu}\tau_1) - \frac{4}{63}(\bar{\nu}\tau_1)^3 + \frac{1}{495}(\bar{\nu}\tau_1)^5 - \frac{1}{32175}(\bar{\nu}\tau_1)^7 + \frac{1}{3439800}(\bar{\nu}\tau_1)^9\right] . \qquad \ldots\ldots (4\text{-}25)$$

Since $q_j(\infty) = 0$, equation (4-23) reduces to

$$Q_i(\tau) = \Re\left[-\frac{i}{\pi}\int_0^\infty \frac{Q_{ij}(\bar{\nu})I(\bar{\nu}\tau_1)}{\bar{\nu}} e^{i\bar{\nu}\tau}\, d\bar{\nu}\right] = \int_{-\infty}^{\infty}\left\{-\frac{iQ_{ij}(\bar{\nu})I(\bar{\nu}\tau_1)}{2\pi\bar{\nu}}\right\} e^{i\bar{\nu}\tau}\, d\bar{\nu} \ , \quad (4\text{-}26)$$

where $Q_{ij}(-\bar{\nu})$ is the complex conjugate of $Q_{ij}(\bar{\nu})$. Equation (4-26) states that $Q_i(\tau)$ is the inverse Fourier transform of the expression in curly brackets.

A fast Fourier transform technique, based on the work of Cooley and Tukey[13], has been used to evaluate equation (4-26) with the aid of a cubic spline to represent the complex generalized force coefficient $Q_{ij}(\bar{\nu})$ and equations (4-24) and (4-25) for $I(\bar{\nu}\tau_1)$. In these calculations it is necessary to truncate the range of $\bar{\nu}$ and straightforward to vary the upper limit $\bar{\nu}_u$. The lower the value of τ_1 , the higher $\bar{\nu}_u$ must be. With $\tau_1 = 10$ and $\bar{\nu}_u = 5.89$ the full calculations of lift due to the trailing-edge control from Fig 8 are reproduced to an accuracy of ±0.001. With $\tau_1 = 5$ near its practical lower limit, results are given in Table 11 for four values of $\bar{\nu}_u$ in the range $1.23 \leqslant \bar{\nu}_u \leqslant 4.91$. For $\bar{\nu}_u = 4.91$ the accuracy of the Fourier transform calculations is ±0.0012 and the rms error in the range $0.5 \leqslant \tau \leqslant 5.0$ is 0.1%. Table 11 shows how this rms error increases to 9.6% as $\bar{\nu}_u$ is reduced to 1.23. To keep the errors within ±0.01 of the maximum quasi-steady lift, it is advisable to keep $\bar{\nu}_u$ to 2.4 or above. For most practical purposes, therefore, the range of frequency parameter $0 \leqslant \bar{\nu} \leqslant 2.4$ should suffice. The upper limit is roughly proportional to $1/\tau_1$, so that for many applications it would only be necessary to consider $\bar{\nu}$ up to flutter frequencies; on the other hand, the extreme examples in Fig 16 with $\tau_1 = 2$ require the whole range of the lifting-surface calculations in Tables 2 and 3.

Unless the calculations involve step changes in control displacement or rate, the oscillatory data for infinite frequency are clearly irrelevant in practical cases*. It follows from equations (3-35) that the behaviour of the history function $H(\sigma)$ as $\sigma \to$ is likewise irrelevant. Similar remarks apply to the position and velocity functions $F_0(\sigma)$ and $F_1(\sigma)$ with greater force, and with particular reference to equation (3-24) no serious concern need be felt about the inability to produce reliable curves of $F_0(\sigma)$ in Figs 4a & 4b. Some idea of the importance of $F_1(\sigma)$ for small σ can be gleaned from equation (4-6) by setting a suitable lower limit to the time required to deflect a control surface.

Latitude in the accuracy to which high-frequency aerodynamic data are required encourages alternative approaches. Thus the aerodynamic modelling discussed by Woodcock[8], which exploits Fourier transforms, can be seen in a practical light. The analysis that follows from representation of the coefficients $Q_{ij}(\bar{\nu})$ as the ratio of polynomials in $\bar{\nu}$, as proposed by Veps[14] for example, becomes credible. Although such an approximation could hardly be expected to reproduce the undulations of the Argand diagram of $Q_{13}(\bar{\nu})$ in Fig 2, it would surely be capable of representing the region $0 < \bar{\nu} < 1$ to good

---

* This might not be the case for motion which ultimately diverges, *eg* $q(\tau) = \tau^2$, $(\tau \geqslant 0)$.

accuracy and of continuing without undulations through $1 < \bar{\nu} < 3$ to give usable results for active control studies. Some evidence to this effect is provided in columns (c) and (d) of Table 6, since the former largely excludes the undulations. The present calculations stand as a yard-stick for various approximations discussed in Ref 8.

5 INVERSE CALCULATIONS

In general, as discussed in Refs 4, 8 and 14, the time-dependent aerodynamic forces occur as terms in the equations of an aeroelastic system; for simplicity, the present application is confined to the aerodynamics without any modelling of the aircraft response. In practice, an active control is subject to a sensor, such as an accelerometer, attached to the aircraft structure; within a purely aerodynamic framework no attempt is made to simulate a sensor or any associated control laws. Instead, perfect knowledge of the aerodynamic input is assumed, and in section 5.2 this amounts to the growth of lift due to a step gust.

In section 5.1 we address the question of determining the motion of a control surface to produce a given time-dependent aerodynamic force. Equation (2-21)

$$Q''_{ij}(\infty)\,\frac{dq_j(\tau)}{d\tau} + Q'_{ij}(0)\int_0^\tau \frac{dq_j(\tau_0)}{d\tau_0}\,F_1(\tau-\tau_0)\,d\tau_0 = Q_i(\tau) \qquad (5\text{-}1)$$

is to be solved for $q_j(\tau)$, given $Q_i(\tau)$, the velocity factor $F_1(\sigma)$ from equation (2-22), and the coefficients $Q'_{ij}(0)$ and $Q''_{ij}(\infty)$. The program, mentioned at the end of section 3.3, provides numerical values of $F_1(\sigma)$ for selected σ up to and including some arbitrary large value σ_1, beyond which equation (3-30) is used to give

$$F_1(\sigma) = 1 + \frac{Q'_{1j}(0)Q'_{i2}(0)(\sigma-\sigma_1)}{8\pi Q'_{ij}(0)\sigma^3} + \frac{\{F_1(\sigma_1)-1\}\sigma_1^3}{\sigma^3} \quad . \qquad (5\text{-}2)$$

5.1 Alternative approaches

One scheme of calculation is to iterate by taking equation (5-1) in the form

$$Q'_{ij}(0)q_j(\tau) + Q''_{ij}(\infty)\,\frac{dq_j(\tau)}{d\tau} + Q'_{ij}(0)\int_0^\tau \frac{dq_j(\tau_0)}{d\tau_0}\,\{F_1(\tau-\tau_0)-1\}\,d\tau_0 = Q_i(\tau) \qquad (5\text{-}3)$$

and by evaluating $q_j^{(n+1)}(\tau)$ from a previous approximation $q_j^{(n)}(\tau)$ from the relationship

$$q_j^{(n+1)}(\tau) = \frac{Q_i(\tau)}{Q'_{ij}(0)} - \frac{Q''_{ij}(\infty)}{Q'_{ij}(0)}\,\frac{dq_j^{(n)}(\tau)}{d\tau} - \int_0^\tau \frac{dq_j^{(n)}(\tau_0)}{d\tau_0}\,\{F_1(\tau-\tau_0)-1\}\,d\tau_0 \quad . \qquad (5\text{-}4)$$

There is the disadvantage that each iteration involves the numerical differentiation of $q^{(n)}(\tau)$, and the procedure is often unstable.

Instead, greater success is obtained from the linear differential equation

$$Q'_{ij}(0)q_j^{(n+1)}(\tau) + Q''_{ij}(\infty)\frac{dq_j^{(n+1)}(\tau)}{d\tau} = Q_i(\tau) - Q'_{ij}(0)\int_0^\tau \frac{dq_j^{(n)}(\tau_0)}{d\tau_0}\left\{F_1(\tau-\tau_0) - 1\right\}d\tau_0 \quad \text{..... (5-5)}$$

which gives

$$q_j^{(n+1)}(\tau) = \frac{\exp\left[-Q'_{ij}(0)\tau/Q''_{ij}(\infty)\right]}{Q''_{ij}(\infty)}\int_0^\tau\left[Q_i(\tau') - R^{(n)}(\tau')\right]\exp\left[\frac{Q'_{ij}(0)\tau'}{Q''_{ij}(\infty)}\right]d\tau' \quad (5\text{-}6)$$

where $$R^{(n)}(\tau) = Q'_{ij}(0)\int_0^\tau \frac{dq_j^{(n)}(\tau_0)}{d\tau_0}\left\{F_1(\tau-\tau_0) - 1\right\}d\tau_0 \ . \quad (5\text{-}7)$$

The iterations can be started by taking $q_j^{(0)}(\tau) \equiv 0$ and hence $R^{(0)}(\tau) \equiv 0$. Then by equations (5-6) and (5-5) respectively

$$q_j^{(1)}(\tau) = \frac{\exp\left[-Q'_{ij}(0)\tau/Q''_{ij}(\infty)\right]}{Q''_{ij}(\infty)}\int_0^\tau Q_i(\tau')\exp\left[\frac{Q'_{ij}(0)\tau'}{Q''_{ij}(\infty)}\right]d\tau' \quad (5\text{-}8)$$

and

$$\frac{dq_j^{(1)}(\tau)}{d\tau} = -\frac{Q'_{ij}(0)q_j^{(1)}(\tau)}{Q''_{ij}(\infty)} + \frac{Q_i(\tau)}{Q''_{ij}(\infty)} \ . \quad (5\text{-}9)$$

Then equations (5-7) to (5-9) determine $R^{(1)}(\tau)$, equation (5-6) and $R^{(1)}(\tau)$ determine $q_j^{(2)}(\tau)$, and its derivative is obtained by differentiating equation (5-6) to give

$$\frac{dq_j^{(n+1)}(\tau)}{d\tau} = -\frac{Q'_{ij}(0)q_j^{(n+1)}(\tau)}{Q''_{ij}(\infty)} + \frac{Q_i(\tau) - R^{(n)}(\tau)}{Q''_{ij}(\infty)} \quad (5\text{-}10)$$

with $n = 1$. This procedure has been used successfully for the lift ($i = 1$) and the modes $j = 3$ and 5 corresponding to the trailing-edge and all-moving-tip controls, when the exponent outside the integral in equation (5-6) is negative.

For the leading-edge control $Q'_{ij}(0)$ and $Q''_{ij}(\infty)$ are of opposite sign and numerical errors, however small, magnify from iteration to iteration. This poses a problem which cannot be overcome, for example, by subtracting $2Q''_{ij}(\infty)dq_j(\tau)/d\tau$ from both sides of equation (5-3) and allowing for the extra term on the right hand side in the definition of $R^{(n)}(\tau)$. The difficulty is apparently the basic one that there exists a divergent motion of the leading-edge control, which produces zero lift. There are indications for very high frequency from piston theory, considered in section 3.2, that the ultimate value of the generalized force coefficient,

$$Q'_{14}(\infty) + i\bar{\nu}Q''_{14}(\infty) = -0.977 + 0.0514\, i\bar{\nu} \qquad (5\text{-}11)$$

from Table 3, vanishes for the rapidly divergent motion corresponding roughly to $i\bar{\nu} = 19.0$. In this unusual situation any iterative method is doomed to failure and a different approach must be adopted.

We therefore take $q_4(\tau)$ as a series of exponential terms

$$q_4(\tau) = \sum_{k=1}^{K} \alpha_k e^{-\beta_k \tau} \quad , \qquad (5\text{-}12)$$

where the factors $\beta_k \geq 0$ are suitably chosen and the K coefficients α_k are determined so as to satisfy equation (5-3) to a sufficient approximation. A good procedure is to evaluate the left hand side of equation (5-3) for, say, $2K$ values of τ in the range of interest and then to solve the set of linear simultaneous equations that satisfy the initial condition on $q_4(0)$ and minimize the root mean square error in the quantities $Q_i(\tau)$.

5.2 Neutralization of gust force

We first calculate the lift on the wing of Fig 1 as it enters a step gust at $M = 0.8$ in the direction normal to the gust front. As discussed in section 2.2 and reproduced from Fig 2b in Fig 17, the lift $L(\sigma)/L(\infty)$ or L/L_1 grows more slowly than that due to a step change in the trailing-edge control angle, which also involves impulsive lift at $\sigma = 0$. Clearly a less violent change in control angle is needed to neutralize the growth of lift from the step gust. The iterative calculation, based on equations (5-5) to (5-10), gives the curve of δ/δ_1 with alternating long and short dashes in Fig 17. The most striking feature of this curve is that it attains 98% of its final value and remains within ±2% of it after just four mean chords of travel, at which stage the lift from the step gust is only approaching 80%.

The same method of calculation is used for the all-moving-tip control, but for the leading-edge control satisfactory results are obtained by means of equation (5-12) with $K \geq 4$. Fig 18 compares the neutralizing curves of δ/δ_1 for the three types of control surface, which show the inverse characteristics of their velocity factors $F_1(\sigma)$ from Fig 5. The overshoot in lift from the leading-edge control, typified by $F_1(\sigma) > 1$ for $\sigma < 0.5$, leads to the less rapid demand for δ in Fig 18, while the all-moving-tip shows intermediate characteristics, just as it has done in Fig 5 and Table 10. The relative magnitudes of δ_1 for the three controls in Fig 18 show the high ratio 10.8 for the leading-edge control, which is much less effective than the trailing-edge control in producing lift. For each control δ remains within ±1% of its final value δ_1 after a gust penetration of only $5.4\bar{c}$, although the growth of lift due to the gust takes at least three times as long to do so. This remarkable result is peculiar to lift because of the invariant asymptotic behaviour found in equations (2-17) and (3-5). Nevertheless, the rapid control rates implied in Fig 18 are indicative of the targets that can be set in active control technology. Such applications require the full treatment of flow history.

6 CONCLUDING REMARKS

6.1 Recapitulation

A double integral for the time-dependent aerodynamic force due to arbitrary wing or control-surface motion in equation (2-19) forms the basis of calculations in either the time or the frequency domain. In the time domain various expressions involving different hereditary functions are derived, in particular, equation (2-34) containing two quasi-steady terms and a 'history term' involving the history function $H(\sigma)$. A program in ICL 1900 Extended Fortran has been written to calculate the hereditary functions as accurately as possible. The hereditary functions for a high-aspect-ratio wing at $M = 0.8$ with various control surfaces (Fig 1) are used to determine aerodynamic forces due to transient deployment of these controls in the form of equation (4-1). For this particular form of control deployment, analytical integration with respect to the time variable leads to the expression in equation (4-26), which has been evaluated via its Fourier transform in the frequency domain to give good agreement with the time-dependent lift calculated from the hereditary functions in the time domain.

Special attention has been paid to the asymptotic behaviour of the various functions. The evaluation of each hereditary function takes account of the asymptotic expansions of the generalized forces $Q_{ij}(\bar{\nu})$ for small and large frequency in equations (3-1), (3-2), (3-16) and (3-17). The hereditary functions $F_n(\sigma)$ and $H(\sigma)$ are discussed in relation to their asymptotic expansions for small and large time in equations (3-24) to (3-33). The contribution of the history term to lift due to the trailing-edge control is examined in relation to the limiting expressions in equations (4-7) and (4-10) for very rapid and very slow control rates. Having a well-defined asymptotic expansion for small σ , the history function $H(\sigma)$ is considered from the standpoint of empirical correction. The factor $\kappa(\sigma)$ in equation (3-36) or (3-37) is proposed, but there is a simpler alternative in equation (3-39).

Transient deployment of the controls according to equation (4-1) with variable duration τ_1 is considered, and calculations are made of the time-dependent lift, pitching moment or hinge moment for pitching or control-surface motion. The relative importance of the quasi-steady and history terms is analysed in Tables 7 to 9. Analysis is also carried out on the direct use of oscillatory aerodynamic forces in approximating to the time-dependent lift, as in equation (4-22). This has considerable qualitative merit, but the quantitative predictions can seriously exaggerate the results.

The Fourier transform results for time-dependent lift in Table 11 confirm the minimal consequences of neglecting the logarithmic term at small frequency in equation (3-2) and show that, important though it is for the hereditary functions, the asymptotic expansion for large frequency can be ignored altogether by truncating the frequency range in equation (4-26). Roughly, in the frequency domain, an upper limit of $|\bar{\nu}| = \bar{\nu}_u = 12/\tau_1$ appears to be satisfactory (section 4.4).

Methods of inverting the equations to determine the motion that will give a required aerodynamic force are discussed in section 5.1. The iterative scheme in equations (5-5) to (5-10) appears to work unless the coefficients $Q_{ij}(\bar{\nu})$ imply a zero in the lower half

of the complex frequency plane. When this seems to happen for the particular case of lift due to the leading-edge control, a more crude approach of the collocation type has been adopted. The illustrative calculations of control-surface motion to neutralize the growth of lift on entering a step gust show different normalized control rates for the three types of control, which should be considered in relation to their lift effectiveness (Fig 18).

6.2 General conclusions

(1) From the consideration of both small and large frequency, it is preferable to calculate the hereditary functions from integrals involving the in-quadrature force coefficients $Q''_{ij}(\bar{v})$ than from alternative integrals with the in-phase coefficients $Q'_{ij}(\bar{v})$.

(2) When the time-dependent lift is expressed in terms of quasi-steady displacement and rate terms and the additional history term, the history term is likely to be important whenever the rate term is important.

(3) In calculations of time-dependent hinge moment the two quasi-steady terms without the history term seem to cover all practical needs.

(4) During transient deployment of a trailing-edge control the streamwise centre of pressure of the incremental loading moves rapidly from an axis intersecting the control to one slightly upstream of the wing aerodynamic centre before tending asymptotically to the aerodynamic centre as the incremental lift disappears.

(5) The time-dependent lift due to rapid control-surface motion shows sluggish behaviour in the case of a trailing-edge control, but over-reacts to a leading-edge control. An all-moving tip has intermediate characteristics and produces lift that sometimes leads and sometimes lags the control displacement slightly.

(6) The steady two-dimensional chordwise loadings for leading-edge and trailing-edge controls provide a qualitative explanation of their time-dependent lift characteristics on the basis that the growth of loading more remote from the control surface is subject to the major delay.

(7) For many applications of active controls it would be unnecessary to take into account frequencies beyond the flutter range. For this approximation a much simpler aerodynamic modelling would become practicable.

(8) The calculated control-surface motion required to neutralize the growth of lift on entering a step gust stabilizes within about one third of the corresponding distance for the growth of lift itself.

Appendix A

FORMULATION OF TIME-DEPENDENT FORCES

Consider a flat-plate wing displaced upwards from the plane $z = 0$ according to the equation

$$z(x,y,t) = z_j(x,y)q(\tau) \tag{A-1}$$

where $\tau = Ut/\bar{c}$ is non-dimensional time. The motion starts at $\tau = 0$, so that $q(\tau) = 0$ for $\tau \leq 0$ and thereafter

$$q(\tau) = \int_0^\tau \frac{dq(\tau_0)}{d\tau_0}\, d\tau_0 \quad . \tag{A-2}$$

Remembering that

$$\int_0^\infty \frac{\sin \bar{\nu}\tau}{\bar{\nu}}\, d\bar{\nu} = \pm \tfrac{1}{2}\pi \quad \text{according as} \quad \tau \gtrless 0 \ , \tag{A-3}$$

we may write

$$\begin{aligned} q(\tau) &= \int_0^\infty \frac{dq(\tau_0)}{d\tau_0} \left\{ \frac{1}{2} - \frac{1}{\pi} \int_0^\infty \frac{\sin[\bar{\nu}(\tau_0 - \tau)]}{\bar{\nu}}\, d\bar{\nu} \right\} d\tau_0 \\ &= \tfrac{1}{2}q(\infty) - \frac{1}{\pi} \int_0^\infty \int_0^\infty \frac{dq(\tau_0)}{d\tau_0} \frac{\sin[\bar{\nu}(\tau_0 - \tau)]}{\bar{\nu}}\, d\bar{\nu} d\tau_0 \quad . \end{aligned} \tag{A-4}$$

The integrand, regarded as a function of τ, corresponds to the sinusoidal wing motion

$$z_0(x,y,t) = \Re\left[\frac{i}{\bar{\nu}}\, z_j(x,y)\, \frac{dq(\tau_0)}{d\tau_0}\, e^{i\bar{\nu}(\tau - \tau_0)} \right] \tag{A-5}$$

which provides the generalized force coefficient in mode i

$$\begin{aligned} Q_0(\tau) &= \Re\left[\frac{i}{\bar{\nu}} \frac{dq(\tau_0)}{d\tau_0} \left\{ Q'_{ij}(\bar{\nu}) + i\bar{\nu}Q''_{ij}(\bar{\nu}) \right\} e^{i\bar{\nu}(\tau - \tau_0)} \right] \\ &= -\frac{dq(\tau_0)}{d\tau_0} \left\{ \frac{1}{\bar{\nu}}\, Q'_{ij}(\bar{\nu}) \sin[\bar{\nu}(\tau - \tau_0)] + Q''_{ij}(\bar{\nu}) \cos[\bar{\nu}(\tau - \tau_0)] \right\} \quad . \end{aligned} \tag{A-6}$$

Then the generalized force coefficient corresponding to the wing motion given by equations (A-1) and (A-4) is

$$Q_i(\tau) = \tfrac{1}{2}q(\infty)Q'_{ij}(0) - \frac{1}{\pi} \int_0^\infty \int_0^\infty Q_0(\tau)\, d\bar{\nu} d\tau_0 \quad . \tag{A-7}$$

81060

It is important to note that, since the expression for $q(\tau)$ in equation (A-4) is identically zero for $\tau < 0$ and covers the whole range $-\infty < \tau < \infty$, so does the quantity $Q_i(\tau)$ defined by equations (A-6) and (A-7).

With a little rearrangement of terms and the removal of the subscripts i and ij, we may write

$$Q(\tau) = \int_0^\infty \frac{dq(\tau_0)}{d\tau_0} \left\{ \tfrac{1}{2}Q'(0) + \frac{1}{\pi} \int_0^\infty \frac{1}{\bar{\nu}} Q'(\bar{\nu}) \sin[\bar{\nu}(\tau - \tau_0)]\, d\bar{\nu} \right\} d\tau_0$$

$$+ \frac{1}{\pi} \int_0^\infty \int_0^\infty \frac{dq(\tau_0)}{d\tau_0} \{Q''(\bar{\nu}) - Q''(\infty)\} \cos[\bar{\nu}(\tau - \tau_0)]\, d\bar{\nu} d\tau_0$$

$$+ \frac{1}{\pi} Q''(\infty) \int_0^\infty \int_0^\infty \frac{dq(\tau_0)}{d\tau_0} \cos[\bar{\nu}(\tau - \tau_0)]\, d\bar{\nu} d\tau_0 \quad . \qquad \text{(A-8)}$$

Given that $dq(\tau_0)/d\tau_0 = 0$ at $\tau_0 = 0$ and $\tau_0 = \infty$, the factor of $Q''(\infty)$ in the last term of equation (A-8) simplifies on integration by parts with respect to τ_0. Hence

$$\frac{1}{\pi} \int_0^\infty \int_0^\infty \frac{dq(\tau_0)}{d\tau_0} \cos[\bar{\nu}(\tau - \tau_0)]\, d\bar{\nu} d\tau_0 = \frac{1}{\pi} \int_0^\infty \int_0^\infty \frac{d^2q(\tau_0)}{d\tau_0^2} \frac{\sin[\bar{\nu}(\tau - \tau_0)]}{\bar{\nu}} d\bar{\nu} d\tau_0$$

$$= \frac{1}{2} \int_0^\tau \frac{d^2q(\tau_0)}{d\tau_0^2} d\tau_0 - \frac{1}{2} \int_\tau^\infty \frac{d^2q(\tau_0)}{d\tau_0^2} d\tau_0 = \frac{dq(\tau)}{d\tau} , \qquad \text{if } \tau > 0, \quad \text{(A-9)}$$

and vanishes identically if $\tau < 0$. Since $Q(\tau)$ must vanish identically when $\tau \leq 0$, equation (A-8) yields the identity

$$\int_0^\infty \frac{dq(\tau_0)}{d\tau_0} \left[\tfrac{1}{2}Q'(0) + \frac{1}{\pi} \int_0^\infty \left\{ -\frac{1}{\bar{\nu}} Q'(\bar{\nu}) \sin[\bar{\nu}(\tau_0 - \tau)] + [Q''(\bar{\nu}) - Q''(\infty)] \cos[\bar{\nu}(\tau_0 - \tau)] \right\} d\bar{\nu} \right] d\tau_0 = 0$$

whatever the motion $q(\tau_0)$. Therefore for $\sigma \geq 0$

$$\tfrac{1}{2}Q'(0) - \frac{1}{\pi} \int_0^\infty \frac{1}{\bar{\nu}} Q'(\bar{\nu}) \sin \bar{\nu}\sigma \, d\bar{\nu} + \frac{1}{\pi} \int_0^\infty [Q''(\bar{\nu}) - Q''(\infty)] \cos \bar{\nu}\sigma \, d\bar{\nu} = 0 \quad . \qquad \text{(A-10)}$$

This identity allows the upper limits of integration with respect to τ_0 to be changed from ∞ to τ in the first two terms of equation (A-8), which simply expresses that future motion cannot influence the present. Thus by equations (A-8) and (A-9)

$$Q(\tau) = Q''(\infty)\frac{dq(\tau)}{d\tau} + \int_0^{\tau}\frac{dq(\tau_0)}{d\tau_0}\left\{\left\{Q'(0) + \frac{1}{\pi}\int_0^{\infty}\frac{1}{\bar{\nu}}Q'(\bar{\nu})\sin[\bar{\nu}(\tau-\tau_0)]d\bar{\nu}\right\}d\tau_0\right.$$

$$\left. + \frac{1}{\pi}\int_0^{\tau}\int_0^{\infty}\frac{dq(\tau_0)}{d\tau_0}\{Q''(\bar{\nu}) - Q''(\infty)\}\cos[\bar{\nu}(\tau-\tau_0)]d\bar{\nu}d\tau_0\right. . \qquad \text{(A-11)}$$

The relationship in equation (A-10) also allows the elimination of either $Q'(\bar{\nu})$ or $Q''(\bar{\nu})$ from the double integrals for $Q(\tau)$ when $\tau > 0$, so that we obtain alternative expressions

$$Q(\tau) = Q''(\infty)\frac{dq(\tau)}{d\tau} + Q'(0)q(\tau) + \frac{2}{\pi}\int_0^{\tau}\int_0^{\infty}\frac{dq(\tau_0)}{d\tau_0}\{Q''(\bar{\nu}) - Q''(\infty)\}\cos[\bar{\nu}(\tau-\tau_0)]d\bar{\nu}d\tau_0$$

..... (A-12)

and

$$Q(\tau) = Q''(\infty)\frac{dq(\tau)}{d\tau} + \frac{2}{\pi}\int_0^{\tau}\int_0^{\infty}\frac{dq(\tau_0)}{d\tau_0}\frac{Q'(\bar{\nu})}{\bar{\nu}}\sin[\bar{\nu}(\tau-\tau_0)]d\bar{\nu}d\tau_0 \quad . \qquad \text{(A-13)}$$

Appendix B

EVALUATION OF HEREDITARY FUNCTIONS

Three Integrals

The hereditary functions in equations (3-23) involve the following integrals

$$\left.\begin{aligned} I_0(\sigma) &= \int_0^\infty f(\bar{\nu})\bar{\nu} \sin \bar{\nu}\sigma \, d\bar{\nu} \\ I_1(\sigma) &= \int_0^\infty f(\bar{\nu}) \cos \bar{\nu}\sigma \, d\bar{\nu} \\ I_2(\sigma) &= \int_0^\infty f(\bar{\nu}) \frac{\sin \bar{\nu}\sigma}{\bar{\nu}} \, d\bar{\nu} \end{aligned}\right\} \qquad \text{(B-1)}$$

where
$$f(\bar{\nu}) = \frac{Q''_{ij}(\bar{\nu}) - Q''_{ij}(\infty)}{Q'_{ij}(0)} \, . \qquad \text{(B-2)}$$

Each integral is evaluated in three parts by subdividing the range of integration into $0 < \bar{\nu} < \bar{\nu}_\ell$, $\bar{\nu}_\ell < \bar{\nu} < \bar{\nu}_u$ and $\bar{\nu}_u < \bar{\nu} < \infty$. Different integration procedures are used in the three regions.

$0 < \bar{\nu} < \bar{\nu}_\ell$

As explained in section 2.1, $Q''_{ij}(\bar{\nu})$ is given by equation (3-2) so that equation (B-2) becomes

$$f(\bar{\nu}) = \frac{B''_0 - Q''_{ij}(\infty) + B''_1\bar{\nu} + B''_2\bar{\nu}^2 \log \bar{\nu} + B''_3\bar{\nu}^2}{Q'_{ij}(0)} \, . \qquad \text{(B-3)}$$

Typically we take $\bar{\nu}_\ell = 0.08$, subdivide the range into 16 equal parts and evaluate the contributions to the integrals (B-1) by Simpson's Rule, for example

$$\int_0^{0.08} f(\bar{\nu}) \cos \bar{\nu}\sigma \, d\bar{\nu} = \frac{1}{200}\left[\frac{1}{3} f(0) + \frac{4}{3}\sum_{k=1}^{8} f\left(\frac{2k-1}{200}\right) \cos \frac{(2k-1)\sigma}{200}\right.$$

$$\left. + \frac{2}{3}\sum_{k=1}^{7} f\left(\frac{k}{100}\right) \cos \frac{k\sigma}{100} + \frac{1}{3} f(0.08) \cos (0.08\sigma)\right] . \qquad \text{(B-4)}$$

$\bar{\nu}_\ell < \bar{\nu} < \bar{\nu}_u$

All the available values of $Q''_{ij}(\bar{\nu})$ from lifting-surface theory, excluding $\bar{\nu} = 0$, are used to fit a standard cubic spline. Typically the region $0.08 < \bar{\nu} < 6.00$ is subdivided into $2n = 148$ equal parts and the integrands of (B-1) are evaluated without the trigonometrical factor $\sin \bar{\nu}\sigma$ or $\cos \bar{\nu}\sigma$. They are then represented by quadratics over successive double intervals

$$\bar{\nu}_\ell + (2k-2)h < \bar{\nu} < \bar{\nu}_\ell + 2kh \qquad \left(h = \frac{\bar{\nu}_u - \bar{\nu}_\ell}{2n}, \quad k = 1,2,\ldots,n\right) \tag{B-5}$$

as for Simpson's Rule, but in the subsequent integration the trigonometrical factor is treated analytically. The procedure is known as Filon's Rule and is used in preference to Simpson's Rule to ensure the necessary accuracy when σ is large and the trigonometrical factor is of small wavelength. The resulting contributions to $I_1(\sigma)$ and $I_2(\sigma)$ are as follows:

$$\begin{aligned}\int_{\bar{\nu}_\ell}^{\bar{\nu}_u} f(\bar{\nu}) \cos \bar{\nu}\sigma \, d\bar{\nu} = h\Bigg[&\alpha\{f(\bar{\nu}_u) \sin \bar{\nu}_u\sigma - f(\bar{\nu}_\ell) \sin \bar{\nu}_\ell\sigma\} \\ &+ \beta\Bigg\{\sum_{k=1}^{n-1} f(\bar{\nu}_\ell + 2kh) \cos[\sigma(\bar{\nu}_\ell + 2kh)] \\ &\quad + \tfrac{1}{2}f(\bar{\nu}_\ell) \cos \bar{\nu}_\ell\sigma + \tfrac{1}{2}f(\bar{\nu}_u) \cos \bar{\nu}_u\sigma\Bigg\} \\ &+ \gamma \sum_{k=1}^{n} f(\bar{\nu}_\ell + (2k-1)h) \cos[\sigma(\bar{\nu}_\ell + (2k-1)h)]\Bigg]\end{aligned} \tag{B-6}$$

and

$$\begin{aligned}\int_{\bar{\nu}_\ell}^{\bar{\nu}_u} \frac{f(\bar{\nu})}{\bar{\nu}} \sin \bar{\nu}\sigma \, d\bar{\nu} = h\Bigg[&-\alpha\left\{\frac{f(\bar{\nu}_u)}{\bar{\nu}_u} \cos \bar{\nu}_u\sigma - \frac{f(\bar{\nu}_\ell)}{\bar{\nu}_\ell} \cos \bar{\nu}_\ell\sigma\right\} \\ &+ \beta\Bigg\{\sum_{k=1}^{n-1} \frac{f(\bar{\nu}_\ell + 2kh)}{\bar{\nu}_\ell + 2kh} \sin[\sigma(\bar{\nu}_\ell + 2kh)] \\ &\quad + \frac{f(\bar{\nu}_\ell)}{2\bar{\nu}_\ell} \sin \bar{\nu}_\ell\sigma + \frac{f(\bar{\nu}_u)}{2\bar{\nu}_u} \sin \bar{\nu}_u\sigma\Bigg\} \\ &+ \gamma \sum_{k=1}^{n} \frac{f(\bar{\nu}_\ell + (2k-1)h)}{\bar{\nu}_\ell + (2k-1)h} \sin[\sigma(\bar{\nu}_\ell + (2k-1)h)]\Bigg]\end{aligned} \tag{B-7}$$

where with $\theta = \sigma h$

$$\left.\begin{aligned} \alpha &= \frac{\theta^2 + \theta \sin\theta \cos\theta - 2\sin^2\theta}{\theta^3} \\ \beta &= \frac{2[\theta(1+\cos^2\theta) - 2\sin\theta\cos\theta]}{\theta^3} \\ \gamma &= \frac{4[\sin\theta - \theta\cos\theta]}{\theta^3} \end{aligned}\right\} . \qquad \text{(B-8)}$$

$I_0(\sigma)$ is treated in the same way as $I_2(\sigma)$ with $\bar{\nu}f(\bar{\nu})$ replacing $f(\bar{\nu})/\bar{\nu}$ throughout equation (B-7).

$\underline{\bar{\nu}_u < \bar{\nu} < \infty}$

As explained in section 3.2, $Q''_{ij}(\bar{\nu})$ is given by equation (3-17) so that equation (B-2) becomes

$$f(\bar{\nu}) = \left(\frac{A''_1}{\bar{\nu}^2} + \frac{A''_2}{\bar{\nu}^2}\right) \Big/ Q'_{ij}(0) \quad . \qquad \text{(B-9)}$$

The integrals (B-1) are evaluated analytically in terms of the function

$$S_3(x) = \int_x^\infty \frac{\sin\mu}{\mu^3}\, d\mu \quad . \qquad \text{(B-10)}$$

Successive integration yields the results

$$Q'_{ij}(0)\int_{\bar{\nu}_u}^\infty f(\bar{\nu})\bar{\nu}\sin\bar{\nu}\sigma\, d\bar{\nu} = \left(-2A''_1 + A''_2\sigma^2\right)S_3(\bar{\nu}_u\sigma) + \frac{A''_1}{\bar{\nu}_u^2\sigma^2}\left(\sin\bar{\nu}_u\sigma + \bar{\nu}_u\sigma\cos\bar{\nu}_u\sigma\right) \qquad \text{(B-11)}$$

$$Q'_{ij}(0)\int_{\bar{\nu}_u}^\infty f(\bar{\nu})\cos\bar{\nu}\sigma\, d\bar{\nu} = \left(2A''_1\sigma - \frac{A''_2\sigma^3}{3}\right)S_3(\bar{\nu}_u\sigma) - \frac{A''_1}{\bar{\nu}_u^2\sigma}\sin\bar{\nu}_u\sigma + \frac{A''_2}{3\bar{\nu}_u^3}\cos\bar{\nu}_u\sigma \qquad \text{(B-12)}$$

and

$$Q'_{ij}(0)\int_{\bar{\nu}_u}^\infty f(\bar{\nu})\frac{\sin\bar{\nu}\sigma}{\bar{\nu}}\, d\bar{\nu} = \left(A''_1\sigma^2 - \frac{A''_2\sigma^4}{12}\right)S_3(\bar{\nu}_u\sigma) + \frac{A''_2}{12\bar{\nu}_u^4}\left(3\sin\bar{\nu}_u\sigma + \bar{\nu}_u\sigma\cos\bar{\nu}_u\sigma\right) . \qquad \text{(B-13)}$$

The quantity $S_3(x)$ from equation (B-10) is obtained from expansions in series of Chebyshev polynomials by the procedure described in Ref 15. The formulae, due to Davies and hitherto unpublished, are

for $0 < x \leq 7$

$$S_3(x) = -\frac{\pi}{4} + \frac{1}{x} {\sum_{r=0}^{10}}' D_r T_{2r}\left(\frac{x}{7}\right) \qquad \text{(B-14)}$$

and for $7 \leq x < \infty$

$$S_3(x) = \frac{\sin x}{x^4} {\sum_{r=0}^{14}}' A_r T_{2r}\left(\frac{7}{x}\right) - \frac{\cos x}{x^3} {\sum_{r=0}^{12}}' B_r T_{2r}\left(\frac{7}{x}\right) \qquad \text{(B-15)}$$

where the dash $'$ beside the summation sign indicates that the term $r = 0$ is halved. The Chebyshev polynomials $T_{2r}(z)$ are defined in section 3 of Ref 15 and are evaluated by a recurrence relationship. The coefficients A_r, B_r and D_r are given in Table 12 and ensure high accuracy.

Table 1

DEFINITION OF FORCE AND UPWASH MODES

i or j	Force mode		Upwash mode	
	Force	$z_i/\bar{c}$	Motion	w_j/U
1	Lift	1	Heaving	$i\bar{\nu}$
2	Pitching moment	$(x-x_a)/\bar{c}$	Pitching	$1 + i\bar{\nu}(x-x_a)/\bar{c}$
3	Hinge moment	$(x-x_{h3})/\bar{c}$	Trailing-edge control	$1 + i\bar{\nu}(x-x_{h3})/\bar{c}$
4	Hinge moment	$(x-x_{h4})/\bar{c}$	Leading-edge control	$1 + i\bar{\nu}(x-x_{h4})/\bar{c}$
5	Hinge moment	$(x-x_{h5})/\bar{c}$	All-moving tip	$1 + i\bar{\nu}(x-x_{h5})/\bar{c}$
6	Bending moment	$\lvert y\rvert/s$	Sinusoidal gust	$\exp(i\bar{\nu}x/\bar{c})$

The axis positions x_a, $x_{h3}(y)$, $x_{h4}(y)$ and x_{h5} and the spanwise extent of the control surfaces $y_i < y < s$ are defined in Fig 1. In modes 3, 4 and 5 the formulae for $z_i/\bar{c}$ and w_j/U apply over the extent of the control surface, but both quantities are nominally zero over the rest of the planform ($y < y_i$ or $x < x_{h3}(y)$ in mode 3, or $x > x_{h4}(y)$ in mode 4).

Table 2

FORCE COEFFICIENTS FOR OSCILLATING TRAILING-EDGE CONTROL (M = 0.8)

$\tilde{\nu}$	Lift		Pitching moment		Hinge moment	
	$-Q'_{13}$	$-Q''_{13}$	$-Q'_{23}$	$-Q''_{23}$	$-Q'_{33}$	$-Q''_{33}$
0	1.7879	-2.6491	1.8843	-1.1691	0.01827	0.00946
0.05	1.7625	-2.4487	1.8748	-1.0902	0.01827	0.00952
0.15	1.6350	-1.9144	1.8281	-0.8954	0.01826	0.00964
0.40	1.3271	-0.8774	1.7035	-0.5526	0.01834	0.00987
0.60	1.2257	-0.4838	1.6210	-0.4072	0.01856	0.00995
0.75	1.2083	-0.3544	1.5701	-0.3232	0.01881	0.00993
1.00	1.1707	-0.2967	1.5220	-0.2324	0.01929	0.00981
1.20	1.0927	-0.2464	1.4880	-0.1987	0.01974	0.00979
1.50	1.0652	-0.1638	1.4376	-0.1555	0.02082	0.00966
1.80	1.0040	-0.1582	1.3868	-0.1340	0.02181	0.00936
2.10	0.9495	-0.1026	1.3341	-0.1043	0.02316	0.00913
2.40	0.9259	-0.0977	1.2891	-0.0889	0.02425	0.00868
2.70	0.8691	-0.0672	1.2427	-0.0682	0.02533	0.00840
3.00	0.8485	-0.0557	1.1964	-0.0545	0.02616	0.00800
3.30	0.8142	-0.0382	1.1580	-0.0372	0.02673	0.00777
3.60	0.7931	-0.0262	1.1233	-0.0235	0.02721	0.00756
3.90	0.7784	-0.0143	1.0994	-0.0102	0.02767	0.00745
4.20	0.7683	-0.0049	1.0819	+0.0015	0.02830	0.00739
4.50	0.7673	+0.0023	1.0738	0.0104	0.02922	0.00732
4.80	0.7662	0.0082	1.0700	0.0182	0.03024	0.00722
5.10	0.7711	0.0117	1.0706	0.0229	0.03135	0.00709
5.40	0.7694	0.0145	1.0690	0.0270	0.03240	0.00693
5.70	0.7725	0.0168	1.0699	0.0299	0.03331	0.00675
6.00	0.7735	0.0177	1.0712	0.0317	0.03406	0.00658
∞	0.582	0.0514	0.874	0.0735	0.0354	0.00516
$-B'_1$ =	1.8046	-	0.7462	-	0.00058	-

Table 3

FORCE COEFFICIENTS FOR OSCILLATING LEADING-EDGE CONTROL (M = 0.8)

$\bar{\nu}$	Lift		Pitching moment		Hinge moment	
	$-Q'_{14}$	$-Q''_{14}$	$-Q'_{24}$	$-Q''_{24}$	$-Q'_{44}$	$-Q''_{44}$
0	0.1658	-0.0776	0.0220	0.0847	-0.05667	0.00312
0.05	0.1640	-0.0609	0.0214	0.0915	-0.05666	0.00294
0.15	0.1558	-0.0228	0.0190	0.1065	-0.05661	0.00252
0.40	0.1357	+0.0406	0.0174	0.1284	-0.05672	0.00181
0.60	0.1243	0.0714	0.0212	0.1318	-0.05720	0.00166
0.75	0.1209	0.0923	0.0236	0.1320	-0.05775	0.00184
1.00	0.1372	0.1130	0.0284	0.1379	-0.05861	0.00244
1.20	0.1559	0.1072	0.0408	0.1424	-0.05922	0.00270
1.50	0.1564	0.1071	0.0630	0.1424	-0.06076	0.00330
1.80	0.1986	0.1172	0.0948	0.1435	-0.06134	0.00418
2.10	0.2252	0.1022	0.1291	0.1381	-0.06209	0.00453
2.40	0.2505	0.1080	0.1681	0.1365	-0.06222	0.00521
2.70	0.2988	0.1009	0.2126	0.1309	-0.06196	0.00533
3.00	0.3333	0.0969	0.2604	0.1268	-0.06203	0.00555
3.30	0.3782	0.0921	0.3137	0.1206	-0.06185	0.00567
3.60	0.4244	0.0867	0.3688	0.1140	-0.06178	0.00578
3.90	0.4711	0.0807	0.4252	0.1070	-0.06172	0.00590
4.20	0.5206	0.0746	0.4847	0.0994	-0.06141	0.00604
4.50	0.5700	0.0678	0.5444	0.0914	-0.06095	0.00616
4.80	0.6197	0.0607	0.6046	0.0825	-0.06019	0.00624
5.10	0.6665	0.0533	0.6609	0.0734	-0.05941	0.00628
5.40	0.7112	0.0460	0.7162	0.0643	-0.05845	0.00631
5.70	0.7544	0.0386	0.7678	0.0549	-0.05734	0.00631
6.00	0.7928	0.0309	0.8146	0.0454	-0.05608	0.00626
∞	0.977	-0.0514	0.982	-0.0477	-0.0531	0.00516
$-B'_1$ =	0.1674	-	0.0692	-	-0.00165	-

Table 4

FORCE COEFFICIENTS FOR OSCILLATING ALL-MOVING TIP (M = 0.8)

$\bar{v}$	Lift		Pitching moment		Hinge moment	
	$-Q'_{15}$	$-Q''_{15}$	$-Q'_{25}$	$-Q''_{25}$	$-Q'_{55}$	$-Q''_{55}$
0	1.0368	-0.9826	0.9567	-0.0945	0.00029	0.06800
0.05	1.0239	-0.8739	0.9520	-0.0514	0.00027	0.06800
0.15	0.9616	-0.6036	0.9306	+0.0478	0.00016	0.06797
0.40	0.8128	-0.0995	0.8816	0.2092	-0.00078	0.06821
0.60	0.7622	+0.1018	0.8548	0.2675	-0.00208	0.06890
0.75	0.7604	0.1778	0.8382	0.3008	-0.00322	0.06946
1.00	0.7777	0.2039	0.8314	0.3429	-0.00570	0.07029
1.20	0.7546	0.2071	0.8369	0.3544	-0.00834	0.07152
1.50	0.7520	0.2552	0.8423	0.3672	-0.01123	0.07378
1.80	0.7849	0.2361	0.8604	0.3661	-0.01485	0.07550
2.10	0.7418	0.2589	0.8605	0.3720	-0.01587	0.07841
2.40	0.8075	0.2542	0.8880	0.3695	-0.01660	0.07940
2.70	0.7668	0.2572	0.8947	0.3722	-0.01471	0.08196
3.00	0.8182	0.2587	0.9233	0.3659	-0.01170	0.08193
3.30	0.8055	0.2573	0.9290	0.3674	-0.00788	0.08357
3.60	0.8363	0.2562	0.9579	0.3619	-0.00144	0.08285
3.90	0.8356	0.2549	0.9649	0.3605	+0.00241	0.08306
4.20	0.8521	0.2534	0.9820	0.3572	0.00768	0.08244
4.50	0.8600	0.2536	0.9984	0.3566	0.01262	0.08229
4.80	0.8764	0.2512	1.0165	0.3528	0.01713	0.08148
5.10	0.8854	0.2508	1.0324	0.3517	0.02113	0.08134
5.40	0.9036	0.2486	1.0539	0.3487	0.02697	0.08079
5.70	0.9140	0.2465	1.0720	0.3458	0.03208	0.08023
6.00	0.9258	0.2442	1.0859	0.3427	0.03680	0.07952
∞	0.855	0.2331	0.986	0.3271	0.0111	0.07557
$-B'_1$ =	1.0465	-	0.4327	-	0.00026	-

Table 5

VARIOUS CALCULATIONS OF HEREDITARY POSITION FACTOR FOR LIFT DUE TO TRAILING-EDGE CONTROL

σ	Values of $F_0(\sigma)$				
	(a)	(b)	(c)	(d)	(e)
0	−0.0003	0.2270	1.0474	1.3842	1.3842
0.05	+0.0048	0.2274	0.8772	1.0991	1.0991
0.10	0.0095	0.2234	0.7351	0.8676	0.8676
0.20	0.0189	0.2142	0.5265	0.5456	0.5456
0.30	0.0281	0.2056	0.3954	0.3638	0.3638
0.40	0.0370	0.1971	0.3184	0.2752	0.2752
0.60	0.0539	0.1800	0.2494	0.2288	0.2288
0.80	0.0689	0.1631	0.2129	0.2117	0.2117
1.00	0.0816	0.1467	0.1687	0.1664	0.1663
1.40	0.0986	0.1158	0.0785	0.0702	0.0702
1.80	0.1033	0.0887	0.0489	0.0563	0.0563
2.20	0.0964	0.0663	0.0462	0.0531	0.0530
2.60	0.0806	0.0488	0.0369	0.0435	0.0434
3.00	0.0597	0.0364	0.0327	0.0389	0.0388
4.00	0.0136	0.0231	0.0318	0.0309	0.0308
5.00	0.0072	0.0240	0.0307	0.0254	0.0253
6.00	0.0284	0.0255	0.0242	0.0208	0.0206
8.00	0.0139	0.0133	0.0111	0.0180	0.0178
10.00	0.0017	0.0033	0.0059	0.0006	0.0005
12.00	0.0054	0.0039	0.0029	0.0032	0.0032
16.00	0.0013	0.0005	0.0009	0.0008	0.0010
20.00	0.0004	0.0002	0.0005	0.0005	0.0006
30.00	0.0001	0.0001	0.0001	0.0001	0.0001

(a) With $Q''_{13}(\bar{\nu})$ set to zero when $\bar{\nu} > 1.2$.

(b) With $Q''_{13}(\infty) = 0.0514$ and $Q''_{13}(\bar{\nu})$ unspecified for $1.2 < \bar{\nu} \leq 6.0$.

(c) Given 14 values of $Q''_{13}(\bar{\nu})$ in $0 \leq \bar{\nu} \leq 6$ and $Q''_{13}(\infty)$.

(d) Given 24 values of $Q''_{13}(\bar{\nu})$ in $0 \leq \bar{\nu} \leq 6$ and $Q''_{13}(\infty)$.

(e) As for (d), except that $B'_1 = 0$ to suppress logarithmic behaviour for small $\bar{\nu}$.

Table 6

VARIOUS CALCULATIONS OF HISTORY FUNCTION FOR LIFT DUE TO TRAILING-EDGE CONTROL

σ	Values of $H(\sigma)$				
	(a)	(b)	(c)	(d)	(e)
0	1.4817	1.5104	1.5104	1.5104	1.5104
0.05	1.4631	1.4854	1.4788	1.4783	1.4783
0.10	1.4446	1.4610	1.4494	1.4489	1.4489
0.20	1.4076	1.4138	1.3959	1.3963	1.3963
0.30	1.3707	1.3687	1.3477	1.3492	1.3492
0.40	1.3342	1.3257	1.3035	1.3058	1.3059
0.60	1.2623	1.2456	1.2243	1.2271	1.2272
0.80	1.1926	1.1726	1.1552	1.1576	1.1577
1.00	1.1256	1.1062	1.0946	1.0965	1.0967
1.40	1.0018	0.9903	0.9915	0.9919	0.9922
1.80	0.8936	0.8929	0.9020	0.8999	0.9002
2.20	0.8017	0.8099	0.8206	0.8169	0.8172
2.60	0.7252	0.7375	0.7465	0.7423	0.7427
3.00	0.6614	0.6730	0.6783	0.6747	0.6752
4.00	0.5367	0.5348	0.5310	0.5317	0.5322
5.00	0.4291	0.4209	0.4155	0.4195	0.4200
6.00	0.3311	0.3311	0.3303	0.3328	0.3330
8.00	0.2209	0.2224	0.2243	0.2209	0.2204
10.00	0.1694	0.1680	0.1654	0.1684	0.1666
12.00	0.1288	0.1308	0.1308	0.1306	0.1272
16.00	0.0909	0.0923	0.0914	0.0910	0.0850
20.00	0.0682	0.0695	0.0681	0.0681	0.0623
30.00	0.0415	0.0421	0.0415	0.0415	0.0277

(a) With $Q''_{13}(\bar{\nu})$ set to zero when $\bar{\nu} > 1.2$.

(b) With $Q''_{13}(\infty) = 0.0514$ and $Q''_{13}(\bar{\nu})$ unspecified for $1.2 < \bar{\nu} \leq 6.0$.

(c) Given 14 values of $Q''_{13}(\bar{\nu})$ in $0 < \bar{\nu} \leq 6$ and $Q''_{13}(\infty)$.

(d) Given 24 values of $Q''_{13}(\bar{\nu})$ in $0 < \bar{\nu} \leq 6$ and $Q''_{13}(\infty)$.

(e) As for (d), except that $B'_1 = 0$ to suppress logarithmic behaviour for small $\bar{\nu}$.

Table 7

CONTRIBUTIONS TO FORCES DUE TO TRANSIENT DEPLOYMENT OF TRAILING-EDGE CONTROL

(a) Lift, $\tau_1 = 5$

τ	Quasi-steady terms		History term $\Delta L/L_0$	Total force L/L_0
	Control angle	Control rate		
0.5	0.047	-0.369	0.350	0.028
1.0	0.262	-0.874	0.765	0.153
1.5	0.593	-1.004	0.773	0.362
2.0	0.885	-0.655	0.349	0.578
2.5	1.000	0.000	-0.292	0.708
3.0	0.885	0.655	-0.842	0.698
3.5	0.593	1.004	-1.038	0.558
4.0	0.262	0.874	-0.777	0.359
4.5	0.047	0.369	-0.218	0.197
5.0	0.000	0.000	+0.125	0.125

(b) Lift, $\tau_1 = 40$

τ	Quasi-steady terms		History term $\Delta L/L_0$	Total force L/L_0
	Control angle	Control rate		
4	0.047	-0.046	0.031	0.032
8	0.262	-0.109	0.049	0.202
12	0.593	-0.125	0.027	0.494
16	0.885	-0.082	-0.016	0.787
20	1.000	0.000	-0.053	0.947
24	0.885	0.082	-0.067	0.899
28	0.593	0.125	-0.050	0.668
32	0.262	0.109	-0.010	0.361
36	0.047	0.046	0.031	0.124
40	0.000	0.000	0.033	0.033

(c) Hinge moment, $\tau_1 = 5$

τ	Quasi-steady terms		History term	Total force
	Control angle	Control rate		
0.5	0.047	0.129	-0.028	0.147
1.0	0.262	0.305	-0.024	0.543
1.5	0.593	0.351	0.011	0.955
2.0	0.885	0.229	0.045	1.159
2.5	1.000	0.000	0.054	1.054
3.0	0.885	-0.229	0.036	0.691
3.5	0.593	-0.351	-0.001	0.241
4.0	0.262	-0.305	-0.038	-0.081
4.5	0.047	-0.129	-0.054	-0.136
5.0	0.000	0.000	-0.024	-0.024

Table 8

USEFULNESS OF QUASI-STEADY APPROXIMATIONS TO TRANSIENT LIFT AND HINGE MOMENT

(Errors are given as percentages of the peak steady value)

Motion	Force	τ_1	One-term approximation		Two-term approximation	
			Maximum error	Rms error	Maximum error	Rms error
Pitching	Lift	5	35.9	20.8	67.1	41.1
		10	18.3	10.1	32.4	19.2
		20	8.4	4.8	13.8	8.0
		40	3.7	2.3	4.9	2.9
		80	1.8	1.2	1.5	0.9
Trailing-edge control	Lift	5	31.2	18.0	103.8	62.9
		10	23.8	14.6	48.5	28.7
		20	16.8	10.9	19.7	11.6
		40	10.4	7.0	6.7	4.0
Trailing-edge control	Hinge moment	5	37.0	24.7	5.4	3.6
		10	18.6	12.5	1.5	0.9
		20	9.1	6.2	0.4	0.2
		40	4.5	3.0	0.1	0.1
Leading-edge control	Lift	20	9.3	5.4	14.2	8.4
		40	3.9	2.4	5.0	3.0
Leading-edge control	Hinge moment	20	0.7	0.4	0.4	0.2
		40	0.4	0.3	0.1	0.1
All-moving tip	Lift	20	11.1	7.1	16.9	10.0
		40	6.5	4.3	5.8	3.5

Table 9

ANALYSIS OF ROOT MEAN SQUARE ERRORS WITH QUASI-STEADY APPROXIMATIONS

Motion	Force	Equal with one and two terms		Errors below 5%	
		Rms error	τ_1	With one term	With two terms
Pitching	Lift	1.6%	55	$\tau_1 > 19$	$\tau_1 > 28$
Trailing-edge control	Lift	10%	23	$\tau_1 > 65$	$\tau_1 > 36$
Leading-edge control	Lift	2.0%	50	$\tau_1 > 21$	$\tau_1 > 28$
All-moving tip	Lift	5.2%	31	$\tau_1 > 33$	$\tau_1 > 32$
Trailing-edge control	Hinge moment	-	-	$\tau_1 > 24$	$\tau_1 > 4$
Leading-edge control	Hinge moment	-	-	$\tau_1 > 4$	$\tau_1 > 2$

Table 10

TRANSIENT LIFT DUE TO WING AND CONTROL-SURFACE MOTIONS

(a) $\tau_1 = 5$

τ	$\frac{\theta}{\theta_0}$ or $\frac{\delta}{\delta_0}$	Values of L/L_0			
		Pitching	Trailing-edge control	Leading-edge control	All-moving tip
0.25	0.0069	0.0439	0.0050	0.0089	0.0232
0.5	0.0467	0.1567	0.0280	0.1069	0.0943
1.0	0.2621	0.4875	0.1529	0.5213	0.3420
1.5	0.5927	0.7996	0.3624	0.9145	0.6170
2.0	0.8847	0.9397	0.5782	1.0558	0.7891
2.5	1.0000	0.8463	0.7082	0.8865	0.7835
3.0	0.8847	0.5660	0.6981	0.4962	0.6085
3.5	0.5927	0.2334	0.5580	0.0734	0.3502
4.0	0.2621	0.0102	0.3590	−0.1735	0.1362
4.5	0.0467	−0.0118	0.1974	−0.1282	0.0628
5.0	0.0000	+0.0532	0.1251	+0.0893	0.0879
6.0	0.0000	0.0424	0.0821	0.1033	0.0726
8.0	0.0000	0.0351	0.0539	0.0648	0.0494
12.0	0.0000	0.0115	0.0116	0.0131	0.0042
18.0	0.0000	0.0021	0.0027	0.0015	0.0026
30.0	0.0000	0.0004	0.0004	0.0004	0.0004

(b) $\tau_1 = 40$

τ	$\frac{\theta}{\theta_0}$ or $\frac{\delta}{\delta_0}$	Values of L/L_0			
		Pitching	Trailing-edge control	Leading-edge control	All-moving tip
0.8	0.0005	0.0012	0.0003	0.0010	0.0008
2.0	0.0069	0.0102	0.0043	0.0107	0.0076
4.0	0.0467	0.0538	0.0320	0.0554	0.0441
8.0	0.2621	0.2638	0.2019	0.2641	0.2347
12.0	0.5927	0.5756	0.4940	0.5744	0.5363
16.0	0.8847	0.8513	0.7870	0.8495	0.8197
20.0	1.0000	0.9638	0.9466	0.9621	0.9547
24.0	0.8847	0.8614	0.8994	0.8608	0.8791
28.0	0.5927	0.5925	0.6677	0.5931	0.6286
32.0	0.2621	0.2848	0.3614	0.2863	0.3221
36.0	0.0467	0.0800	0.1238	0.0816	0.1018
40.0	0.0000	0.0231	0.0325	0.0232	0.0278
46.0	0.0000	0.0062	0.0072	0.0062	0.0065
52.0	0.0000	0.0025	0.0028	0.0025	0.0026
64.0	0.0000	0.0007	0.0008	0.0007	0.0007
80.0	0.0000	0.0002	0.0003	0.0002	0.0002

Table 11

LIFT DUE TO RAPID DEPLOYMENT OF TRAILING-EDGE CONTROL ($\tau_1 = 5$)

τ	Full* calculation	Truncation† in frequency parameter at:			
		$\bar{\nu}_u = 4.91$	$\bar{\nu}_u = 2.45$	$\bar{\nu}_u = 1.84$	$\bar{\nu}_u = 1.23$
0	0.0000	-0.0010	-0.0066	-0.0280	0.0326
0.1	0.0006	+0.0002	-0.0039	-0.0203	0.0517
0.5	0.0280	0.0288	+0.0325	+0.0410	0.1411
1.0	0.1529	0.1528	0.1559	0.1871	0.2720
1.5	0.3624	0.3631	0.3601	0.3829	0.4035
2.0	0.5782	0.5787	0.5777	0.5686	0.5113
2.5	0.7082	0.7088	0.7114	0.6792	0.5748
3.0	0.6981	0.6986	0.6983	0.6755	0.5821
3.5	0.5580	0.5586	0.5548	0.5640	0.5330
4.0	0.3590	0.3588	0.3612	0.3924	0.4391
4.5	0.1974	0.1983	0.2033	0.2248	0.3205
5.0	0.1251	0.1239	0.1193	0.1106	0.2008
5.5	0.0964	0.0971	0.0927	0.0643	0.1012
6.0	0.0821	0.0815	0.0859	0.0666	0.0354
7.0	0.0650	0.0650	0.0631	0.0872	0.0115
8.0	0.0538	0.0540	0.0538	0.0488	0.0632
10.0	0.0396	0.0386	0.0366	0.0497	0.0500
12.0	0.0116	0.0120	0.0104	0.0016	-0.0087
16.0	0.0045	0.0051	0.0065	0.0030	-0.0098
20.0	0.0012	0.0019	0.0010	0.0069	+0.0064
Rms error $0.5 \leq \tau \leq 5.0$		0.1%	0.4%	2.3%	9.6%

* Total force as in Table 7(a).

† Fourier transform calculations with finite range of integration $0 \leq \bar{\nu} \leq \bar{\nu}_u$.

Table 12

COEFFICIENTS IN EQUATIONS (B-14) AND (B-15) OF APPENDIX B

r	A_r	B_r	D_r
0	5.18081405	-1.81985802	7.1517184311
1	-0.36052882	0.08176881	2.2011779268
2	0.04113346	-0.00718178	-0.3109142653
3	-0.00635944	0.00092653	0.0555982922
4	0.00121010	-0.00015385	-0.0074123262
5	-0.00026811	0.00003058	0.0007046314
6	0.00006679	-0.00000697	-0.0000490713
7	-0.00001827	0.00000177	0.0000025918
8	0.00000540	-0.00000049	-0.0000001070
9	-0.00000170	0.00000015	0.0000000035
10	0.00000057	-0.00000004	-0.0000000001
11	-0.00000020	0.00000002	-
12	0.00000007	-0.00000001	-
13	-0.00000003	-	-
14	0.00000001	-	-

LIST OF SYMBOLS

a_p	coefficients (p = 0,1,2) in equation (3-13)
A'_p	coefficients (p = 0,1,2) in equation (3-16)
A''_p	coefficients (p = 0,1,2) in equation (3-17)
A_r, B_r, D_r	coefficients (r = 0,1,2,....) in Table 12
b_p	coefficients (p = 0,1,2,3) in equation (3-13)
B'_p	coefficients (p = 0,1,2,3) in equation (3-1)
B''_p	coefficients (p = 0,1,2,3) in equation (3-2)
c	local chord of wing
$\bar{c}$	mean chord of wing (see Fig 1)
c_K, c_R, c_T	crank chord, root chord, tip chord (see Fig 1)
e	subscript denoting empirical value
f	function in equation (B-2)
F_0	hereditary position factor in equations (2-25)
F_1	hereditary velocity factor in equation (2-22) or (2-23)
F_2	hereditary acceleration factor in equation (2-31)
g	planform rounding function in equation (2-7)
h	subdivided interval in equation (B-5)
H	history function in equation (2-35)
i	$\sqrt{-1}$; integer or subscript denoting force mode (see Table 1)
I	integral in equation (4-24) or (4-25)
I_p	integrals (p = 0,1,2) in equations (B-1)
j	integer or subscript denoting upwash mode (see Table 1)
J	hereditary function in equation (4-12)
k	variable integer
K	Küssner kernel function in equation (2-3)
K	number of terms of series in equation (5-12)
ℓ_j	complex wing loading in equation (2-4)
L	instantaneous lift force in equations (2-13) and (4-22)
L_0	peak value of quasi-steady lift force
L_1	final steady lift force
m	number of spanwise terms
M	Mach number of stream
$\mathcal{M}$	instantaneous pitching moment
(n)	superscript denoting nth iteration
N	number of chordwise terms
q_i	integers (i = 1,2,...,N) (see Ref 5)

LIST OF SYMBOLS (continued)

q, q_j	time-dependent factor for mode j in equations (2-18), (4-1) and (A-1)
Q_0	elementary generalized force coefficient in equation (A-6)
Q_i	time-dependent force coefficient in mode i
Q_{ij}	complex generalized force coefficient in equation (2-6)
Q'_{ij}	real part of Q_{ij}
Q''_{ij}	imaginary part of $Q_{ij}/\bar{v}$
Q_H, Q_R	quantities in equation (4-3)
$R^{(n)}$	iterative integral in equation (5-7)
$\mathcal{R}$	real part of
s	semi-span of wing
S_3	integral in equation (B-10)
t	time
t_1	duration of wing or control-surface motion
T_{2r}	Chebyshev polynomials (r = 0,1,2,....)
U	speed of stream
w_j	upwash angle in mode j (see equation (2-2) and Table 1)
x	streamwise coordinate (see Fig 1)
x_a	location of pitching axis (see Fig 1)
x_{hj}	local x-coordinate of hinge line (j = 3,4,5 in Fig 1)
x_ℓ	x-coordinate of local leading edge
$x_{\ell T}$	location of tip leading edge (see Fig 1)
x_t	x-coordinate of local trailing edge
y	spanwise coordinate (see Fig 1)
y_i	y-coordinate of inboard end of control surface (i = 3,4,5)
y_K	y-coordinate of crank station (see Fig 1)
z	upward displacement from planform
z_0	elementary sinusoidal wing motion in equation (A-5)
z_i, z_j	force mode in Table 1, displacement in equation (2-1)
α, β, γ	functions in equations (B-8)
α_k, β_k	coefficients and factors in equation (5-12)
δ	instantaneous control deflection angle in streamwise plane (radians)
δ_0	peak value of δ (radians unless otherwise stated)
δ_1	final control deflection angle

LIST OF SYMBOLS (concluded)

ΔC_p	lift per unit area/$\frac{1}{2}\rho U^2$
ΔL	contribution to L from integral in equation (2-34)
θ	instantaneous angle of pitch with heave constraint
θ_0	peak value of θ
$\kappa, \bar{\kappa}$	empirical correction factors
λ	planform rounding variable in equations (2-8) and (2-9)
$\bar{\nu}$	frequency parameter, $\omega\bar{c}/U$
$\bar{\nu}_\ell, \bar{\nu}_u$	lower and upper values subdividing the range $0 < \bar{\nu} < \infty$
ρ	density of stream
σ	distance of travel in mean chords, $Ut/\bar{c}$
σ_1	value of σ above which equation (5-2) is used for F_1
σ_m	value of σ, if any, where $H(\sigma)$ is a maximum
τ	non-dimensional time, $Ut/\bar{c}$
τ_1	non-dimensional duration of motion, $Ut_1/\bar{c}$
τ_2	value of τ when L/L_0 has fallen to 0.01
ϕ, ϕ_h	angular chordwise parameters in equations (4-21)
ω	circular frequency

REFERENCES

No.	Author	Title, etc
1	H. Lomax	Indicial aerodynamics. AGARD Manual on Aeroelasticity, Vol II, Chapter 6 (1960)
2	C.G.B. Mitchell	Calculation of the response of a flexible aircraft to harmonic and discrete gusts by a transform method. RAE Technical Report 65264, ARC R&M 3498 (1965)
3	H. Körner	Theoretical aerodynamic methods for active control devices. Aerodynamic Characteristics of Controls, AGARD-CP-262, Paper 1 (1979)
4	G.J. Hancock	Role of unsteady aerodynamics in aircraft response. Special Course on Unsteady Aerodynamics, AGARD-R-679, Paper 8 (1980)
5	D.E. Davies	Theoretical determination of subsonic oscillatory airforce coefficients. RAE Technical Report 76059, ARC R&M 3804 (1976)
6	D.E. Davies	On the use of Fortran programs for evaluating the generalised airforces and aerodynamic loading on a flat plate wing oscillating harmonically in subsonic flow. RAE Technical Memorandum Structures 881 (1976)
7	J.A. Drischler	Calculation and compilation of the unsteady-lift functions for a rigid wing subjected to sinusoidal gusts and to sinusoidal sinking oscillations. NACA Technical Note 3748 (1956)
8	D.L. Woodcock	Aerodynamic modelling for studies of aircraft dynamics. RAE Technical Report 81016 (1981)
9	H.C. Garner	A phenomenon of subsonic aerodynamic loading from rapid aileron oscillations. RAE Technical Report 80025 (1980)
10	H.C. Garner R.D. Milne	Asymptotic expansion for transient forces from quasi-steady subsonic wing theory. Aeronaut. Q., Vol XVII, pp 343-350 (1966)
11	H. Ashley G. Zartarian	Piston theory - A new aerodynamic tool for the aeroelastician. J. Aeronaut. Sci., Vol 23, pp 1109-1118 (1956)
12	H.C. Garner Doris E. Lehrian	The theoretical treatment of slowly oscillating part-span control surfaces in subsonic flow. ARC R&M 3676 (1969)

REFERENCES (concluded)

No.	Author	Title, etc
13	J.W. Cooley J.W. Tukey	An algorithm for the machine calculation of complex Fourier series. Mathematics of Computation, Vol 19, No.90, pp 297-301 (1965)
14	R. Vepa	Finite state modelling of aeroelastic systems. NASA-CR-2779 (1977)
15	D.E. Davies	Expansions in series of Chebyshev polynomials of a function occurring in linear unsteady aerodynamic theory. RAE Technical Report 77110 (1977)

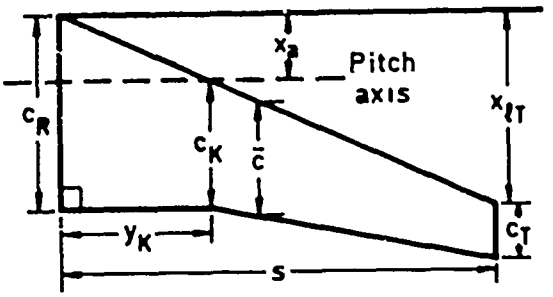

$\bar{c}$ = 1.000 s = 3.996
c_R = 1.690 y_K = 1.389
c_K = 1.101 x_a = 0.592
c_T = 0.478 $x_{\ell T}$ = 1.693

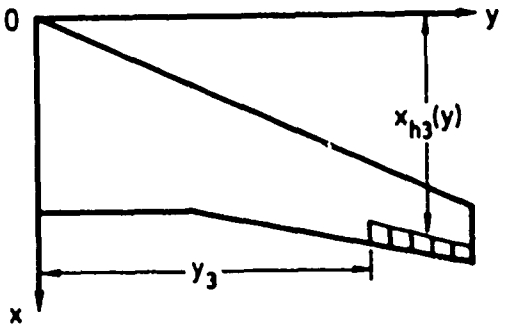

Trailing - edge control
25% chord
y_3 = 3.061
$x_{h3}(y) = 1.075 + 0.244y$

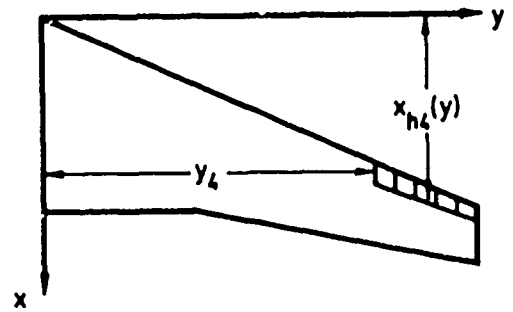

Leading - edge control
25% chord
y_4 = 3.061
$x_{h4}(y) = 0.358 + 0.364y$

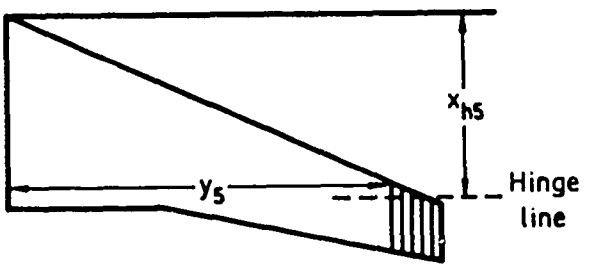

All - moving tip
y_5 = 3.529
x_{h5} = 1.638

TR 81060

Fig 1 Planform of wing and control surfaces

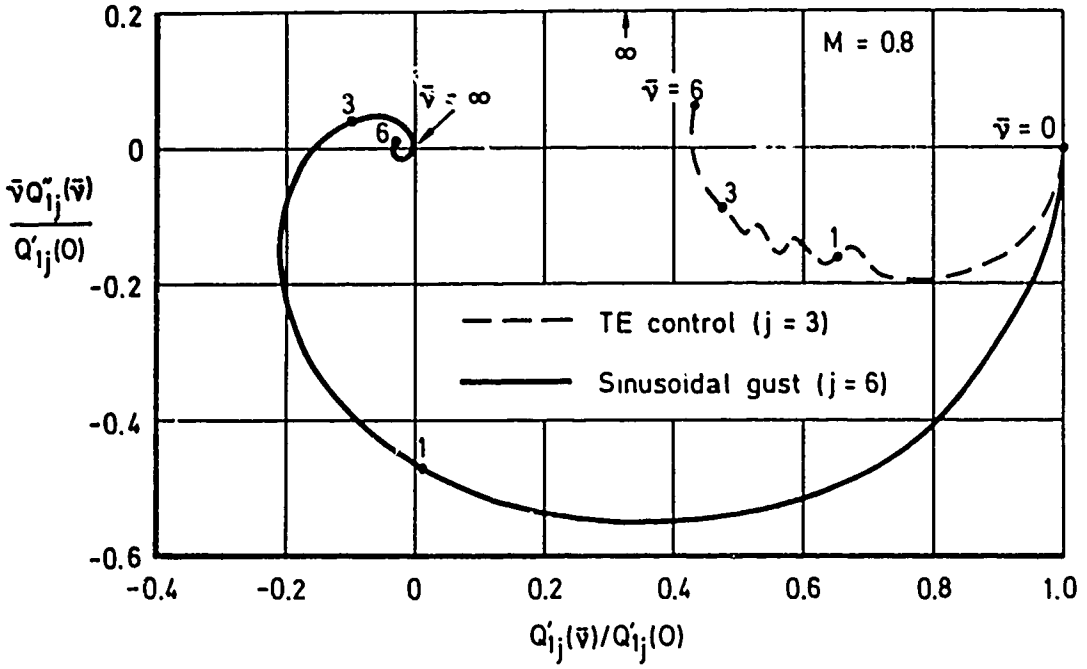

a Argand diagrams for oscillatory motion

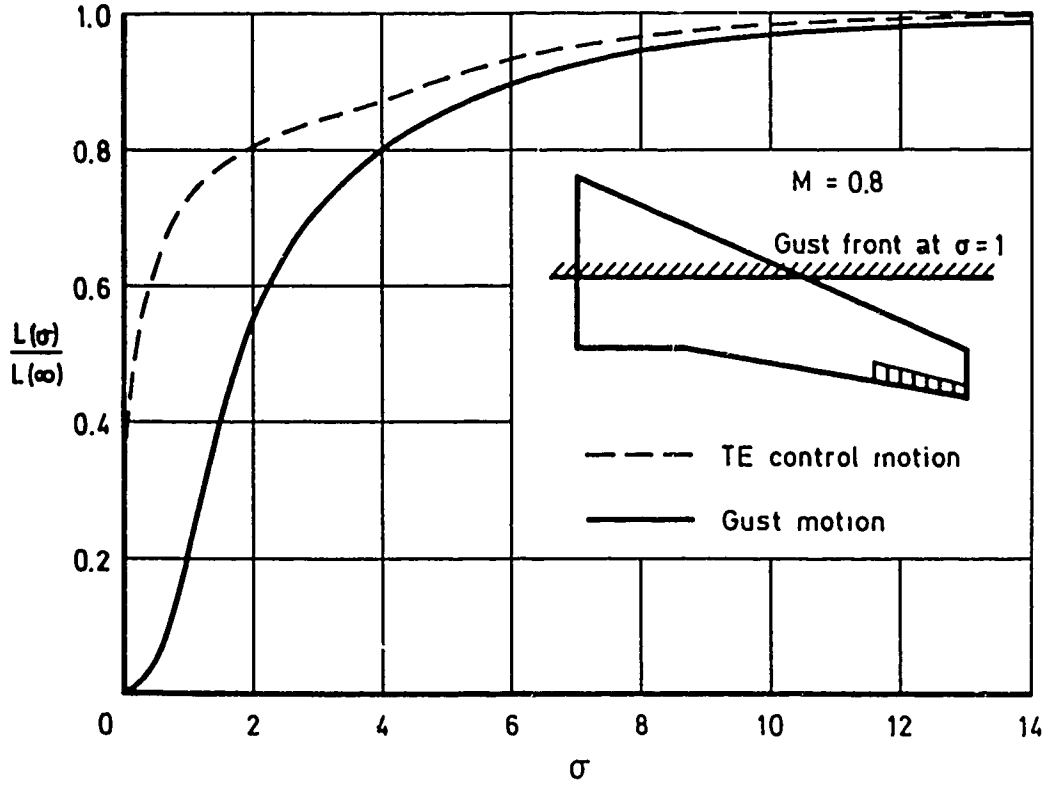

b Growth of lift for step motions

TR 81060

Fig 2a&b Normalized lift from oscillatory and step motions

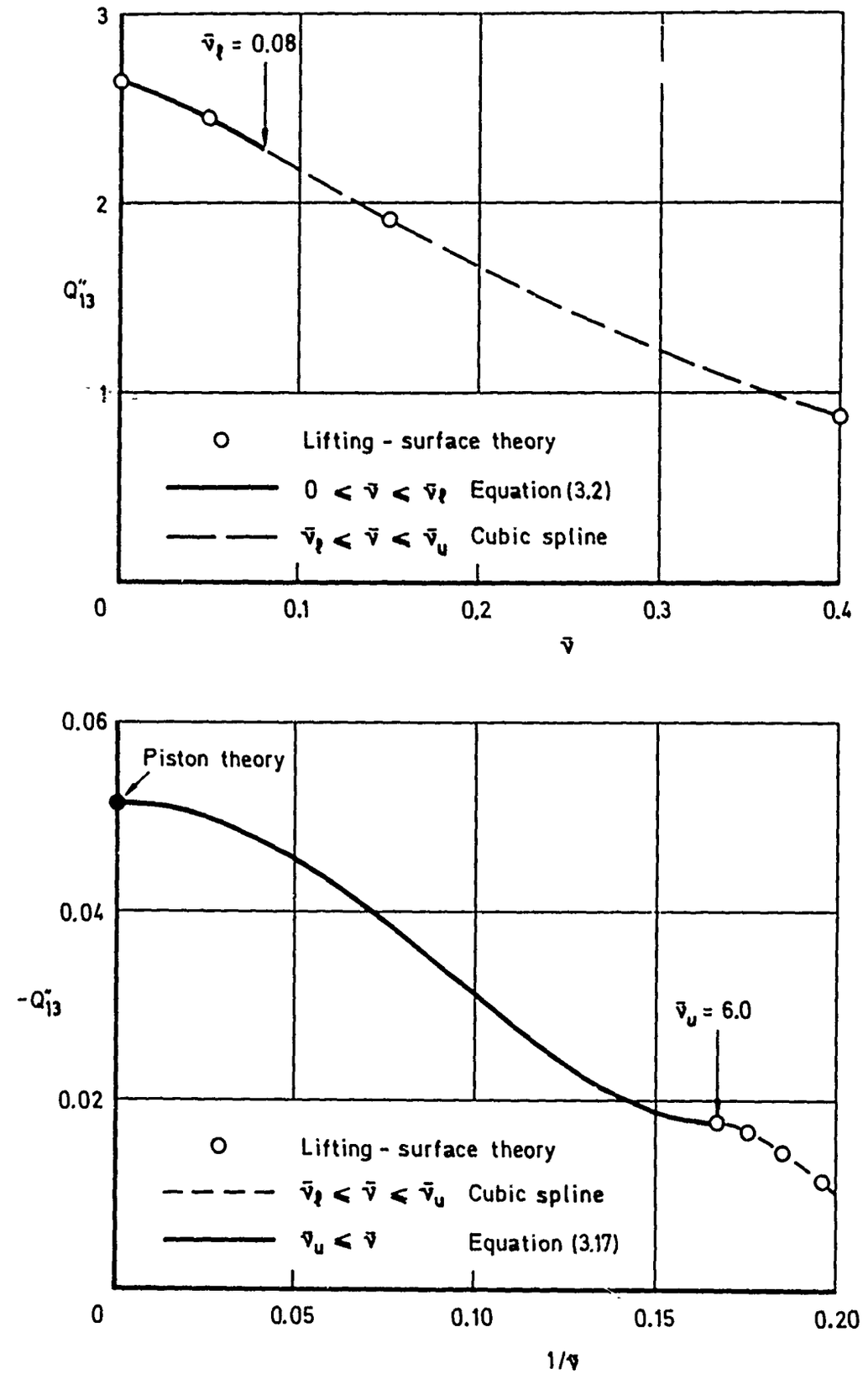

TR 81060

Fig 3 Matching of $Q''_{13}(\bar{\nu})$ at $\bar{\nu} = \bar{\nu}_\ell$ and $\bar{\nu} = \bar{\nu}_u$

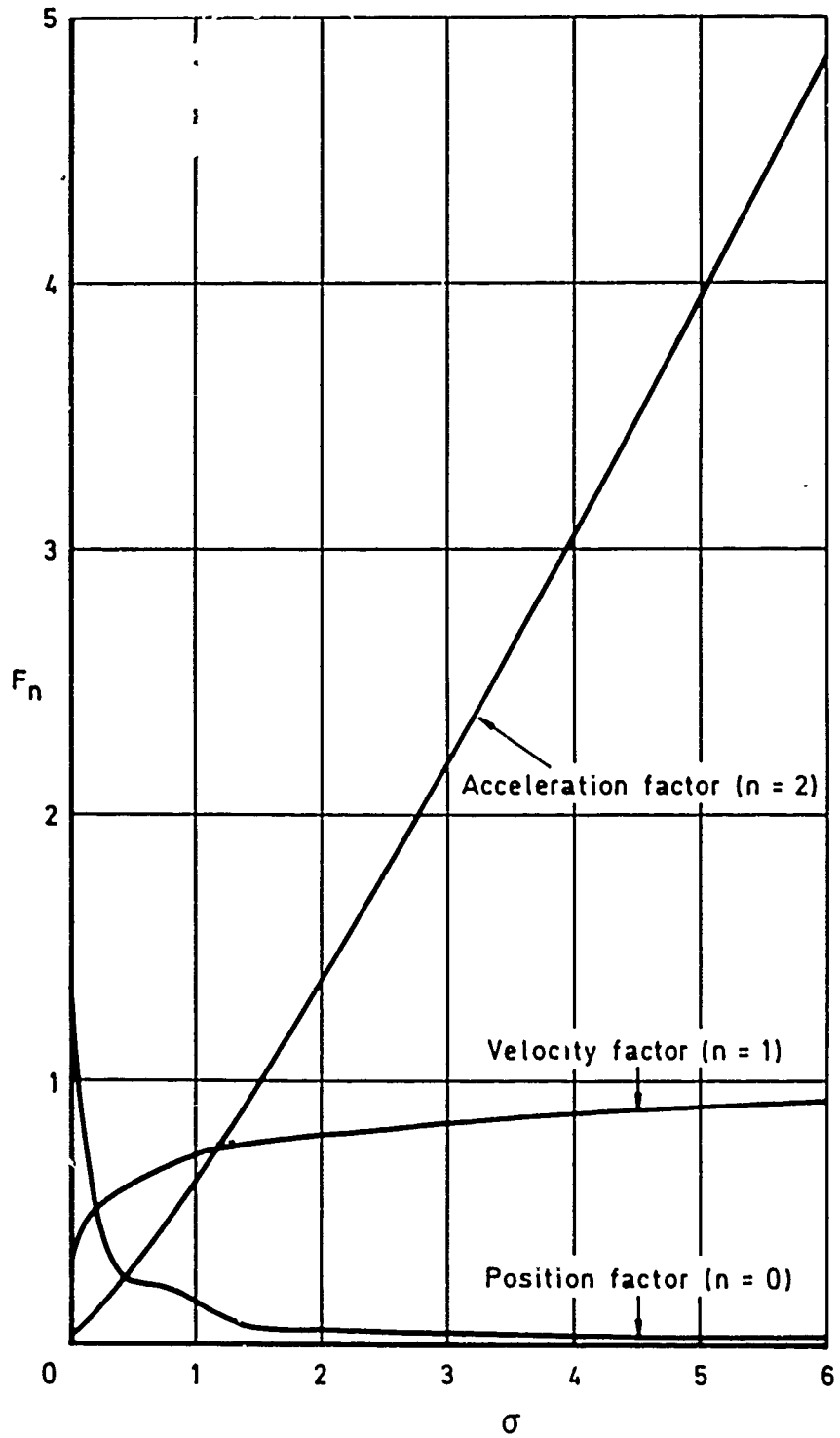

a Lift due to trailing - edge control at M = 0.8

Fig 4a Three hereditary functions

TR 81060

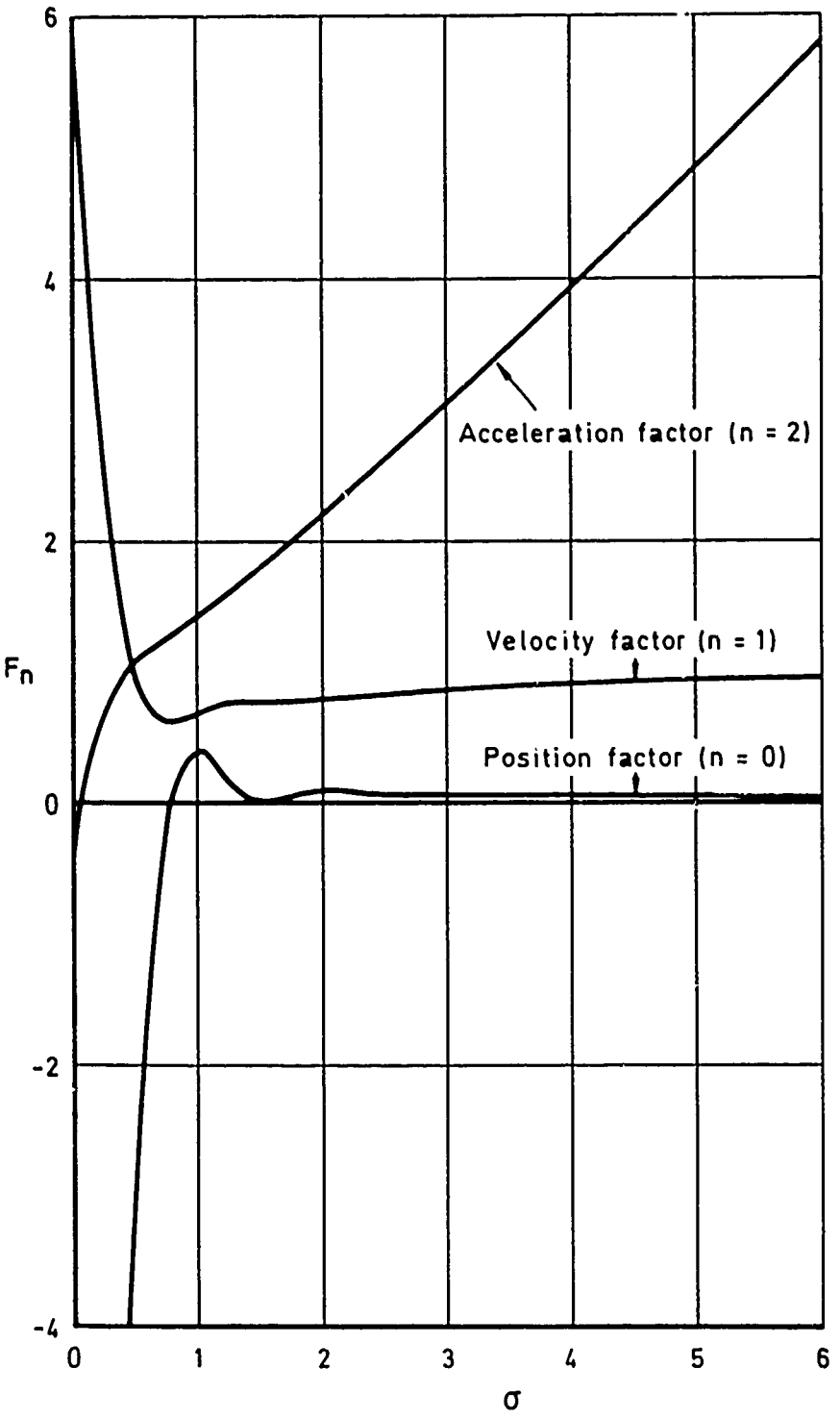

b Lift due to leading-edge control at M = 0.8

Fig 4b Three hereditary functions

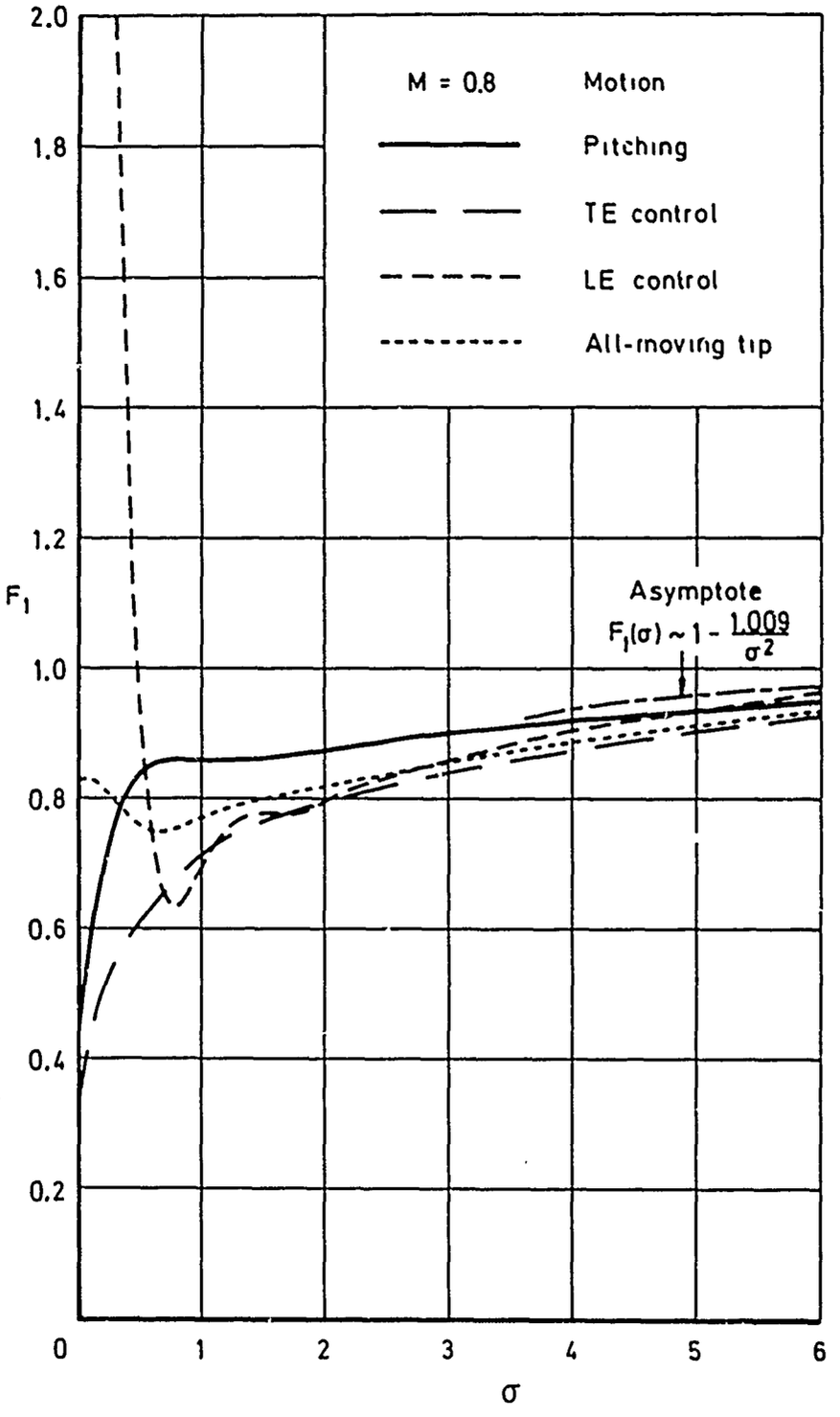

Fig 5 Velocity factors for lift in various motions

TR 81060

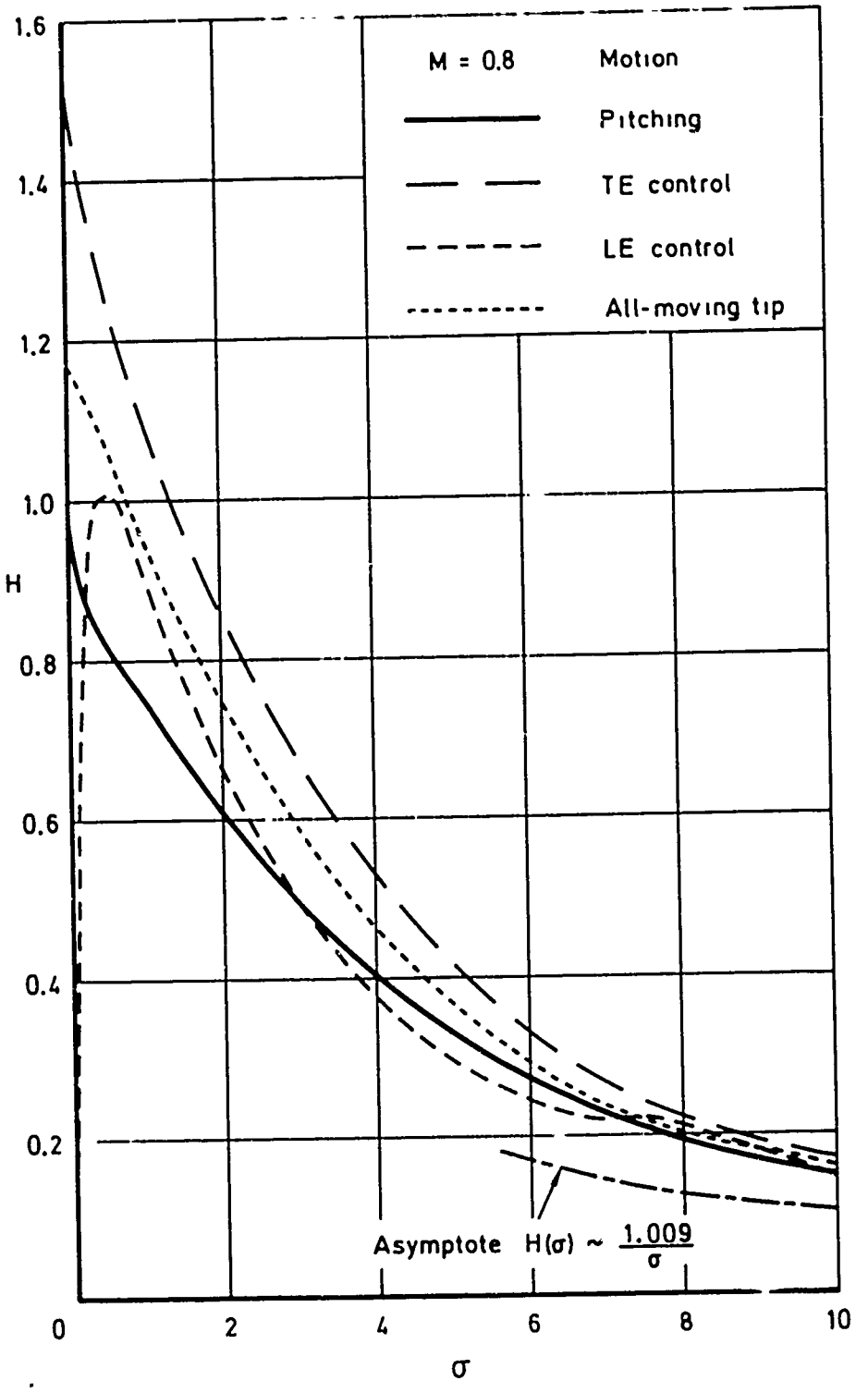

Fig 6 History functions for lift in various motions

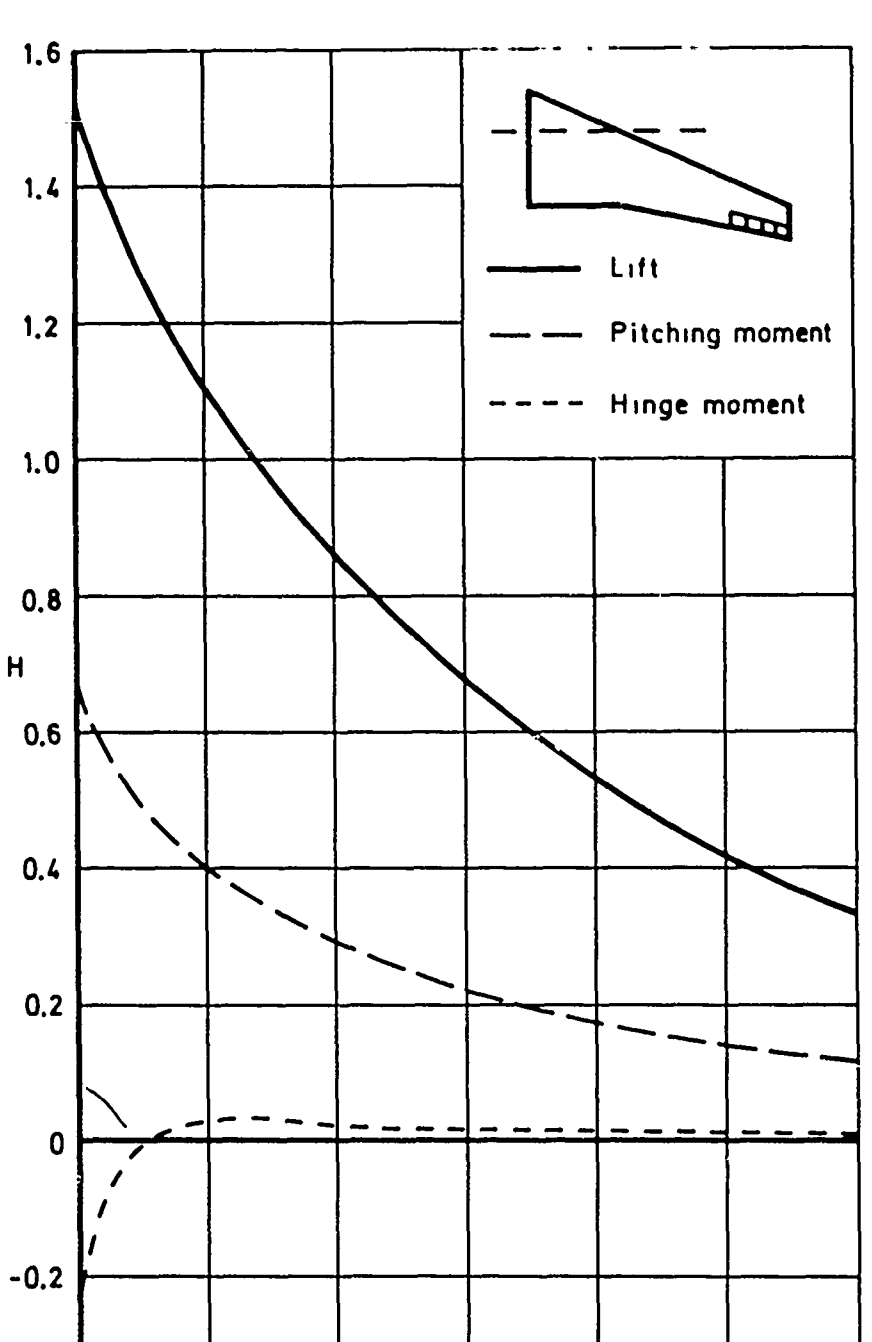

Fig 7 Various history functions for trailing-edge control motion

TR 81060

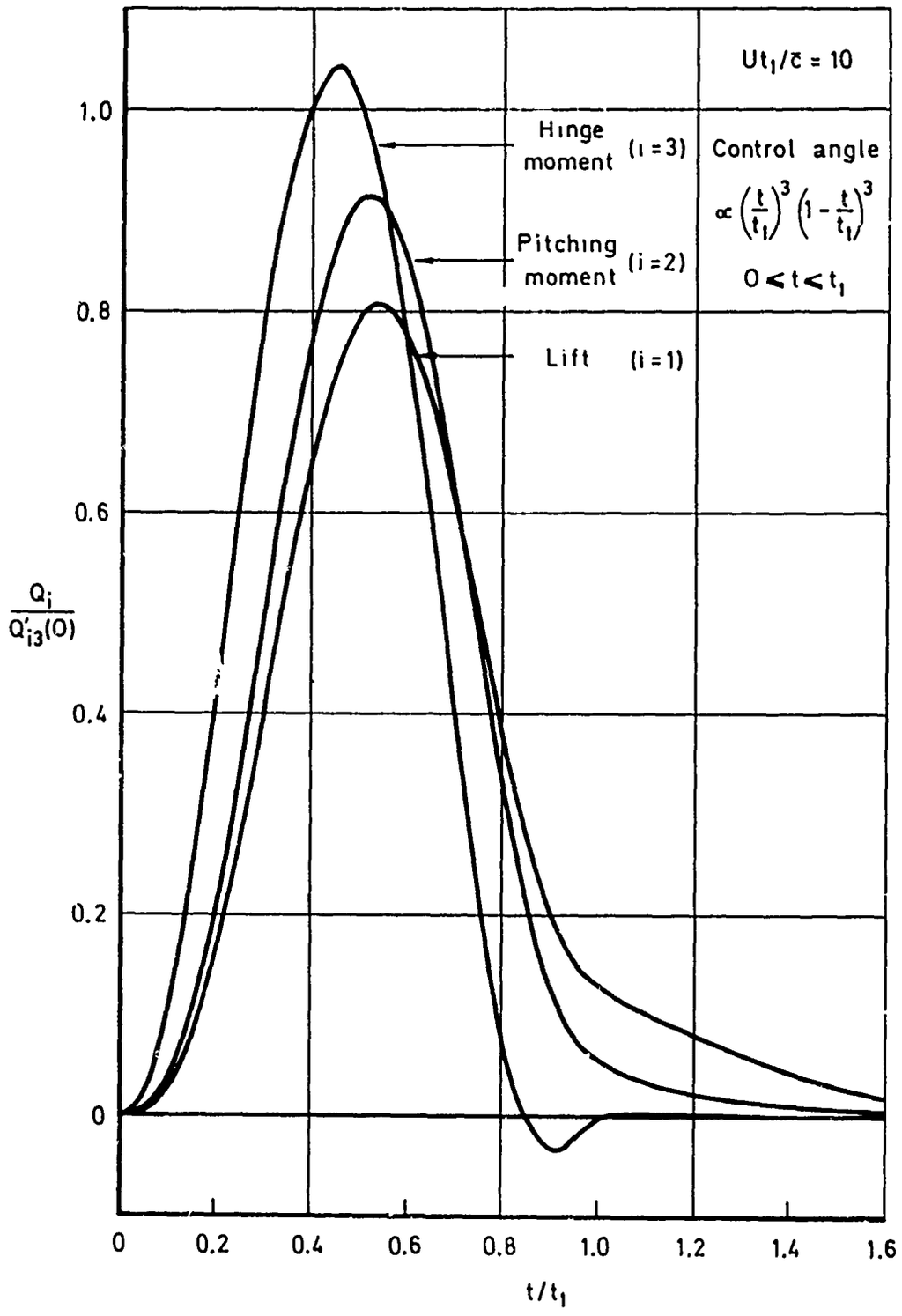

Fig 8 Time-dependent forces for trailing-edge control motion

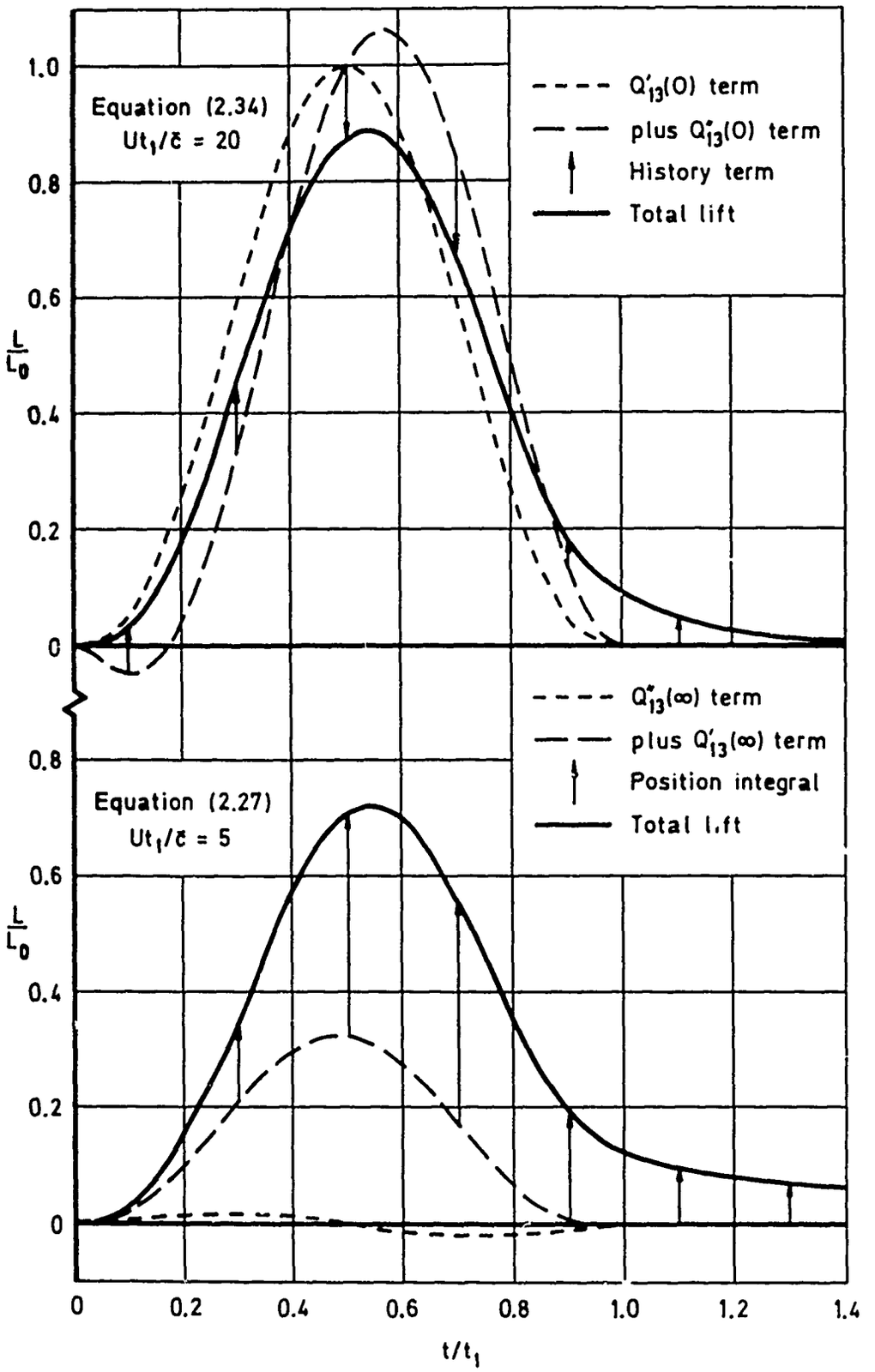

TR 81060

Fig 9 Contributions to lift from trailing-edge control

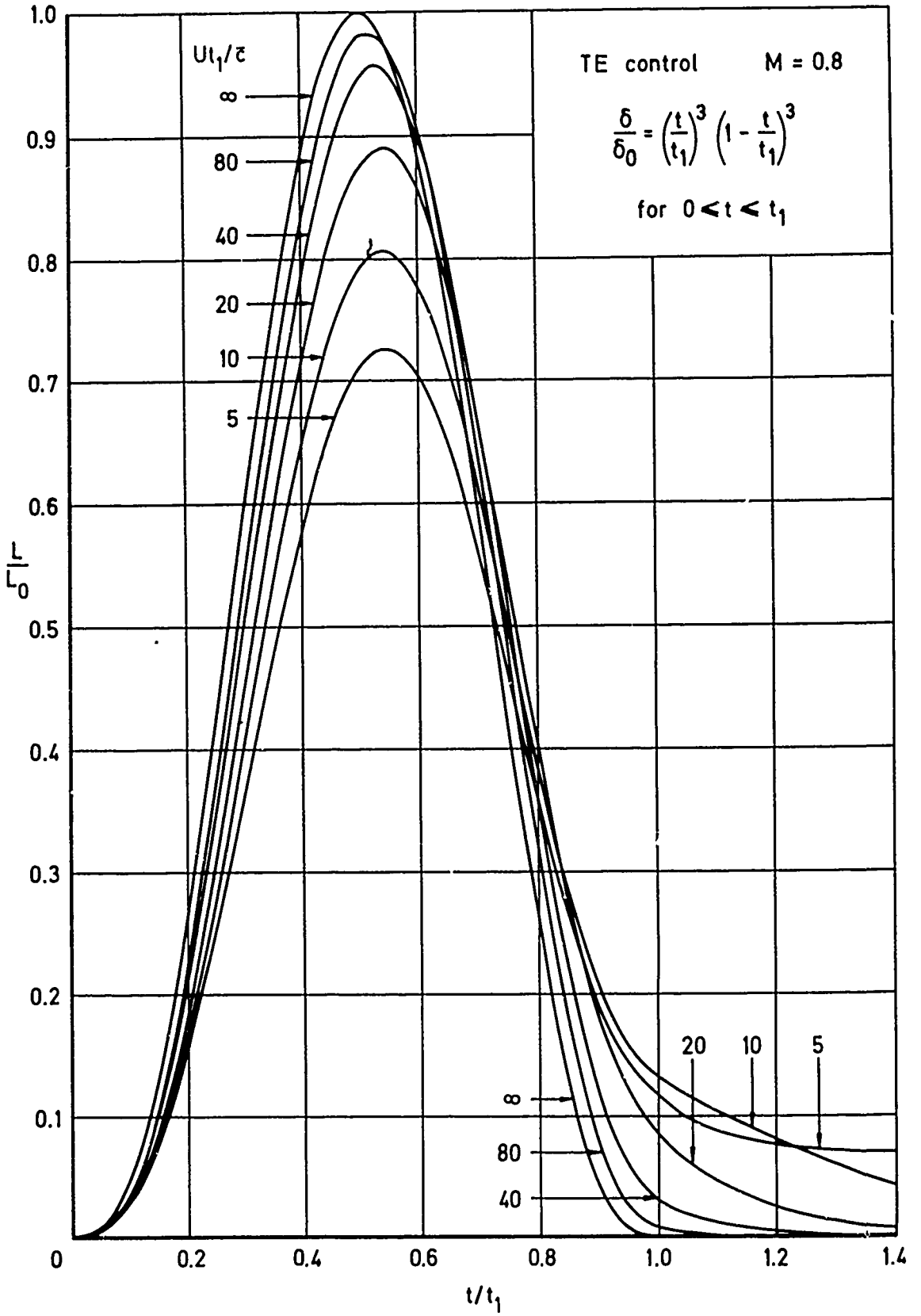

TR 81060

Fig 10 Influence of excursion time on transient lift

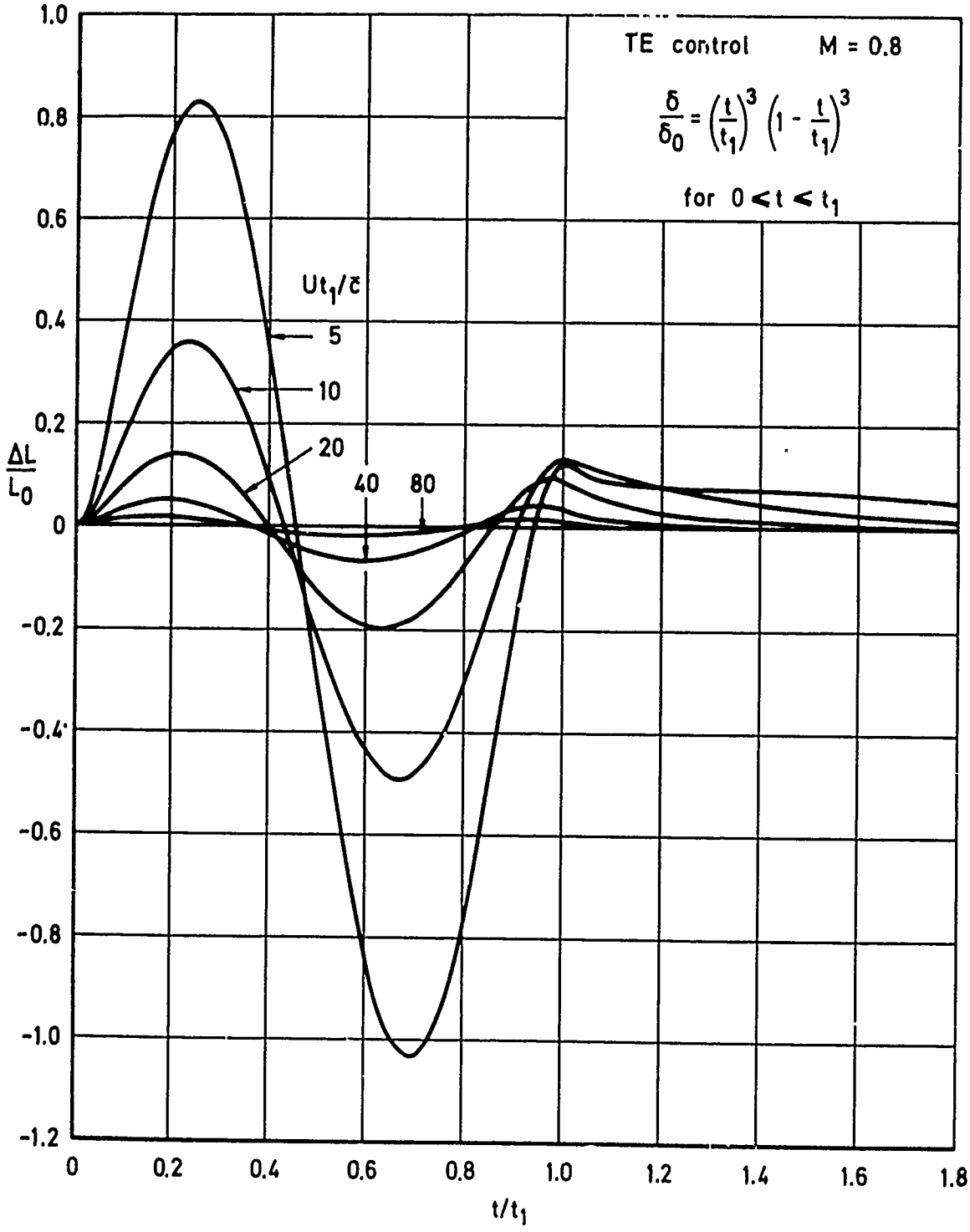

Fig 11 Contribution of history function to L/L_0

TR 81060

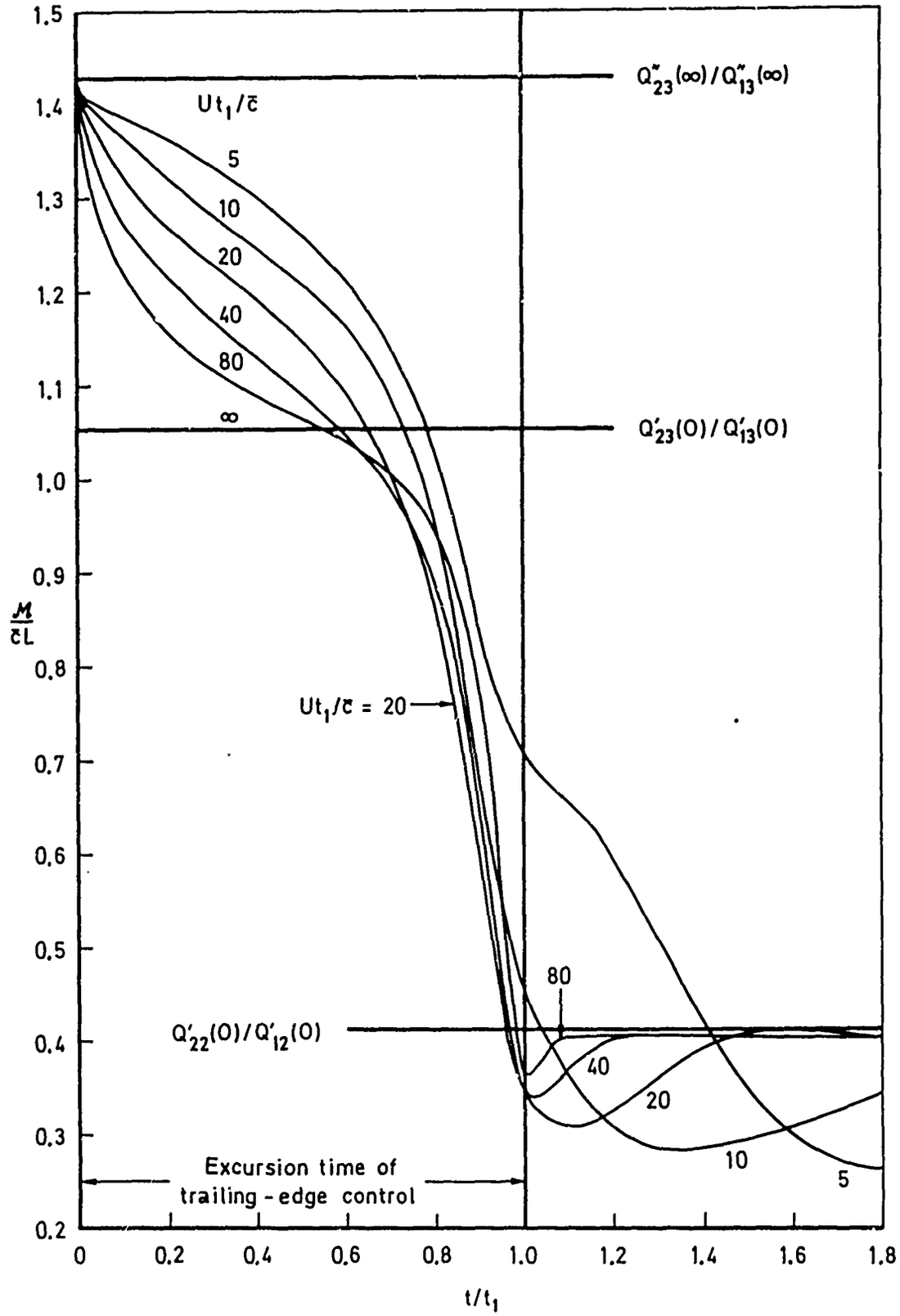

TR 81060

Fig 12 Time-dependent streamwise centre of pressure

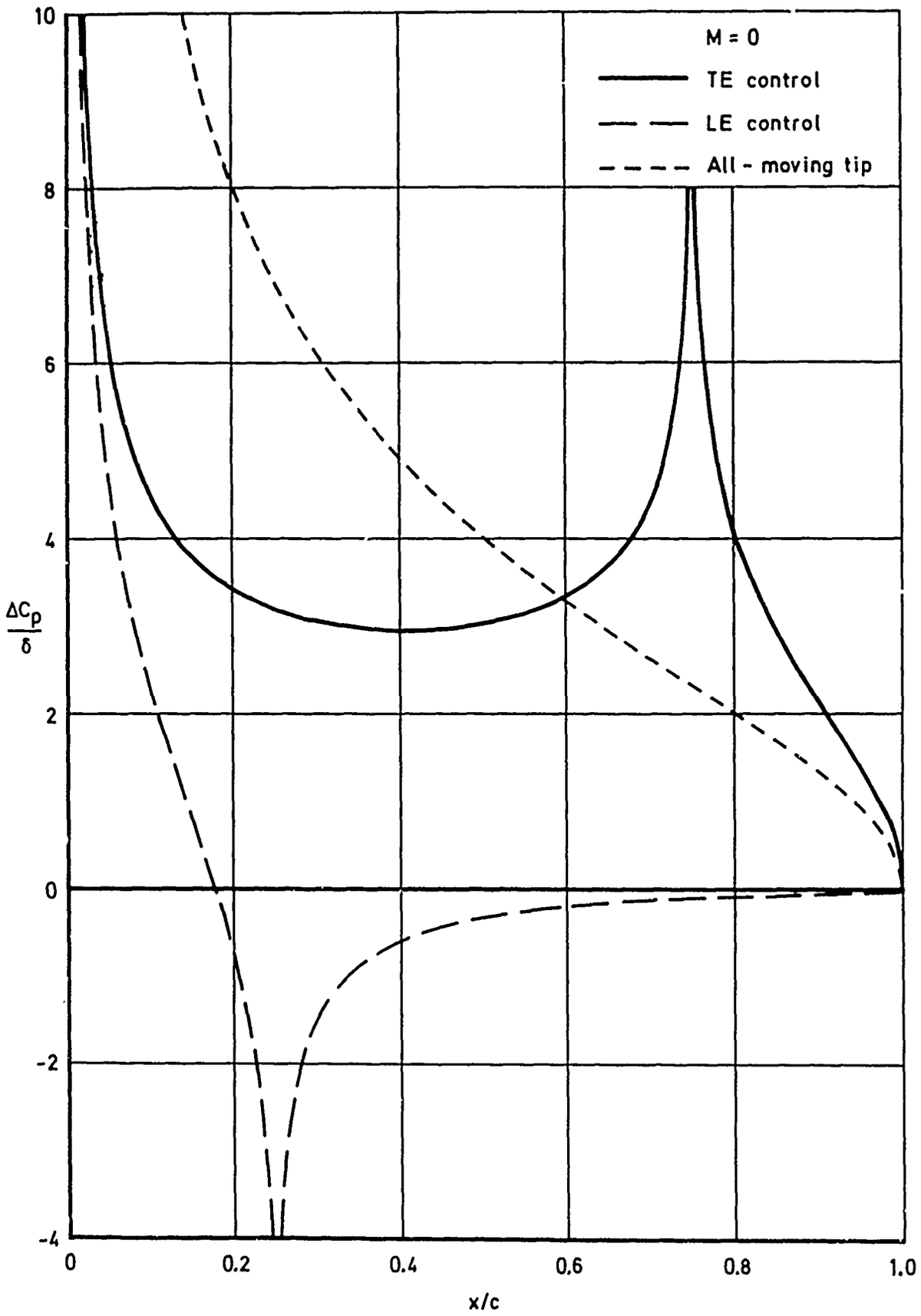

TR 81060

Fig 13 Steady two-dimensional loadings for three types of control

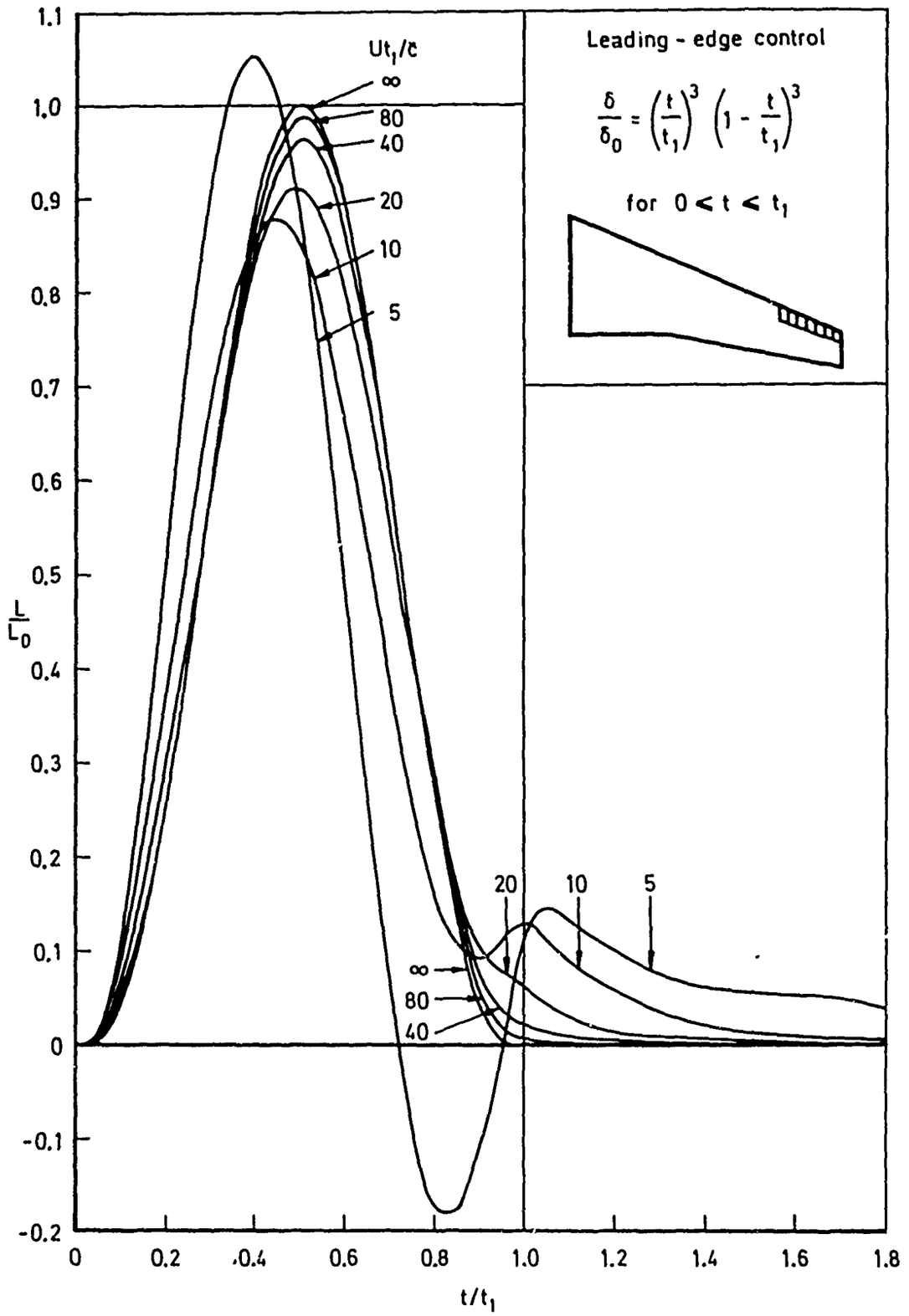

Fig 14 Influence of excursion time on transient lift

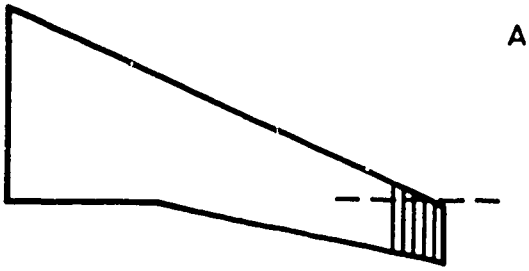

All - moving tip M = 0.8

$$\frac{\delta}{\delta_0} = \left(\frac{t}{t_1}\right)^3 \left(1 - \frac{t}{t_1}\right)^3$$

for $0 < t < t_1$

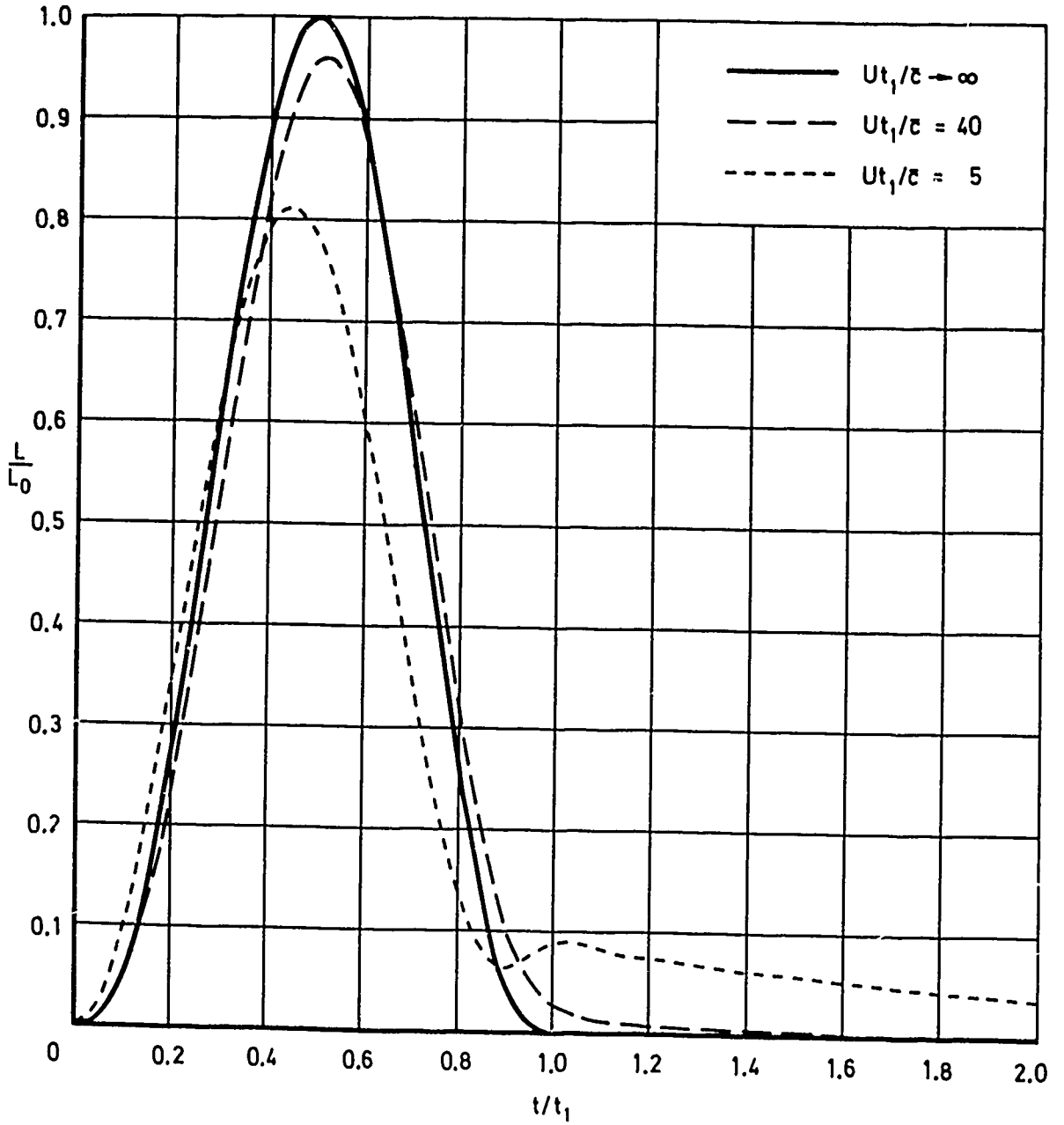

TR 81060

Fig 15 Influence of excursion time on transient lift

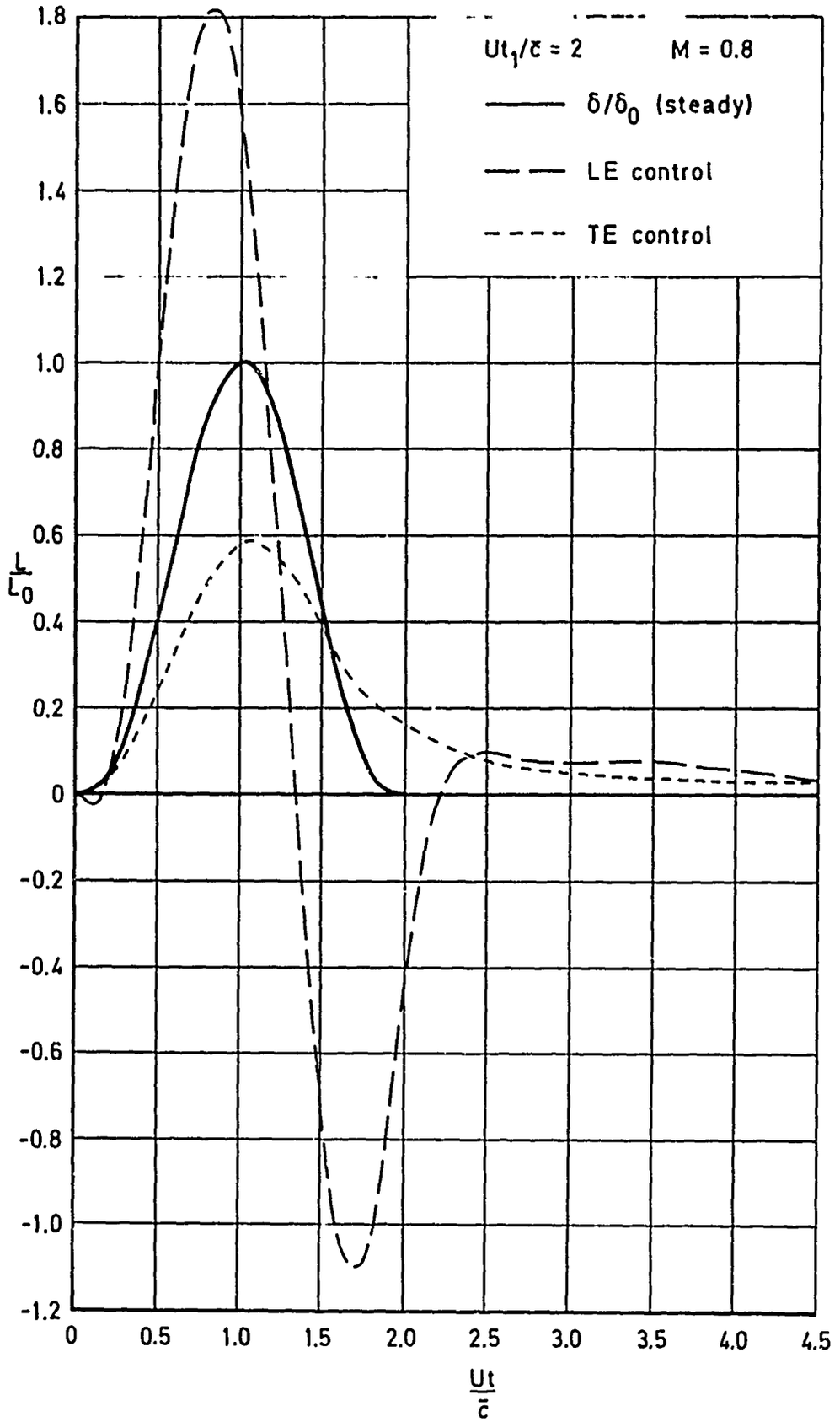

TR 81060

Fig 16 Transient lift due to rapid motion of leading-edge and trailing-edge controls

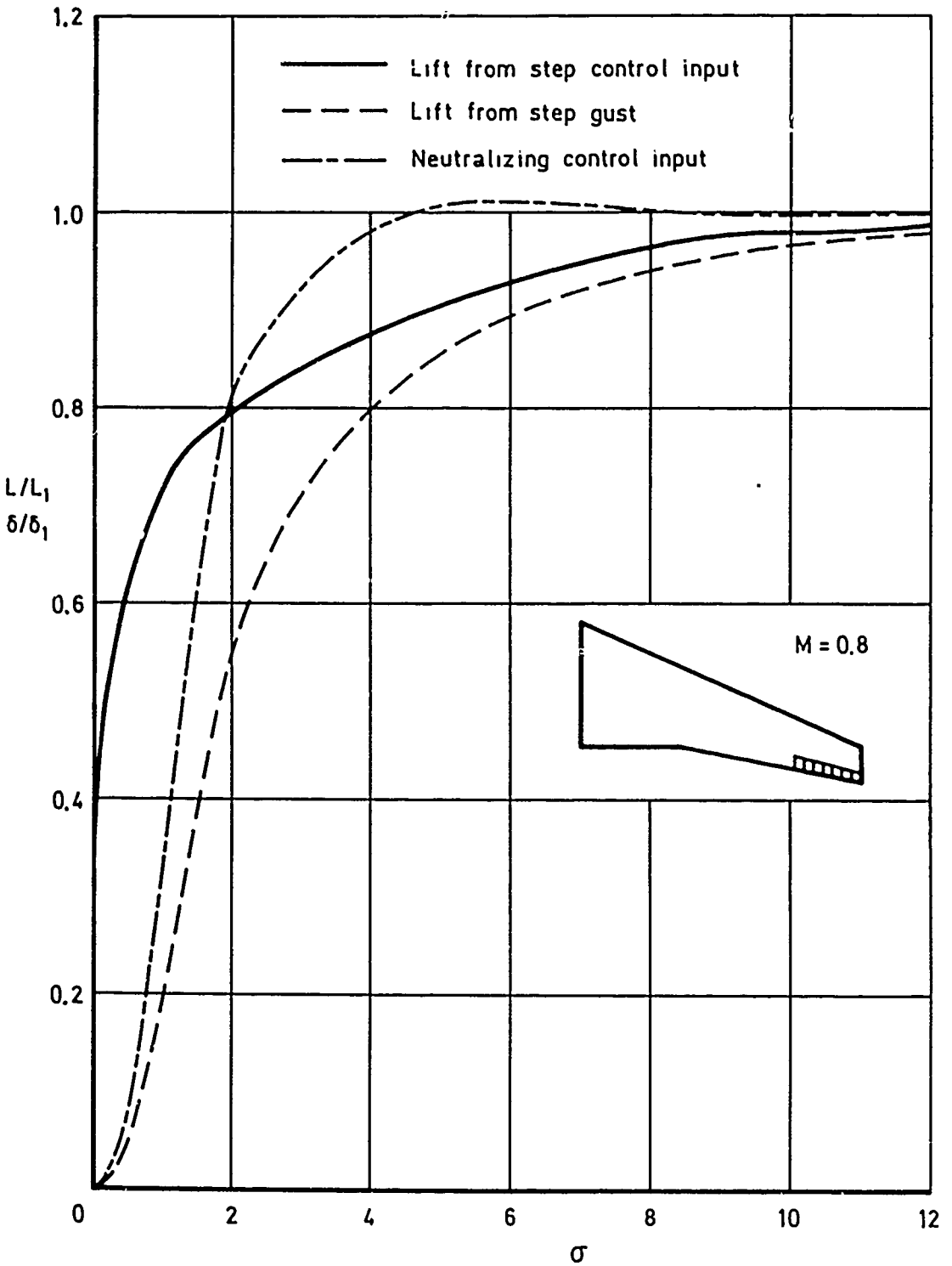

Fig 17 Trailing-edge control input to cancel lift from step gust

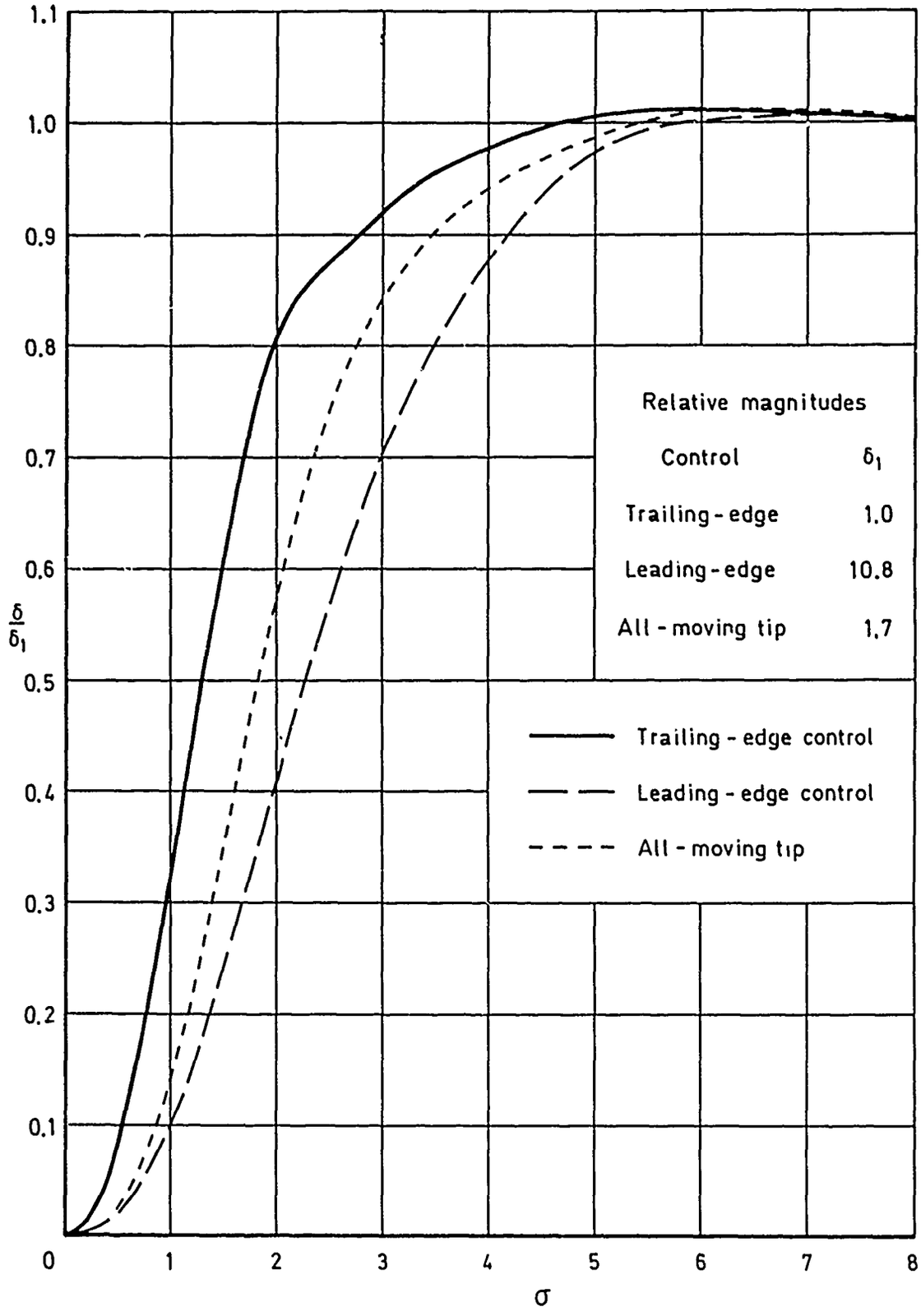

TR 81060

Fig 18 Control surface motions to neutralize lift due to step gust

REPORT DOCUMENTATION PAGE

Overall security classification of this page

UNLIMITED

As far as possible this page should contain only unclassified information. If it is necessary to enter classified information, the box above must be marked to indicate the classification, e.g. Restricted, Confidential or Secret.

1. DRIC Reference (to be added by DRIC)	2. Originator's Reference	3. Agency Reference	4. Report Security Classification/Marking
	RAE TR 81060	N/A	UNCLASSIFIED

5. DRIC Code for Originator	6. Originator (Corporate Author) Name and Location
7673000W	Royal Aircraft Establishment, Farnborough, Hants, UK
5a. Sponsoring Agency's Code	6a. Sponsoring Agency (Contract Authority) Name and Location
N/A	N/A

7. Title The application of subsonic theoretical aerodynamics to active controls

7a. (For Translations) Title in Foreign Language

7b. (For Conference Papers) Title, Place and Date of Conference

8. Author 1. Surname, Initials	9a. Author 2	9b. Authors 3, 4	10. Date	Pages	Refs.
Garner, H.C.	-	-	May 1981	81	15

11. Contract Number	12. Period	13. Project	14. Other Reference Nos.
N/A	N/A		Structures BF/B/0860

15. Distribution statement

(a) Controlled by – RAE/ST4

(b) Special limitations (if any) – N/A

16. Descriptors (Keywords) (Descriptors marked * are selected from TEST)

Active controls. Aerodynamic loads*. Indicial aerodynamics. Lift*. Potential theory*. Subsonic flow*. Three-dimensional flow*. Unsteady flow*.

17. Abstract

Analytical and numerical studies are made of aerodynamic forces for wing and control-surface motion with general time-dependence in linearized subsonic flow. Alternative formulations are discussed, with particular attention to one where quasi-steady displacement and rate terms are combined with a residual history term. An accurate calculation procedure is devised, and results are illustrated for trailing-edge, leading-edge and all-moving-tip controls. Emphasis is placed on asymptotic behaviour at small and large times. Individual control characteristics are compared over a wide range of control rate. The usefulness of the quasi-steady approximation is established for hinge moments and is analysed for lift, where the rate and history terms become important together. The rapid lift response to the leading-edge control and the sluggish lift response to the trailing-edge control are explained. Confirmatory Fourier transform calculations show the extent to which the range of frequency can be truncated. The control-surface motion to produce a known time-dependent force is determined. It is remarkable how rapidly the controls can neutralize the growth of lift as the wing enters a step gust.